SISSA - SCUOLA INTERNAZIONALE SUPERIORE DI STUDI AVANZATI
TRIESTE
Strada Costiera 11

ISAS - INTERNATIONAL SCHOOL FOR ADVANCED STUDIES

On deconstruction and roughening phase transitions in Au(110) and Pt(110) surfaces

Thesis submitted for the degree of

"Magister Philosophiæ"

CANDIDATE

Marco Bernasconi

SUPERVISORS

Prof. Erio Tosatti

Dr. Furio Ercolessi

July 1992

TRIESTE

On deconstruction and roughening phase transitions in Au(110) and Pt(110) surfaces

Thesis submitted for the degree of

"Magister Philosophiæ"

CANDIDATE

Marco Bernasconi

SUPERVISORS

Prof. Erio Tosatti

Dr. Furio Ercolessi

July 1992

Table of Contents

Introduction

The (110) surfaces of noble and near noble metals belongs to two different classes. The first class includes the lighter metals (Cu,Ag,Ni,Pd) whose (110) surface remains unreconstructed when clean (although a suitable coverage of alkali adatoms may lead them to reconstruct [1, 2, 3, 4]).At sufficiently high temperatures these surfaces are expected to show a roughening transition [5, 6, 7, 8, 9, 10]. The second class includes the heavier metals (Au,Pt,Ir) which at low temperature reconstruct in the 2x1 missing row phase (Au, Pt), or in other closely related missing-row geometries (Ir) [11]. The unreconstructed (110) surface of fcc crystal is formed by an array of atomic rows along the $[1\bar{1}0]$ direction, separated by a distance a_0 in the [001] direction, a_0 being the bulk lattice constant. Missing-row reconstruction may be rationalized in a simple way. The surface tend to increase its atomic density by forming of (111) microfacets resulting in a closely packed surface with lower surface energy than the 1x1 surface, despite the increase in microscopic surface area. The lowest order possibility of such microfaceting is precisely the 2x1 reconstruction, where alternating $[1\bar{1}0]$ top rows are removed. The occurrence of reconstruction depends on the relative value of the surface energy per atom in the unreconstructed (110) and in the (111) surfaces, namely one expects roughly the reconstruction to take place if $\Delta > 0$, where $\Delta = \sigma_{110} - \sqrt{3/2}\sigma_{111}$, and σ are surface energy per unit area. Actually if $\Delta > 0$ one must consider some additional interaction in order to stabilize the 2x1 phase

with respect to macroscopic faceting towards the more stable (111) structure. Elastic attractions between "ridge" and "valley" have been invoke to explain the stability of the 2x1 structure [17]. A variety of techniques , have established the existence of the missing row structure in gold [12] and Pt [13]. Recent work [11] has shown that Ir(110) is more complex. Theoretically, the missing row (MR) phase has been shown to be favourable by tight binding [14] and pseudo-potential density functional calculations [15] as well as by calculation using phenomenological many body hamiltonians [16, 18, 19]. Among the latter only the "glue model" by Ercolessi et al [16, 18] produces for gold a 2x1 phase which at zero temperature is stable with respect to (111) faceting.

As temperature rises, excitations begin to disorder the ideally reconstructed 2x1 surface until eventually a continuous deconstruction transition takes place. Assuming that atoms in the outermost plane behave as a lattice gas at half coverage the deconstruction transition should belong to the 2D Ising universality class [20, 21]. However it has been recognized soon that there is no a priori reason for the surface to stay confined into two levels. For example the glue model for gold predicts the higher order missing-row reconstructions, which affect more atomic layers, to be very close in energy to the 2x1 structure. Therefore deconstruction could arise from the proliferation of defects with different reconstruction index, 1x1, 3x1, 4x1 ..., as well as adatoms and vacancies. This suggest the existence of a possible link between deconstruction and roughening [5]. Roughening derives from the proliferation of thermally excited steps [22, 23]. The interplay between steps and deconstructive defects may provide the connection between the two transitions which is the subject on much recent experimental [24, 25, 26, 27, 28, 29, 30] and theoretical work [30-45]. Furthermore the possibility of a single phase transition from the reconstructed flat phase to a deconstructed rough phase cannot be excluded theoretically. In this latter scenario there is the possibility that reconstruction might induce a change of the universality class of

the roughening transition from the Kosterlitz-Thouless, expected for the unreconstructed fcc(110) [5].

Experimentally the deconstruction and roughening transitions can be observed by means of X-ray, electrons and He-atom scattering techniques, measuring the surface structure factor directly related to elastic scattering intensities. In Au(110) the deconstruction transition has been located at $T_D \sim 700K$ through the vanishing of the $(00\frac{1}{2})$ Bragg peak in LEED [24, 29], X-ray [25] and atom scattering [26, 27] experiments. The critical exponents have been reported to be in the 2D Ising universality class. This is agreement with the lattice gas model prediction, but if the off-plane degree of freedom are included the Ising point must be produced in a rather non trivial fashion. Roughly 50 K above the deconstruction temperature T_D, a roughening transition has been reported for Au(110) by atom scattering [26]. Conversely X-rays scattering measurements in Pt(110) by Robinson *et al* [30], have been interpreted as an indication of a single phase transition ($T_D = T_R$) from reconstructed smooth to deconstructed rough, albeit with exponents near the 2D Ising universality class. The roughening of the surface was deduced from the observed shift in the position of the $(00\frac{1}{2})$ Bragg peak above T_D. Such a shift, not observed in gold just above T_D, originates from the translation of the uppermost layer along [001] direction by $a_0/2$, generated by a monoatomic step. The temperature dependence of the shift detected on Pt implies a proliferation of steps at the deconstruction temperature.

One problem is to understand if the apparently different experimental results for gold and platinum really require that T_D and T_R do coincide in platinum or if they can be explained by a different structure of the deconstructed phase for the two materials. Moreover in the former case one should ask which parameters control the separation between T_D and T_R, if topology alone is not sufficient to guarantee the existence of two distinct phase transitions. Actually the MR (2x1) structure has four degenerate ground states:

in the fcc(110) the outermost layer may be formed by two different sublattices and the missing rows can be chosen in two possible ways, odd rows and even rows. Two different order parameter can be defined: the reconstruction order parameter P_{2x1} vanishing at T_D, and the order parameter P_{EO}, determining which of two the sublattices of fcc(110) corresponds to the atoms in the top rows (the "even" sublattice, or the "odd" sublattice).

In chapter 1 we show that P_{EO} can discriminate between two different possible structures of the deconstructed flat phase. In one phase, domain walls with finite width proliferate destroying the reconstruction order parameter P_{2x1}, but still P_{EO} is finite, the domain walls being formed by a bound pair of steps of opposite sign. Inside the reconstructed domains only the two ground states with the same sublattice, say the even sublattice, on the top rows positions are involved. We call this phase " deconstructed, even, flat" (DEF). The other phase is a realization of the disordered flat phase (DOF) introduced by Rommelse and den Nijs [40, 42, 43]. The step free energy vanishes at the deconstruction transition; steps are no longer bound, but they have long range up-down up-down order and the surface is still flat on average. All the four MR ground states are involved locally in the reconstructed domains with the same probability, implying the vanishing of the P_{EO} order parameter, as well as of P_{2x1}.

Next we suggest that if the DEF phase is realized at T_D, an intermediate phase transition should in principle occur before roughening. The new critical line is located by the vanishing of P_{EO} and corresponds to the transition between the DEF and DOF. At this transition the step free energy vanishes, and steps proliferate on the already deconstructed surface. Yet the surface is still flat due to the long range up down order of steps typical of DOF.

The experimental fingerprint of the two deconstructed phases are compared in chapter 2 with experimental data available for Au(110) and Pt(110) . The experimental results are

seen to be consistent with the hypothesis that gold and platinum at T_D might be physical realizations of the former DEF, and of the latter DOF phases respectively.

As it turns out, the DEF deconstructed phase with a nonzero value of P_{EO} has already been studied within well-defined statistical mechanical models. Conversely the deconstruction-"preroughening" transition, producing a DOF phase has not been properly analysed up to now, nor has the role of the P_{EO} order parameter been clearly pointed out. In chapter 3 we briefly review the models proposed so far for deconstruction and roughening and we discuss the behaviour of the order parameter P_{EO} in the different cases; the lattice gas model, which is the first model introduced for the deconstruction of fcc(110)(2x1) surfaces is discussed instead in appendix B. We propose in chapter 3 that the deconstructed phase, produced by the a solid-on-solid (SOS) model recently studied by Mazzeo *et al* [44], is precisely a realization of the DOF phase.

Finally we discuss possible modifications of the existing models, in order to exhibit a full sequence of three phase transitions T_D, (where $P_{2x1} = 0$), T_{EO} (where $P_{EO} = 0$) and T_R (roughening) which fully characterize the interplay between reconstruction and roughening for the missing-row reconstructed fcc(110) surfaces.

All the statistical mechanics models studied have as input parameters the energies of the defects supposed to be involved in the disordering mechanism. The hierarchy of the energies of the different defects is a crucial ingredient in order to discriminate between the possible scenarios, and it is greatly simplified in the SOS analysed so far. In appendix C we discuss to which extent a SOS model as that proposed by Mazzeo *et al* [44] is able to describe the true hierarchy of the energy of defects in fig.(1.1) for a real surface. In order to do this we compare the defects energy as predicted by the SOS model of Mazzeo *et al* [44], with the energies deduced by molecular dynamics simulation with two different phenomenological classical potential, namely the glue model [16, 18, 17] and the Voters'

potential [46] for gold. It turns out that the results are strongly potential dependent, hence we have investigated the structure of the deconstructed phase obtained with both the previous continuum models. Unfortunately the kinetics of the deconstruction transition is very low, so the thermodynamical characterization of the phase trasition by molecular dynamics is very computer demanding. Nevertheless we get a picture of the deconstrucetd phase by warming up the sample at temperature higher than the expected T_D, where the kinetics is much faster. The deconstructed phase for the Voters' and glue models are indeed very different. It turns out that the glue model, widely and successfully employed to predict the stability of reconstructed phases of all the low index surfaces of gold, does not deconstruct properly; as a matter of fact at 980 K our samples are deconstructed, but the surface atoms have lost the registry with the underlying bulk lattice, producing satellite peaks in the surface structure factor, not observed experimentally. Conversely the Voters' potential does not present this anomaly, suggesting that the incommensuration is an artificial result, produced by the stronger surface contractive forces of the glue model. Unfortunately with the Voters' potential the 2x1 phase is not stabilized with respect to faceting in the (111) surface, hence the decostructed phase obtained by molecular dynamics is only metastable. The ability to reproduce the structure of the deconstructed phase seems thus a stringent test for the quality of phenomenological continuum potentials. A phenomenological many-body potential such as the glue and Voters' potentials, able to describe properly the deconstructed phase of Au(110)(2x1) is thus still lacking.

Most of the existing concepts in the theory of the MR deconstruction/roughening have been produced by three groups of authors, namely Den Nijs [39, 40, 43, 45], Villain and Vilfan [31, 32, 33, 34, 35] and Levi, Jug, Kohanoff, Mazzeo, Tosatti and Trayanov [5, 36, 37, 38, 44]. Our work represents an attempt at extending and clarifying further the physical situation and, without really attempting any comprehensive review of these

earlier contributions, will make free abundant use of ideas, concepts and nomenclature, and even schematic drawing of steps, etc., contained therein.

1 Scenarios for the deconstruction and roughening phase transitions

We first introduce the order parameters which characterize the reconstruction and the roughness of the surface. The missing-row reconstruction order parameter can be defined as

$$P_{2x1} =< \rho_{\mathbf{G}} >=< \frac{1}{N} \sum_l e^{i\mathbf{G}\,\mathbf{R}_l} > \tag{1.1}$$

where $\mathbf{G} = \frac{2\pi}{a_0}(0, 0, \frac{1}{2})$, a_0 being the bulk lattice constant, and $\mathbf{R}_l$ are coordinates of all top atoms, a top atom being defined as an atom with all nearest neighbors at a lower levels. Here $< ... >$ denotes configurational averages, and N is the number of 2x1 unit cells.

A side view of 2x1 ideal surface is shown in figure 1.1a, the directions of most important relaxation are depicted, as deduced from first principle calculations [15]. The atoms (circles) are projected onto the $(1\bar{1}0)$ plane, empty and full circles denotes the two surface sublattices of the unreconstructed phase. One notes that the 2x1 ground state is fourfold degenerate: the top rows may belong either to the even sublattice or to the odd sublattice, and the missing rows can be chosen in two possible ways, odd rows and even rows. The four ground states correspond to the four values of the complex order parameter $< \rho_{\mathbf{G}} >$: $(1,0), (-1,0), (0,1), (0,-1)$. In the four ground states the phase θ of $< \rho_{\mathbf{G}} >$ is respectively 0, π, (even atoms on the top rows), and $\frac{\pi}{2}$, $-\frac{\pi}{2}$ (odd atoms on top rows).

The deconstruction transition T_D is defined as the temperature where the reconstruction order parameter vanishes.

Next, we define another order parameter, named P_{EO}, which discriminates between the odd and even sublattice in figure 1.1a. P_{EO} determines which sublattice corresponds to the atoms of the topmost layer. A possible choice is

$$P_{EO} =< \frac{1}{N} \sum_i |\cos \mathbf{G}\,\mathbf{R}_i| - |\sin \mathbf{G}\,\mathbf{R}_i| > \tag{1.2}$$

where the symbols have the same meaning as in (1.1). We remark that $P_{2x1} = 0$ does not implies $P_{EO} = 0$. The order parameter P_{EO} can be zero or finite above deconstruction; we will see that this order parameter can be used to characterize two possible structure of the deconstructed phase. The P_{EO} order parameter can be defined and has been defined also in the smooth unreconstructed fcc(110). Its vanishing locates precisely the preroughening transition to a disordered flat phase, introduced by Rommelse and den Nijs [40, 42, 43], and discussed further chapter 3. The role of this order parameter for the reconstructed surfaces, however, does not seem to have received attention.

Finally we come to roughening. The statistical mechanical definition of a rough surface is introduced through the analysis of the height-height correlation function expressed as

$$G(R_{ij}) =< [h(\mathbf{R}_i) - h(\mathbf{R}_j)]^2 > \tag{1.3}$$

where $h(\mathbf{R}_i)$ is the coordinate perpendicular to the surface of surface atom at lattice site $\mathbf{R}_i$. A surface is rough if the height-height correlation function diverges when $R_{ij} = |\mathbf{R}_i - \mathbf{R}_j| \rightarrow \infty$, and smooth otherwise. The general features of the roughening phase transition have been discussed in many review papers, notably by Weeks [23] and by van Beijeren and Nolden [22].

Different varieties of SOS models, some of them exactly solved, predict a roughening

transition of infinite order in the Kosterlitz-Thouless (KT) universality class. This conclusion was first drawn from a discrete gaussian model by Chui and Weeks [47]. Subsequently van Beijeren [48] mapped a body centered SOS model for isotropic bcc(100) surface on the exactly solved six vertex model [49, 50], exhibiting a KT roughening. For the fcc(110) surface an analogous mapping on the anisotropic six vertex model has been provided by Jayaprakash and Saam [51], and used by Trayanov *et al* [5].

The KT critical behaviour prescribes at the roughening temperature T_R an essential singularity in the free energy, no divergence in the specific heat but a rounded maximum at a temperature T^* usually lower than T_R, and the asymptotic behaviour [22]

$$\begin{aligned} G(R) &\sim 2\,K(T)\ln\xi,\ T < T_R \\ &\sim 2\,K(T)\ln R,\ T > T_R \end{aligned} \tag{1.4}$$

for $R \to \infty$. ξ being the correlation length for height-height correlation function (1.3), which is divergent for all $T > T_R$. The coefficient K(T) behaves in a characteristic way for a KT transition, namely

$$K(T) = \frac{1}{\pi^2} + C\sqrt{T - T_R}\,,\ T \to T_R^+ \tag{1.5}$$

where C is a non universal constant.

At and above the roughening transition temperature the step free energy is zero, and macroscopically this shows up as a divergence of the average interfacial thickness and disappearance of the flat crystal facet [22].

The defects of importance in the deconstruction and roughening of the MR phase are illustrated in figures 1.1 (b)-(l). The defect are supposed to be of infinite length along the $[1\bar{1}0]$ direction.

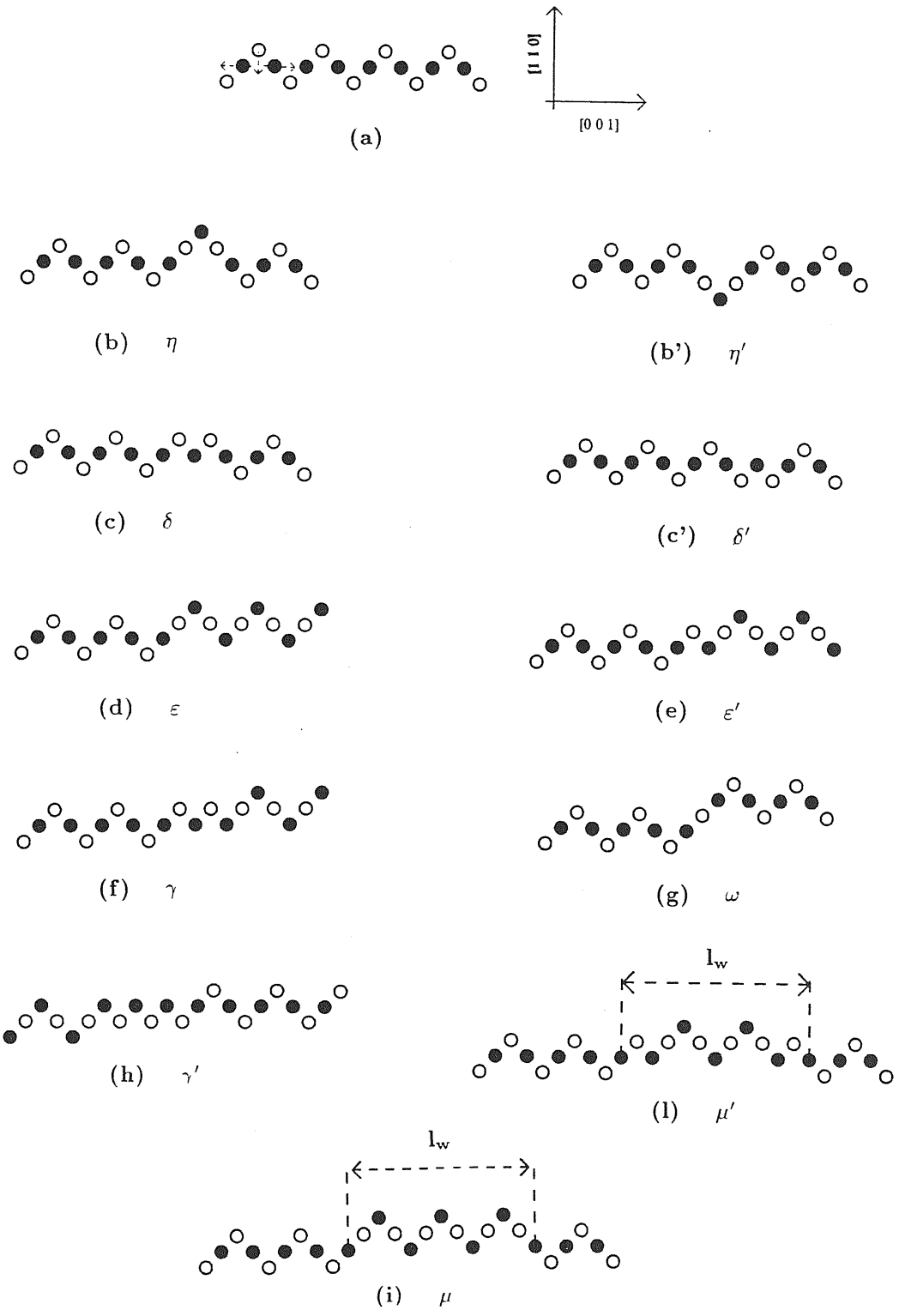

Figure 1.1: Side view of 2x1 phase and possible elementary excitations. (a) Ideal structure. The arrows show the direction of surface-atoms relaxation. (b)-(p) Defects configurations. Greek letters denote creation energy per atom along $[1\bar{1}0]$.

Greek letters below the defects represent creation energy per atomic spacing along the row $[1\bar{1}0]$. We call (b) and (b') 3x1 compact domain wall, (c) and (c') 1x1 compact domain wall, (d) 3x1 step, (e) 1x1 step, (g) 4x1 step, (i) and (l) 3x1 and 1x1 extended domain wall respectively. (f) and (g) are examples of higher energy step excitations. The defects (b), (b') and (i) can be seen as two opposite 3x1 steps bound together. Following den Nijs [43] we may call chirality the difference in energy between step 1x1 and step 3x1. We define "domain wall" a defect dividing two regions of the surface with P_{2x1} of opposite sign, but same P_{EO} i.e. same sublattice on top rows, but different parity of the missing rows. Defects (b), (b'), (c), (c'), (i) and (l) are all domain walls. As usual one can define the domain wall free energy as the difference between the free energies of the two systems with different boundary conditions as illustrated in figure 1.2 [22]. Plus and minus signs refer to the sign of the order parameter. The boundary conditions imposed in figure 1.2b force the system to develop a domain wall. The two domains are actually two different phases coexisting in equilibrium and spatially separated by an interface whose free energy must be positive for stability. At the critical temperature the free energy of the interface vanishes since there are no longer two well-defined phases, but just one homogeneous disordered phase. A step divides two regions of the surface with different sublattice on top rows and opposite sign of P_{EO}. Across a 1x1 step the phase θ changes by $\frac{\pi}{2}$, while across 3x1 step the phase θ changes by $-\frac{\pi}{2}$. The step free energy can be defined analogously to that of the domain wall, imposing the required change in θ as a boundary condition.

The infinite domain walls and steps along $[1\bar{1}0]$ shown in fig.1.1 may be considered as "ground state" configurations of the interface; at finite temperature they are no longer infinite straight lines,as they get interrupted by kinks. The domain wall moves to neighboring atomic rows, through intermediate excited states. This meandering produces a configurational entropy which decreases the free energy per unit length [31, 33]. In the

following we will speak about free energies of a particular domain wall as 3x1 or 1x1 compact domain wall etc., meaning that mainly one particular defect contributes to the effective domain as introduced by the boundary conditions.

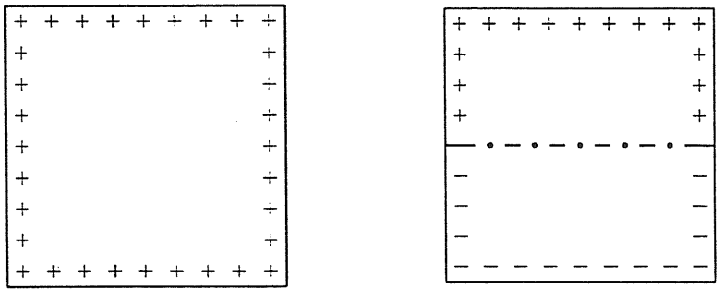

Figure 1.2: Boundary condition for an Ising model favoring (a) the homogeneous $\uparrow$ $-$phase, (b) the coexistence of the $\uparrow$ $-$phase and $\downarrow$ $-$phase.

We remark that when walking along the [001] direction, the order parameter P_{2x1} changes sign after crossing two steps. An important consequence is that overhangs (fig.1.3a) and therefore simple closed terraces (fig.1.3b) are forbidden. The simplest allowed closed terrace (fig.1.3c) and closed reconstruction domain (fig.1.3d) are made up with pairs of simple steps and related terraces, whose edges merge to a point [34].

In the following we analyse different scenarios which are in principle possible for the disordering process of a generic 2x1 reconstructed phase. In chapter 2 we will compare the experimental fingerprints of each possible phase with the experimental data available for Au(110) and Pt(110). In chapter 3 we will present the statistical mechanics models studied so far, dealing with the different pictures of deconstruction and roughening presented. All the scenarios proposed implicitly assume that mainly one type of defect is involved in the deconstruction transition. The scenarios from (i) to (iv) below assume the disordering process occurring in two steps: first a critical deconstruction transition at T_D and a

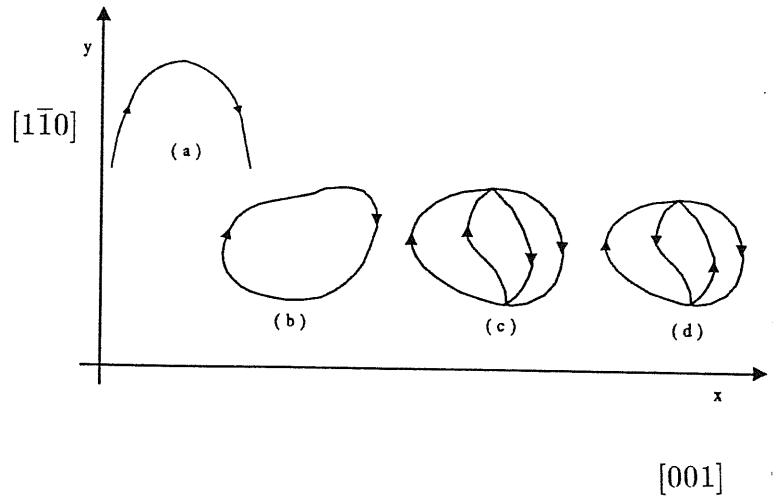

Figure 1.3: Topology of two allowed ((c), (d)), and two forbidden ((a), (b)) configurations of steps in the 2x1 phase. Arrows denote the sign of the steps.

roughening transition at a higher temperature T_R. Conversely scenario (v) considers only one phase transition associated with roughening. We remark that since roughening implies a proliferation of steps, and since across two adjacent steps (either parallel or antiparallel) the reconstruction order parameter changes sign, the rough surface is in some sense deconstructed, i.e. it has $< P_{2x1} >= 0$. The roughening transition always implies a deconstruction transition, if the latter does not occur before, i.e. $T_R \geq T_D$. The exclusion of a reconstructed rough phase is due to the particular topology of the MR structure, where height variable and reconstruction order parameter cannot be disentangled [39]. Moreover in a rough phase P_{EO} is zero if atoms at each level are to have the same probability to be on surface (the interfacial width diverges), so that there is no the predominance of one sublattice on the top rows. The vanishing of $< P_{2x1} >$ and $< P_{ExO} >$ above T_R does not however imply necessarily the absence of any reconstruction-related phase transition above T_R. Examples of this kind will be touched upon later on in section 3.5.

The scenarios proposed are the following:

(i) The free energy of a 1x1 compact domain wall (Fig.1.1c, c') goes to zero at T_D and the free energy of a 3x1 or 1x1 step (Fig.1.1d, e) goes to zero at higher temperature. P_{2x1} vanishes at T_D, but P_{EO} is still finite above T_D. [1]

(ii) The free energy of a 3x1 compact domain wall (Fig.1.1b, b')goes to zero at T_D and the free energy of a 3x1 or 1x1 step goes to zero at higher temperature. P_{2x1} vanishes at T_D, but P_{EO} is still finite above T_D.

(iii) The free energy of a 3x1 or 1x1 extended domain wall (Fig.1.1i, l) with a fixed average width l_w goes to zero at T_D . The mean extension of the wall l_w has non-critical behaviour near T_D . Scenarios (i) and (ii) can be seen as particular case of (iii) with $l_w = a_0$, if the step leading to roughening is of the same kind of the compact domain wall driving deconstruction. At temperatures greater than T_D the domain wall in any case broadens to a greater average width. P_{2x1} vanishes at T_D, but P_{EO} is still finite above T_D. The deconstructed phase in scenarios (i)-(iii) above is a realization of the DEF phase.

(iv) The free energy of a step vanishes at T_D but the surface is stabilized in a disordered flat phase (DOF) by a long range up-down up-down order of steps. The roughening transition at $T_R > T_D$ coincides with the vanishing of the long range up-down up-down order. We assumes the structure of the deconstructed phase to be equivalent to the disordered flat phase (DOF) introduced by Rommelse and den Nijs [40, 42, 43].

(v) There is only one phase transition where the surface simultaneously roughens and deconstructs. This possibility has been investigated by den Nijs (sections 3.3, 3.5), by Villain and Vilfan (section 3.2), and recently by Balents (section 3.5). We will see in

[1] It might seem improbable in scenario (i) that the deconstruction is driven by 1x1 wall, and the roughening by 3x1 steps: one could perhaps expect that if the 1x1 wall costs less in energy than the 3x1 wall, the 1x1 step should cost less than a 3x1 step. Analogous comment deserves scenario (ii). However, as we will see in appendix C, relaxation effects are responsible for the following hierarchy of the energies of defects calculated, for example with the glue model for Au(110) at $T = 0\,K$: $E^{wall}_{1x1} < E^{wall}_{3x1}$, but $E^{step}_{1x1} \gg E^{step}_{3x1}$. Furthermore we remark that, due to relaxation of the isolated defects, $E^{wall}_{1x1} < E^{wall}_{3x1}$ holds also if the energy of the 1x1 phase is greater than the energy of 3x1 phase. So it is entirely possible to have in principle a deconstruction transition driven by 1x1 defect, and a roughening driven by 3x1 step.

section 3.3 that the model hamiltonian proposed by den Nijs [39] provides at zero chirality a simultaneous roughening and deconstruction, still with critical behaviour of the reconstruction order parameter in the 2D Ising universality class. Both ξ_{2x1} and ξ_{EO} diverges as $(\frac{T-T_D}{T_D})^{-1}$ in the model of den Nijs at the simultaneous deconstruction and roughening. Conversely, as we will see in section 3.5, the simultaneous deconstruction and roughening transition is expected to belong to the Pokrovsky-Talapov universality class in the limit of infinite chirality.

1.1 Stability of the DOF phase

Figure 1.4 shows the main difference between the structure of deconstructed phase in scenarios (iv) and (iii). As in the previous figures, continuous lines are steps, the arrows denote their sign. Figure 1.4a describes scenario (iii): a couple of steps is bound to form a domain wall with finite size l_w, the size of the domain between two walls scales as the reconstruction correlation length ξ_{2x1} [32, 33]. In the figure 1.4b the DOF is depicted schematically.

Besides disconnected terraces (fig.1.3c) and disconnected reconstructed domains (fig.1.3d), an infinite fluctuating backbone of steps must exist in order to destroy the long range reconstruction order. The backbone forms a lattice which is not rigid, but fluctuates in its shape and number of bonds. Below T_D the backbone disintegrates and only disconnected terraces survive, restoring the long order reconstruction order. Note the orientation of the axis in fig.1.4b. The lines between two vertices represent steps which can be partly (or mainly) parallel to the [001] or to the $[1\bar{1}0]$ directions. However, since overhangs are forbidden the steps "parallel" to the [001] direction can only have kinks of one type: either all pointing upwards or all pointing downwards.

Six configurations of arrows are possible at each vertex of the backbone cluster, as

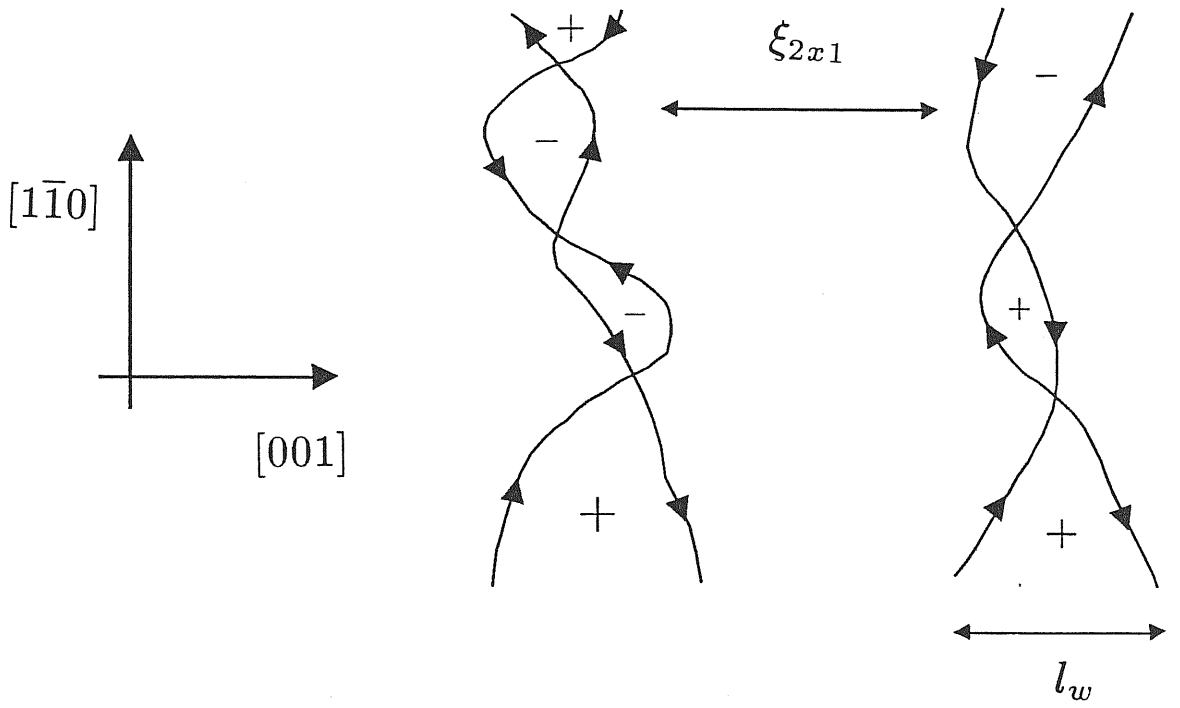

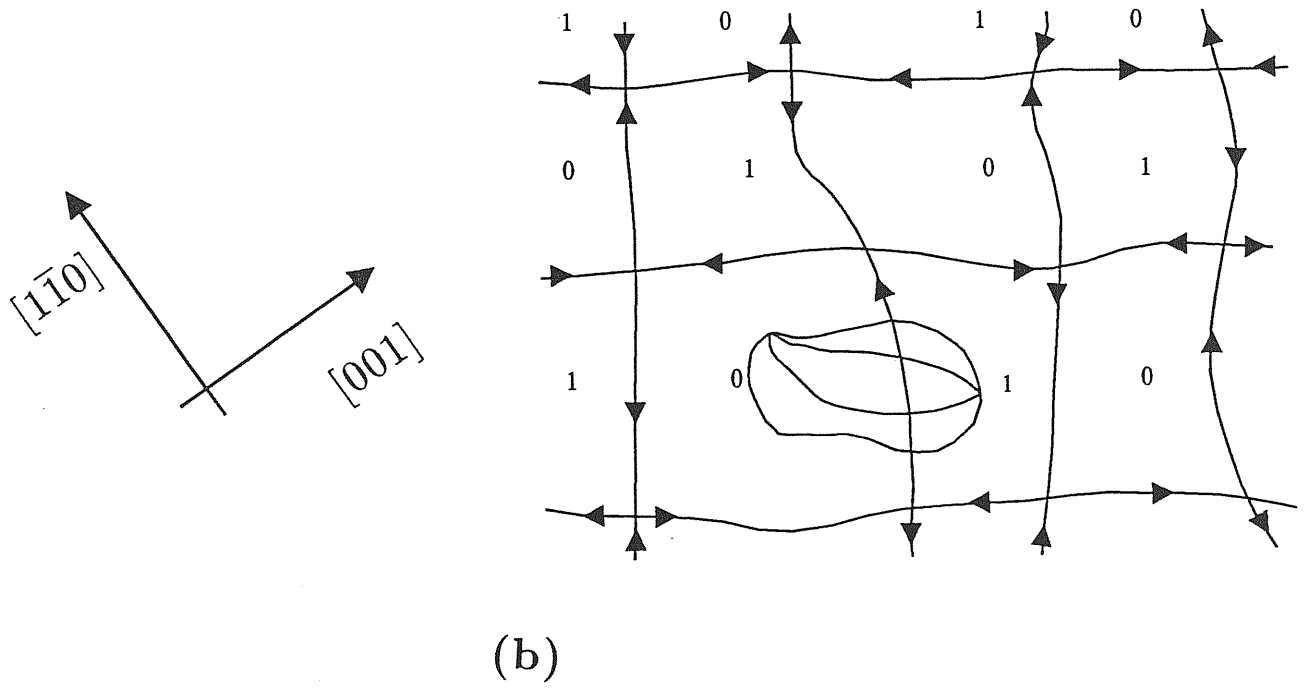

Figure 1.4: (a) Deconstructed flat phase of scenario (iii). + and - refer to the height difference with respect to the reconstructed domains. (b) Disordered flat phase on fcc(110)(2x1) of scenario (iv). The numbers denote the heights of the cells.

depicted in fig.1.5. Step-step interactions assign different Boltzmann weights to each vertex. Statistical mechanics of the six vertex (6V) model [49, 50] associated to this backbone determines the smoothness or roughness of the surface. The smooth phase of the six vertex model corresponds to the DOF phase, the backbone is formed by an array of steps "antiferromagnetically" ordered. The roughening transition of the six vertex model destroys the antiferromagnetic long range order of arrows in the backbone and produces the roughening of the surface [42, 43].

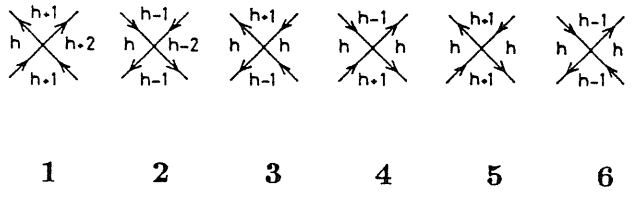

Figure 1.5: Configurations of the vertex in the six vertex model.

In scenario (iv) it is the free energy of a single step which vanishes at T_D and not the free energy of a domain wall. Here steps are not bound in pairs, and their antiferromagnetic order has only long range character. In section 3.1 we will illustrate the work by Rommelse and den Nijs, proving the existence of the DOF phase for a SOS model of sc(100) surface. In section 3.6 we will interpret the Monte Carlo results by Mazzeo *et al* [44] of a SOS hamiltonian for fcc(110)(2x1) as a realization of the DOF phase in fig.1.4b.

The deconstructed flat phase in scenarios (i)-(iii) and (iv) have a different "symmetry", characterized by a different behaviour of the P_{EO} order parameter. P_{EO} is finite in the deconstructed phase of scenarios (i)-(iii): mainly one sublattice occupies top rows positions; reconstructed domains involve just two of the four degenerate MR ground states while the other two ground states configurations are assumed locally inside the domain walls.

Concerning the critical exponent at T_D, we have already mentioned that considering the disordering of only the outermost layer, the deconstruction transition is always in the 2D Ising universality class [20, 21]. This is true in scenario (i). However the universality class can not change if the domain wall has a finite width l_w and is composed by 1x1 or 3x1 bound steps. It is determined by the change of the order parameters across the domain wall and it can not be affected by the internal structure of the wall itself. We further remark that due to relaxation effects also the domain walls in scenario (i) must have a finite width in real systems. The only additional requirement is that l_w is non-critical. Hence in scenarios (i)-(iii) the order parameter P_{2x1} averages to zero by assuming mainly two values at T_D, (say $\theta = 0, \pi$, or $\theta = \pm\frac{\pi}{2}$). Thus, it can be considered an Ising variable, and the deconstruction transition is expected to belong to the 2D Ising universality class. In the DOF of scenario (iv) both P_{2x1} and P_{EO} simultaneously vanish at T_D, and the two sublattices have the same probability to be on top. Adjacent terraces of the backbone cluster in figure 1.4b have opposites value of P_{EO}. We expect that near T_D the size of the terraces scale as the correlation length ξ_{EO} of the order parameter P_{EO}. Terraces can be further deconstructed by compact domain walls, so the relation $\xi_{2x1} \leq \xi_{EO}$ is expected to hold. The deconstructed flat phase of scenario (iv) is formed by reconstructed domains of all the four MR ground states. There are no a priori arguments to predict the universality class of the deconstruction transition in this case, and explicit numerical study of a model able to reproduce scenario (iv) is needed to deduce critical exponents. As we will see in section 3.6, the Monte Carlo simulation by Mazzeo *et al* finds 2D Ising exponents for a deconstruction transition where P_{2x1} and P_{EO} simultaneously vanish. Although further work seems necessary to unambiguously identify scenario (iv) with the deconstruction transition detected, the results by Mazzeo *et al* suggest that also a DOF produced by a proliferation of 3x1 steps could be consistent with the experimental evidence of 2D Ising

critical behaviour. In scenario (iv) the roughening transition is identified with the roughening of of the six vertex model assigned to the backbone cluster. Since the universality class of a phase transition should not change with the shape of the underlying lattice, a conventional KT roughening is expected in this picture.

Let us now discuss the general conditions for the stability of a DOF phase. When the backbone appears, because of the vanishing of the step free energy, the 6V model defined on the backbone must be in its antiferromagnetic phase. This occurs provided that $\Delta = \frac{a_1^2+a_3^2-a_5^2}{2a_1a_3} < -1$, where a_i is the Boltzmann weight $exp(-\beta\varepsilon_i)$ of vertex i with energy ε_i [5, 49, 50]. The symmetric version of the 6V model is assumed, i.e. $a_1 = a_2$, $a_3 = a_4$, $a_5 = a_6$. The condition $\Delta < -1$ is satisfied if the Boltzmann weight of vertices 5 and 6 are sufficiently larger that those of vertices 1-4. In the DOF in fig.1.4b vertex 1 represents the intersection between two parallel steps, i.e. a 4x1 step; vertex 5 represents the intersection between two antiparallel steps, i.e a 3x1 compact wall; vertex 3 corresponds to exchange of sign of two antiparallel steps at their crossing, and requires the breaking of three bonds along $[1\bar{1}0]$ (see fig..3.3a). Because of the large bond-breaking energy, vertex 3 is energetically much more costly than vertex 5. Hence, it seems possible to have $a_1 < a_5$ and stabilize the DOF phase, just by requiring a larger energy of 4x1 step with respect to the 3x1 wall.

In reality a vertex is presumably a rather complex object, instead of a point as assumed so far. Schematically, we may think of a region of radius R, large compared with the lattice parameter a_0, but small compared with the correlation length ξ_{EO}. The steps have no intersections outside R, but they can cross each other many times and have indirect interactions mediated by finite terraces inside R. So we can assign vertex free energy as $f = F_{vertex} - F_{periodic} - 2F_{step}$, where $F_{vertex}, F_{periodic}$, and F_{step} are respectively the free energy of a sample of dimension $\xi_{EO} \times \xi_{EO}$ with the boundary conditions imposed by the

vertex, the free energy of a sample with periodic boundary condition and the free energy of a single step.

We can imagine different mechanisms which favour the configuration with two adjacent antiparallel steps typical of vertex 5, with respect to the configuration in vertex 1 with two adjacent parallel steps. For example, there is an elastic repulsion between parallel steps, which turn out to be an attraction between antiparallel steps [52], or we may simply imagine a larger meander entropy of a 3x1 compact wall, with respect to the 4x1 step (see discussion in section 3.6). The argument presented above, indicating that the exchange of sign of steps in vertex 3 requires a larger number of bond-breaking than vertex 5, is no more sufficient to guarantee that $a_3 < a_5$, if the vertices are not a point, but an extended object. The identification of a mechanism, involving only entropy and not energy, which favours vertex 5 with respect to vertex 3 should be more subtle: we suggest that f_3 can be larger than f_5, because of an indirect interaction between the steps of the backbone, mediated by finite terraces. In figure 1.6 are displayed the configurations of vertices 5 (a), 4 (b) and 1 (c) in the presence of a finite terrace. One recognise the presence of subvertices at the intersections between the steps of the backbone and the finite terrace.

It is easy to recognise that vertex 5 is the only one which does not contain any subvertex of type 1. If we assume that indeed $f_1 > f_5$, then the absence of subvertices 1 in vertex 5 justifies a lower free energy of vertex 5 with respect to vertex 4. In other words, if we assume a stronger repulsion, either energetic or entropic, between parallel steps, one concludes that the presence of finite terraces hinders the crossing (exchange of sign) between two antiparallel steps.

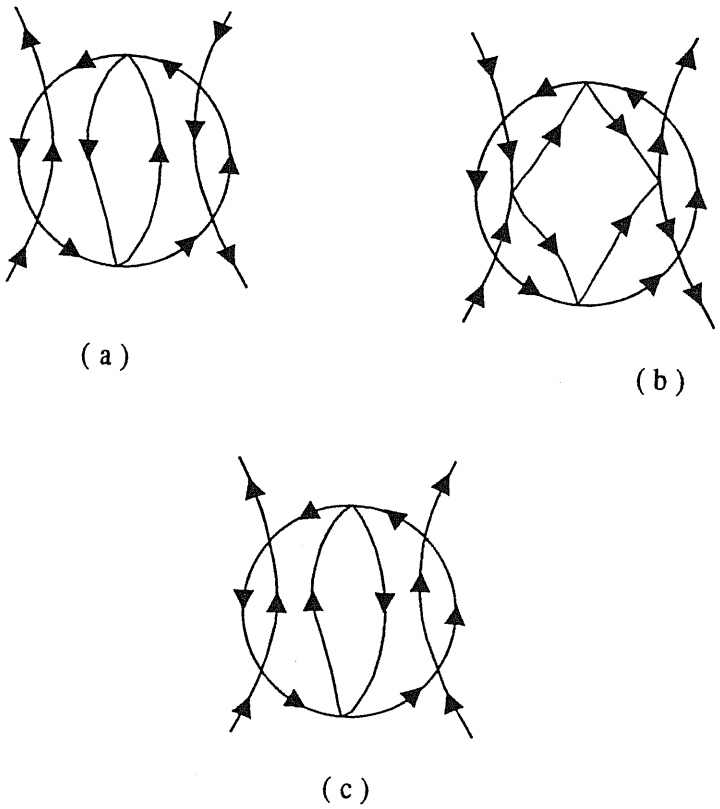

Figure 1.6: Configurations of vertex 5 (a), vertex 4 (b) and vertex 1 (c) in presence of a finite terrace.

1.2 Deconstruction transition and parity-restoring transition

Since there are two order parameters P_{2x1} and P_{EO} one can imagine that the vanishing of P_{2x1} and P_{EO} independently locates two phase transitions at temperature T_D and T_{EO} respectively. The two transitions can coincide as occur in scenario (iv) or they can differ as in scenarios (i)-(iii). What happens to the P_{EO} order parameter between T_D and T_R is an open problem, and different possibilities are conceivable. Let us consider each of them. Assume first that $l_w \ll \xi_{2x1}$ above T_D and up to T_R. The domain wall width does not widen significantly and surface roughening is produced by a proliferation of "individual" steps thought as independent entities with respect to the bound steps which form the domain walls. Depending on the nature of step-step interaction one can contemplate two further possibilities: a) the step free energy vanishes only at the roughening transition and $T_{EO} = T_R$; b) the single step free energy vanishes at $T_{EO} < T_R$. Above T_{EO} steps form a percolating network on the surface already deconstructed by domain walls. The surface is still flat on average due to long range up-down-up- order of steps. T_{EO} locates a phase transition from a DEF phase of the type described in scenarios (i)-(iii) to the DOF of scenario (iv). Once in the DOF phase the roughening transition will occur at higher temperature, following the same mechanism discussed in scenario (iv). In this picture just above T_{EO} there is a percolating network of steps superimposed on a percolating network of domain walls with small width l_w. In summary three phase transitions are predicted at temperatures $T_D < T_{EO} < T_R$.

Conversely, assume l_w to increase significantly above T_D, so that roughening coincides with the unbinding of the two steps form a domain wall, as proposed for example by Villain and Vilfan [33]. In this case something interesting could possibly happen below

roughening, when l_w starts to compete with ξ_{2x1}. In fact if $l_w \approx \xi_{2x1}$ the deconstructed phase is essentially a two levels system and P_{EO} vanishes. Explicit study of a model yielding this picture is necessary in order to understand whether also in this case a third phase transition at $T_{EO} < T_R$ is possible or whether $T_{EO} = T_R$.. For $T_{EO} < T_R$ the step free energy should still be finite at T_{EO}, and vanish only at T_R. At T_{EO} there is only the percolating network of domain walls.

Summarizing four situations are conceivable :

(A) $T_D < T_{EO} = T_R$. This can occur in scenarios (i), (ii), (iii).

(B) $T_D = T_{EO} < T_R$. This can occur in scenario (iv)

(C) $T_D = T_{EO} = T_R$. This can occur in scenario (v).

(D) $T_D < T_{EO} < T_R$. This can occur in scenarios (i), (ii), (iii).

The last possibility has not been explored up to now in literature. In chapter 3 we will illustrate the models proposed so far, dealing with the first three possibility and we will discuss how their enrichment with step-step interactions could produce the new phase transition proposed between deconstruction and roughening.

2 Scattering experiments

In this chapter we discuss how scattering experiments can discriminate between the different scenarios proposed. We also consider how the experimental data available for Pt and Au fits into the picture. We discuss the scattering intensities in the crude kinematic approximation. At this level, there is little difference amongst the various probes, in particular atoms and X-rays [5]. For example, elastic scattering of atoms in the kinematic approximation and in the corrugated hard wall model can be written as an average (configurational or temporal) $< I >$ of

$$\begin{aligned} I(\mathbf{Q}, q_z) &= \sum_{\mathbf{R}} e^{i\mathbf{Q}\,\mathbf{R}} \sum_{\kappa,\kappa'} \sum_{\mathbf{R}'} e^{i\mathbf{Q}\,(\,\mathbf{X}(\mathbf{R}+\mathbf{R}',\kappa)\,-\,\mathbf{X}(\mathbf{R}',\kappa'))} \\ &\cdot\ e^{iq_z\,(\,h(\mathbf{R}+\mathbf{R}',\kappa)\,-\,h(\mathbf{R}',\kappa'))}\,\alpha(\mathbf{R}+\mathbf{R}',\kappa)\,\alpha^*(\mathbf{R}',\kappa') \end{aligned} \tag{2.1}$$

where $\mathbf{Q}$ and q_z are the momentum transfer parallel and perpendicular to the surface. $\mathbf{R}, \mathbf{R}'$ run over the 2x1 surface Bravais lattice. $\mathbf{X}(\mathbf{R}, \kappa)$ is the position of atom in cell $\mathbf{R}$ belonging to the sublattice κ of the MR phase, $\kappa = 0, 1, 2, 3$. Neglecting relaxation $\mathbf{X}(\mathbf{R}, \kappa)$ is independent on $\mathbf{R}$. $h(\mathbf{R}, \kappa)$ is the vertical position of atom $\mathbf{R}$, κ. $\alpha(\mathbf{R}, \kappa)$ is a "shadowing factor" (as introduced by Levi *et al* [36]) depending on the heights of nearest neighbors of atom $\mathbf{R}, \kappa$, included because atoms surrounding a lower atom make the latter less visible to the probing beam. For atom scattering a reasonable approximation is [58]

$$\alpha(\mathbf{R},\kappa) = 2 - \frac{1}{2}n(\mathbf{R},\kappa) \tag{2.2}$$

where $n(\mathbf{R},\kappa)$ is the number of nearest neighbours of atom $\mathbf{R},\kappa$ located at a level higher than the atom itself . Notice that the true experimental intensity contains also other ingredients, such as the Debye Waller factor, an atomic form factor, and other factors not relevant to the present discussion. It is useful to express the configurational average of scattering intensity (2.1) as a sum of two contributions: coherent scattering, which produces the Bragg peaks, and incoherent scattering which is a measure of fluctuations. In the limit $|\mathbf{R}'| \to \infty$ the spatial and configurational average in (2.1)

$$< \sum_{\mathbf{R}'} e^{i\mathbf{Q}\,(\,\mathbf{X}(\mathbf{R}+\mathbf{R}',\kappa)\,-\,\mathbf{X}(\mathbf{R}',\kappa')\,)}\; e^{iq_z\,(\,h(\mathbf{R}+\mathbf{R}',\kappa)\,-\,h(\mathbf{R}',\kappa')\,)}\; \alpha(\mathbf{R}+\mathbf{R}',\kappa)\,\alpha^*(\mathbf{R}',\kappa') > \tag{2.3}$$

can be factorized as

$$N < \overline{e^{i\mathbf{Q}\,\mathbf{X}(\mathbf{R},\kappa)\,+\,iq_z\,h(\mathbf{R},\kappa)}\alpha(\mathbf{R},\kappa)} >< \overline{e^{-i\mathbf{Q}\,\mathbf{X}(\mathbf{0},\kappa')\,-\,iq_z\,h(\mathbf{0},\kappa')}\alpha^*(\mathbf{0},\kappa')} > \tag{2.4}$$

where the bar indicate spatial averages, and N is the number of 2x1 cells. The coherent part is obtained decoupling the spatial and configurational averages in (2.3):

$$< I(\mathbf{Q}) >_{coherent} = N \sum_{\mathbf{R}} e^{i\mathbf{Q}\mathbf{R}}\, |\sum_{\kappa=0}^{3} < \overline{e^{i\mathbf{Q}\mathbf{X}(\kappa)\,+\,iq_z\,h(\kappa)}\alpha(\kappa)} > |^2 \tag{2.5}$$

This expression determines the intensities of the various Bragg peaks. The Bragg peaks of the fcc(110) surface are classified in principal, superlattice and reconstruction peaks. The principal and superlattice peaks are integer peaks of Miller indices (hkl). They are bulk-permitted if all Miller indexes have the same parity and bulk forbidden otherwise. The surface notation assigns to the peak (hkl) in the bulk notation, the "surface Miller

indices" $(h_s k_s)$, related to the bulk ones through $h = k_s, k = -k_s, l = h_s$. An integer peak is said to be principal if its surface Miller indices all have the same parity , otherwise it is called a superlattice peak.

The reconstruction peaks are of type $(q_z\, q_z\, n + \frac{1}{2})$, where q_z is the perpendicular momentum transfer and n is an integer. We will refer to these peaks also as half-integer peaks. For atom scattering, according to eq. (2.5) and (2.2) and neglecting relaxation, the intensities of the latter peaks are independent on the position of q_z along the "rod" in the perfect 2x1 phase. This property is lost in presence of relaxation effects. We remark that, neglecting relaxation, formula (2.1) with the choice (2.2) for the shadowing factors predicts a zero intensity for the specular peak in antiphase (peak (0 0) with $q_z = \frac{\pi}{d}$ in the surface notation, d being the interlayer spacing). This is somewhat unfortunate since specular antiphase scattering is the main situation studied experimentally studied. Its intensity is made nonzero by dynamical deviations from approximation (2.2) and also by the strong inward relaxation of top-row atoms.

The X-rays scattering intensities for bulk forbidden peaks can be approximated still by expression (2.1), with the shadowing factors equal to one for top row atoms and zero otherwise. This procedure, where only the contribution of the top rows in taken into account is adopted by all the work on X-rays referred to in the following.

In appendix A it is shown that for $q_z = 0$ the reconstruction peak intensity is proportional to the square of the reconstruction order parameter (1.1), while the incoherent part is proportional to the susceptibility of the order parameter. At low temperature the upper bound imposed on the long range order correlation length by the finite extension of 2x1 terraces broadens the reconstruction Bragg peaks, which can be accurately fit by a gaussian as a function of function $\mathbf{Q} - \mathbf{G}$ [57]. The area of the gaussian, being proportional to the square of the reconstruction order parameter, is expected to vanish at T_D

approaching zero as $t^{2\beta}$, with $t = \frac{T-T_D}{T_D}$. Nearing T_D, fluctuations start to appear and the peak profile can not be longer fit by a gaussian form alone. The incoherent part is expected to have a Lorenztian shape, whose intensity diverges at T_D as the susceptibility of P_{2x1}, namely $t^{-\gamma}$, while its width is proportional to the correlation length ξ which in turn diverges at the critical temperature as $t^{-\nu}$ [57]. Thus fitting the peak profile near T_D with a superposition of a gaussian plus a lorentzian makes it in principle possible to obtain the critical exponents β, γ, ν. In this way Campuzano *et al* [24] were able to derive from LEED experiments the critical exponents of the deconstruction transition of Au(110) at $T_D = 649\,K$, namely $\beta = 0.13 \pm 0.02$, $\gamma = 1.75 \pm 0.10$, $\nu = 093 \pm 0.09$ in agreement within the experimental accuracy with the 2D Ising values $\beta = \frac{1}{8}, \gamma = \frac{7}{4}, \nu = 0$.

From the incoherent scattering intensity one can extract other useful information on the structure of the surface, particularly since the maximum of the incoherent part of the reconstruction peak can be shifted at **Q** points away from the reconstruction Bragg point $(\frac{1}{2}0)$. The shift reflects the systematic lateral translation of the top rows as occurs for example between 2x1 domains at opposite side of a step, and has also been seen as signifying "incommensurability" of the surface in presence of these steps [37]. From an analysis of the sign and behaviour of the shift with temperature one can obtain information on the type and concentration of defects, which provides insight into the nature of the disordering process. The shift is dependent on the perpendicular momentum transfer q_z. Surprisingly enough, nobody appears to have calculated, as yet, the detailed behaviour including width and shift of incoherent scattering from a well-defined statistical-mechanical model of the surface. Fenter and Lu [59] describes this shift and width by assuming a Markovian distribution of steps on a 2x1 surface, and considering only the contribution of the top rows to the scattering intensities. They assign a probability γ of meeting a 3x1 step either up or down running along the [001] direction. The surface is formed by 2x1

domains of average size $L = 1/\gamma$, separated by 3x1 steps, infinite along the $[1\bar{1}0]$ direction. The oscillation of the shift of half-integer peaks along the rod obtained by Fenter and Lu is shown in figure 2.1 , along with the full width at half maximum (FWHM) of the integer peaks. The shift at $q_z = 0$ in unit $\frac{2\pi}{a_0}$ is

$$\begin{aligned} \Delta Q &= \frac{(-1)^{n+1}}{2} \tan^{-1} \frac{1}{L-1} \\ &\approx \frac{(-1)^{n+1}}{2} \frac{1}{L} \ , \ L \gg 1 \end{aligned} \tag{2.6}$$

n is the order of reconstruction peak $(n + 1/2\ 0)$. The same analysis holds for 1x1 steps (fig.1.1e) but for the sign of the shift, which is reversed. It is worthwhile to repeat that in this approach the steps are assumed to have a Markovian distribution. Hence by assumption the average size of terraces "even" is equal to the average size of terrace "odd". Clearly this approximation does not apply to scenario (iii), where there are 2x1 domains whose size scales as ξ_{2x1} near T_D and terraces forming extended domain walls with fixed average size width (see fig.1.4a).

Either in scenarios (v) and (iv), the distribution of steps is not expected to be Markovian. However in the deconstructed phases of these scenarios $P_{EO} = 0$ and the two sublattices have the same probability to occupy top positions as occur for a Markovian distribution of steps. If this property is the main requirement for the applicability of formula (2.6), one could exstimate the critical properties of the shift in scenarios (iv) and (v) simply by substituting L in eq. (2.6) with the correlation length ξ_{EO}. ξ_{EO} is expected to control the scaling properties of the terraces size near T_D. In this case one obtains:

$$\begin{aligned} \Delta Q &= \pm \frac{1}{2\xi_{EO}} \\ &\sim t^{\nu_{EO}} \ , \ for \ t \ll 1 \end{aligned} \tag{2.7}$$

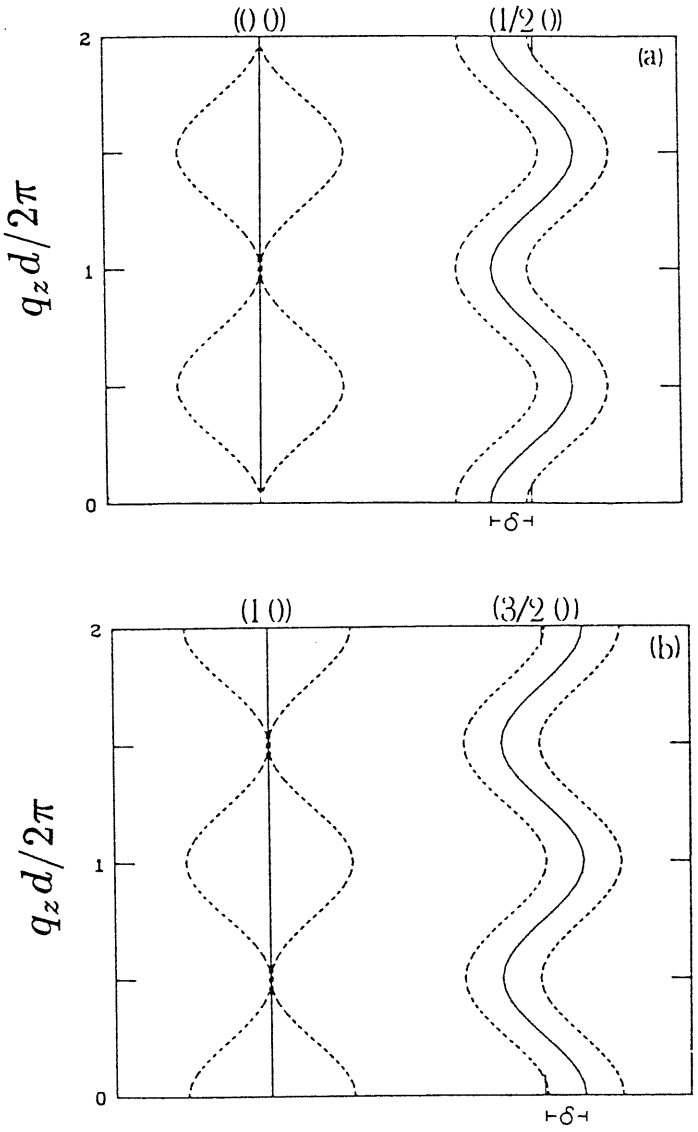

Figure 2.1: A summary of the reciprocal space characteristic for (a) the (00) and $(\frac{1}{2}0)$ peaks, and (b) the (10) and $(\frac{3}{2}0)$ peaks ($\gamma = 0.1$). Solid curves: the Bragg peak positions; dashed curves: the half-intensity positions. The Bragg shift, δ, is shown for $q_z = 0$. The figures are taken from ref. [59].

the sign depending on the order of reconstruction peak and on the type of step considered (1x1 or 3x1). Eq. (2.7) must be considered at best as a heuristic expression for the critical behaviour of the reconstruction peak shift in scenarios (iv) and (v). Its validity is largely questionable although some support to its applicability in presence of steps and domain walls, comes from the calculation of Robinson *et al* [30]. In that situation they still deduce the expression $\Delta \mathbf{Q} = \frac{\gamma}{2}$ for the shift, assuming a Markovian distribution of both steps and compact walls, γ still being the probability of meeting a step (compare to eq.(2.6)). Since the peak width is expected to scale as ξ_{2x1}, the width to shift ratio is assigned by

$$\frac{width}{shift} \sim \frac{\xi_{2x1}}{2\xi_{EO}} \sim t^{\nu_{EO}-\nu_{2x1}} \tag{2.8}$$

ξ_{2x1} is expected to be less than ξ_{EO} if terraces are further deconstructed by compact domains walls (in the model of Fenter and Lu ξ_{2x1} simply coincides with ξ_{EO}).

For scenario (iii) a different behaviour of the shift with temperature is predicted by Villain and Vilfan [32, 33]. They consider an extended domain wall, with uniform thickness l_w (see fig.1.1) and they show that the scattering intensity near the reconstruction peak is the product of the intensity I_0, it would have for vanishing wall thickness, multiplied by a simple function of l_w. Assuming that above T_D, I_0 has the lorentzian shape predicted for the susceptibility of the order parameter, they obtain for $l_w \ll \xi$

$$\Delta \mathbf{Q} \approx \pm \frac{l_w}{2\xi_{2x1}^2} \tag{2.9}$$

the sign has the same meaning as in (2.6). Since l_w is supposed to have a non-critical behaviour in the scenario assumed by Villain and Vilfan, eq. (2.9) is expected to reproduce correctly the dependence of the shift on temperature near T_D although fluctuations in l_w

have been neglected. For $T > T_D$ and l_w nearly constant the shift increases quadratically with $T - T_D$ for an Ising transition in scenarios (i)-(iii). Conversely the shift increases linearly in scenarios (iv) and (v) applying eq. (2.6) , and assigning $\nu_{EO} = 1$ as predicted by Mazzeo *et al* for scenario (iv) and by den Nijs for scenario (v) (see sections 3.4 and 3.6). We remark that for equal concentration of 1x1 and 3x1 defects no shift is predicted. However we notice that the shift is very small near T_D also applying eq. (2.9) with small l_w. In appendix B the lattice gas model for the deconstruction of fcc(110) 2x1 surfaces is presented. It is the first model introduced for the Au(110) surface and can be seen as a description of the deconstruction transition in scenario (i). As a rough estimate of the order of magnitude of the shift, let us consider the results for the reconstruction correlation length within the lattice gas model presented in appendix B, and let us assume that the non universal constant ξ_0^+ in (B.4), takes the Onsager value (B.5) for a square lattice, with the Ising parameters obtained by the calculations of defect with the Voter potential for Au described in appendix C. The corresponding T_D, predicted by the Onsager formula (B.3), is $950\,K$. One obtains for the shift

$$\Delta \mathbf{Q} \approx 0.1676\, t^2 \tag{2.10}$$

and for $t = (T - T_D)/T_D = 0.07$ which is the experimental value for $(T_R - T_D)/T_D$ in Au one obtains

$$\Delta \mathbf{Q} \approx 8.5\, 10^{-4} \tag{2.11}$$

which is indeed very small, compared for example to the shift observed on Pt (see fig.2.2).

From the preceding discussion we recognize that the sign of the shift can discriminate

between the presence of 1x1 and 3x1 defect and the dependence of the half-integer peak shift with temperature above T_D can discriminate between scenarios (i)-(iii) and scenarios (iv)-(v).

However a stronger evidence that deconstruction and roughening are distinct transitions, comes from the analysis of the integer peaks, which can also assign the universality class of the roughening transition. The width of integer peaks is sensitive mainly to step concentration. Its oscillation along the q_z rod in the model of Fenter and Lu [59] is shown in fig.2.1. The width increases by increasing the step density γ previously introduced, and assumes the maximum value in bulk forbidden points. The proliferation of steps both in scenarios (v) and (iv) is thus expected to induce a noticeable broadening of the bulk forbidden integer peaks. Conversely finite domain walls in scenarios (i)-(iii) do not influence the integer peaks width near T_D, where the average width of walls is much less than the size of domains. In atom scattering the coherent part of integer peaks vanishes at T_R [5, 60, 61]. The incoherent part of the principal peaks have a power law shape above T_R for a logarithmically divergent height-height correlation function [5, 60, 61],

$$I(Q_x\,,\,Q_y) \sim (a_x^2\,\tilde{Q}_x^2 + \frac{a_y^2\tilde{Q}_y^2}{g})^{-1+\frac{\tau(q_z,T)}{2}} \tag{2.12}$$

where $\tilde{\mathbf{Q}} = \mathbf{Q}-\mathbf{G}$, $\mathbf{G}$ being a reciprocal lattice principal point. At the superlattice point the power law divergence is suppressed by interference between the shadowing factors in (2.2) [5]. The exponent τ is a function of temperature T and of perpendicular momentum transfer q_z and g is an anisotropy parameter. Theory predicts that for a KT transition $\tau(\pi/d, T_R) = 1$, d being the lattice spacing along [110]. This result is commonly used to locate T_R from scattering data, through the fitting of the power law tails of the peak shape [7, 26]. (At the same time the success of the fitting confirms the KT nature of

the roughening transition.) A KT roughening transition has been detected through the aforementioned lineshape analysis in Pb(110) [62] and Au(110) [26]. Previous analogous results for Ag(110) [8] has been subsequently questioned by Vlieg *et al* [9] who detected the cohexistence of a flat (110) extended region and a slightly inclined rough region, gradually replacing the (110) facet.

We propose that the behaviour of the specular peak in antiphase can be used to discriminate between the two different structures of the deconstructed surface previously discussed, and eventually to detect the critical temperature T_{EO}. Including only the contribution of the top rows in the scattering intensities (2.1), it is straightforward to show that the coherent part of the specular peaks in antiphase is proportional to P_{EO}^2. By taking the shadowing factor (2.2), more appropriate for atom scattering, the same result holds under the additional assumption that the contribution to the scattering intensities of atoms on the boundaries between reconstructed domains can be neglected. We expect that this assumption is quite reasonable if ξ_{2x1} is sufficiently large; anyway a discontinuous increase of the width of the specular peak in antiphase is expected at T_{EO}.

From the simultaneous analysis of the integer and half-integer peaks it is thus possible to discriminate between the different scenarios proposed:

(i)-(iii): the half integer Bragg peaks vanish at T_D, formula (2.9) holds for the shift. Above T_D the specular peak in antiphase still has a δ-function term since P_{EO} is finite. If $T_{EO} \neq T_R$ one expect that above T_{EO} this δ-function term disappears, while the incoherent part is still finite and a large increase of the peak width is expected. At T_R the incoherent scattering intensity diverges as a power law as $\mathbf{Q} \to (00)$, along with all the other principal peaks. Conversely if $T_{EO} = T_R$ the δ-function term in the antiphase specular peak remains finite until $T = T_R$, where the peak shape becomes a power law (incoherent).

(iv): the coherent part of both reconstruction peak and of the antiphase specular peak

vanish at $T_D = T_{EO}$. A noticeable broadening of the specular peak is expected at T_D, but only at T_R the incoherent part of the peak diverges as a power law. Formula (2.7) for the shift of half-integer peaks still holds.

(v): the coherent part of both reconstruction and specular peak in antiphase vanishes at $T_D = T_{EO} = T_R$ as occurs in scenario (iv). The lineshapes of the integer peaks are controlled by the critical properties of the height-height correlation function which were not been provided for scenario (v) by the theoretical models studied up to now. Should the height-height correlation diverge logarithmically one could discriminate between scenario (v) and (iv) through the analysis of power law tails of integer peaks; otherwise one could still discriminate between roughening and the deconstruction-"preroughening" of scenario (iv) observing that in a rough surface the δ component of the specular peak vanishes also for $q_z \neq \frac{\pi}{d}$, while at preroughening it vanishes only for $q_z = 0$.

Critical exponents β, γ, ν for P_{2x1} and ν_{EO}, if relation (2.7) holds, can be obtained from the analysis of half integer peaks lineshape.

We now review the experimental data on Au and Pt following the interpretation scheme illustrated in this section and the possible scenarios previously introduced.

Pt(110). Robinson *et al* [30] measure the behaviour of the reconstruction peak in X-ray scattering. Their results is summarized in fig.2.2. The shift, half-width and intensity of the peak (0.06,0.06,3/2) are shown. The peak shape has been fitted by a lorentzian both above and below T_D, against the prescription previously discussed for the analysis of the reconstruction peak at the critical temperature. Within this fitting procedure they obtain the "critical exponents" $\beta = 0.11$, and $\nu = 0.92$. The shift and half-width both increase linearly with temperature above T_D, and their ratio is around 2.3 and independent of temperature. The experimental results on Pt(110) are consistent with scenario (v) assuming that both P_{EO} and P_{2x1} behave as Ising variables (or at least that

$\nu_{2x1} = \nu_{EO} = 1$!) and that eq. (2.7) for the shift applies. This point of view has been adopted by den Nijs [39] (see section 3.3). The value 2.3 for the width to shift ratio should imply a further deconstruction of terraces due to domain walls (see eq. (2.8)). We propose instead that the experimental data by Robinson *et al* can be explained also assuming a transition to the deconstructed flat phase described in scenario (iv). As a matter of fact the linear increase of the shift and of the width with temperature can be accounted for also by a proliferation of steps in a DOF with $\nu_{2x1} = \nu_{EO} = 1$. Unfortunately experimental analysis on integer peaks, necessary to discriminate between scenario (v) and (iv), are not available. Very recently however, He-scattering evidence [67] has been found, indicating that in reality $T_D \sim 1130K$, $T_R \sim 1180K$, consistent with scenario (iv) as well as with (i)-(iii).

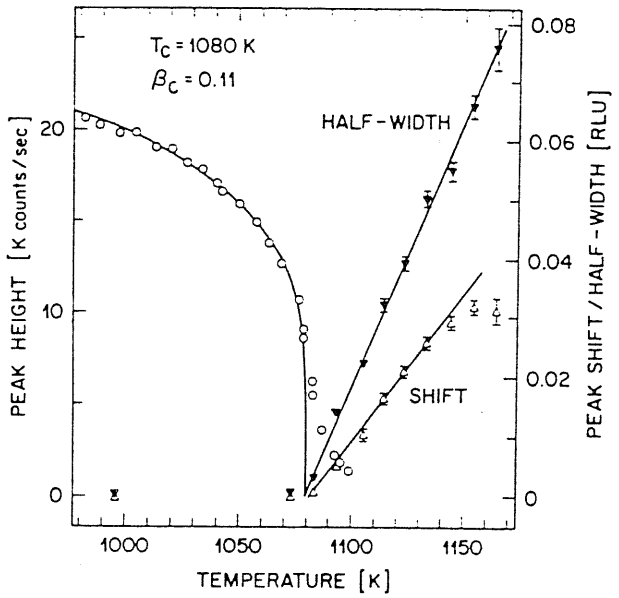

Figure 2.2: Intensity of the half-integer peak, shift of the maximum and half-width as a function of temperature for the Pt(110)(2x1). The figure is taken from ref. [30].

Au(110). We have already mentioned the results of Campuzano *et al* [24] who assign a deconstruction transition at $T_D = 650K$ with Ising exponents. Keane *et al*'s [25] X-ray scattering results show that above 735 K the (0.06,0.06,3/2) peak broaden significantly and exhibits a sharp drop in intensity, however at a temperature as high as 748 K its position is still unchanged. The shape of integer peaks $(0.06, 0.06, 1)$ and $(0.7\pi/d, 0.7\pi/d, 0)$ do not change below 752 K and by 784 K the widths have broadened significantly and the half-integer peak has shifted by $9.8\,10^{-3}\,\frac{2\pi}{a_0}$. The sign of the shift is consistent with the appearance of 3x1 steps. A detailed analysis of the temperature dependence of the shift is not provided. They assign $T_D = 735$ K and $T_R \geq 784$ K, and obtain the critical exponent $\beta = 0.114, \gamma = 1.45, \nu = 0.75$.

Sprosser *et al* [26] report results from He-scattering, as summarized in figure 2.3. They locate T_D at 650 K and a KT roughening at 690 K through fitting of the power law tails of the antiphase specular peak with eq. (2.12). No shift of the reconstruction peak is mentioned.

Cvetko *et al* [27] study the behaviour of reconstruction, specular and superlattice peaks near antiphase condition, also with He-scattering. The reconstruction peaks drops and show a sudden broadening in a narrow temperature range near 700 K. The temperature dependence of the width is consistent a 2D Ising universality class, and they obtained $T_D = 700K$ by a linear extrapolation to zero of the peak width, as a function of temperature. No shift increase is observed above T_D. The specular peak begins to broaden only at 725 K, but at this temperature the tails are not yet consistent with the power law behaviour expected for a rough phase, indicating that roughening will appear at higher temperature.

Van den Riet *et al* [28] observes, 120 K below T_D, an anomaly in ion scattering intensities on Au(110). The authors interpret their data as an indication of the proliferation of single vacancies in the $[1\bar{1}0]$ rows at 520 K, and the onset of surface steps around 650

K. However the proliferation of single vacancies should show up in atom scattering as a diminuished intensity of specular peak in antiphase condition. In the presence of vacancies in the top rows, the second layer becomes more visible to atom beam, and since they scatter in antiphase with respect to the top rows for specular peak near $q_z = \frac{\pi}{d}$, one expect a decrease in peak intensity. To our knowledge the data available on atom scattering [27, 26] do not appear to support the observation of Van den Riet *et al*, and the possible presence of top row vacancies remains controversial.

The apparent inconsistency between T_D reported by different authors may be attributed to finite size of 2x1 terraces and different preparation conditions [63], and perhaps also to small concentration of impurities, like Sn. Previous LEED study found that 0.002 monolayer of Sn on Au(110) resulted in a downward shift of 10 K of the deconstruction transition [64].

Summarizing the results on Au(110), one concludes that $T_R - T_D \approx 40K$, the deconstruction transition is Ising-like and the roughening transition is presumably KT. Perhaps at a third temperature T' around 120 K below T_D, single vacancies in the top rows or some other localized defects proliferate. Scenario (v) is excluded. From the sign of the shift of reconstruction peak above T_R, detected by Keane *et al*, one excludes the predominance of 1x1 steps. The roughening transition is driven by 3x1 steps, and so scenario (iii) with 1x1 extended domain walls at T_D which unbind at T_R is also ruled out. The negligible role of 1x1 step is also confirmed by their low concentration with respect to the abundance of 3x1 steps at low temperature as shown by STM measurements [65, 66]. As shown by the rough calculation leading to (2.10), domain walls with small width are expected to produce a small shift of the reconstruction peaks. Hence, either the proliferation at T_D of 1x1 compact, or 3x1 domain walls with small width l_W seem compatible with experimental results on the shift. Scenario (iv) is at first not excluded for Au(110) by the absence of

a relevant shift in half integer peaks (it could be explained also within the DOF phase invoking small chirality), but is independently ruled out by the absence of broadening of the antiphase specular peak , quite clear at T_D in fig.2.3. In our opinion the possibility that the third phase transition between deconstruction and roughening could take place on Au(110) is not ruled out by available experimental data. A more stringent search for a δ-function term in the integer peaks is necessary to locate T_{EO}.

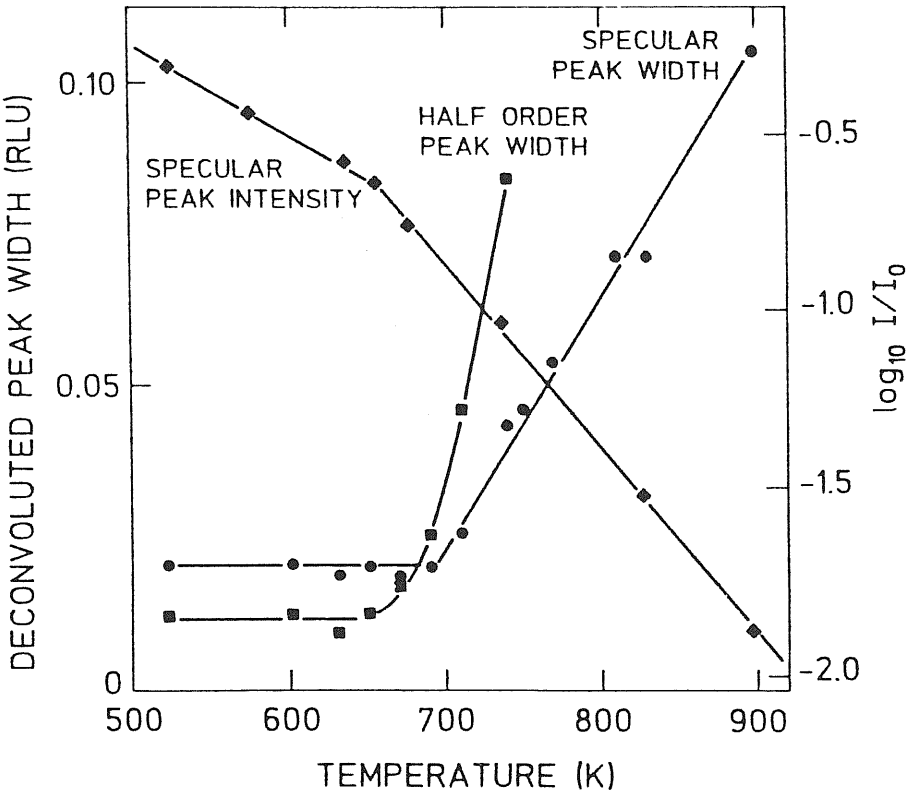

Figure 2.3: Au(110): Intensity of in-phase specular peak (diamonds); width of antiphase specular peak (circles); width of half-order peak (squares). The figure is taken from ref. [26].

Summarizing, from experimental data one argues that scenarios (i)-(iii) with a proliferation of 3x1 steps at roughening are good candidates for Au(110), while scenarios (iv)

seems a better candidate for Pt, although (i)-(ii) are also possible, according to the last experimental results by Kern [67]. The analysis of the shift (not available to us) should discriminate between scenarios (iv) and (i)-(iii) in the recent experimental results by Kern [67].

3 Statistical mechanics models

In this chapter we briefly review the statistical mechanical models introduced to describe scenarios (i)-(v), and we try to analyse which factors favour one disordering mechanism which respect to the others. The description of the lattice gas model which applies only to the deconstruction transition in scenario (i) is postponed in appendix B. Firstly we review the main ideas of the work by Rommelse and den Nijs which introduces the concept of disordered flat phase.

3.1 The preroughening transition of Rommelse and den Nijs

In scenario (iv) the deconstructed phase is flat on average although it contains a disordered array of steps. Rommelse and den Nijs [40, 42, 43] introduced the concept of disordered flat phase (DOF) and studied the conditions for stability of such a phase within a simple model for the sc(100) surface. They show that the DOF is a novel type of phase appearing between the flat and rough phase in presence of short range interactions between steps. As the temperature increases, first the step free energy vanishes at the preroughening transition, leading from the flat ordered into the DOF phase. Next the surface undergoes a KT transition from the DOF phase into the rough disordered phase.

They consider a restricted solid-on-solid model (RSOS) describing the sc(100) surface

and the following hamiltonian:

$$\frac{H}{k_B T} = K \sum_{<\mathbf{R}\mathbf{R}'>} \delta(|h(\mathbf{R}) - h(\mathbf{R}')| - 1) + L_2 \sum_{(\mathbf{R}\mathbf{R}')} \delta(|h(\mathbf{R}) - h(\mathbf{R}')| - 2) \quad (3.1)$$

where $< \mathbf{R}\mathbf{R}' >$ denotes nearest neighbours, and $(\mathbf{R}\mathbf{R}')$ next nearest neighbours on the square lattice. K and L_2 are in units of $k_B T$. The nearest neighbors interaction K contributes to the step energy. Next nearest neighbours interactions (L_2) may cross more than one step. In particular, $L_2 > 0$ produces a short range repulsion between parallel steps. Consider first the extreme limit where the repulsion is infinitely strong, $L_2 \to \infty$. Steps with parallel arrows are forbidden to approach each other closer than the interaction range, while steps with antiparallel arrows are not affected by L_2, and may approach each other at will. Consequently the steps have larger meander entropy in configurations where they alternate in an up-down array, than in configurations where neighbouring steps have the same sign. This argument shows that the long range up-down-up order of steps, producing the disordered flat phase, is favoured by a combination of meander entropy and short range interaction between steps. This argument is indeed very general and not restricted to the particular choice of the model hamiltonian (3.1), but it does not tell whether the effect is strong enough to stabilize the disordered flat phase.

As discussed in chapter 2, a stronger statistical mechanical argument is obtained by considering a six vertex model on the irregular lattice formed by the steps. Assign an Ising spin $\sigma_{\mathbf{R}} = \exp(i\pi h_{\mathbf{R}})$ to each column height, representing its parity. Den Nijs shows that the RSOS model can be rewritten as an Ising model coupled with the 6V model. In this formulation the partition function reads:

$$Z = \sum_{\{\sigma_{\mathbf{R}}\}} exp[-\frac{1}{2} K \sum_{<\mathbf{R},\mathbf{R}'>} (\sigma_{\mathbf{R}}\sigma_{\mathbf{R}'} + 1)] Z_{6V}(\{\sigma_{\mathbf{R}}\}, L_2) \quad (3.2)$$

K governs the Ising-type order, i.e. the structure of the annealed fluctuating lattice

of steps. L_2 governs the antiferromagnetic order of arrows on the lattice of steps. The Boltzmann weight is e^{-L_2} for vertices 1-4, and 1 for vertices 5-6. The phase diagram is shown in fig.3.1. It has been obtained numerically by den Nijs who studied the properties of suitable defined interface free energies that we will discuss later on. First let us analyse the structure of the phase diagram. For $K \to -\infty$ the Ising spin are antiferromagnetically ordered and the model reduces to the exact solvable BCSOS model on the square lattice. The BCSOS flat sector in fig. 3.1, obtained for large L_2 and negative K, represents the reconstructed phase of the model, since the Ising spins remains antiferromagnetically ordered for $K \ll 0$. Starting from this state, the system undergoes a KT roughening to a reconstructed rough phase along the line M-B.

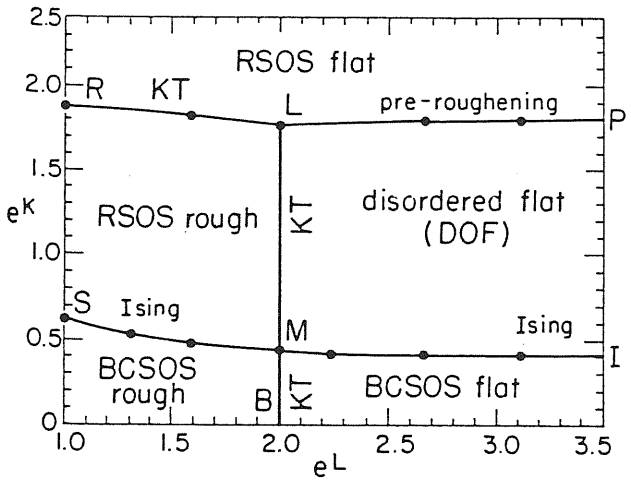

Figure 3.1: Phase diagram of hamiltonian (3.1). The figure is taken from ref. [42].

If we now increase K gradually, the Ising spins disorder along the Ising critical line S-M-I, corresponding to the deconstruction transition. (Note that the point (1,1) on this diagram corresponds to $T \to \infty$). For $K \approx 0$ the Ising spins are disordered, even at low temperature, and Ising-Bloch walls (steps) form a disordered array. This state contains

disconnected finite terraces, but always includes an infinitely large connected backbone cluster, necessary to destroy long range ferromagnetic order of spins. The backbone is not rigid, but it has annealed fluctuations in its shape and number of bonds. The 6V model defined on the backbone is controlled by L_2, and its stiffness for large L_2 is solely responsible for the long range up-down-up order of steps (antiferromagnetic order of arrows). This flat phase at large values of L_2 represents the DOF phase. On the other hand, the rough phase of the 6V at small values of L_2 represents the conventional rough phase of the RSOS. Since in general the universality class of a phase transition does not depend critically on the shape of the underlying lattice, one may expect that the six vertex model on the backbone undergoes a conventional KT roughening (line L-M). The density of steps in the backbone is expected to decrease approaching the line R-L-P from above and the backbone disintegrates on line R-L-P. Above, only finite terraces survive, restoring the long range ferromagnetic Ising order of the RSOS flat phase. Along the line R-L-P the single step free energy vanishes as required for the appearance of the backbone (for finite step free energy only finite terraces can be present; the infinitely long steps of the backbone would cost an infinite free energy). Along the preroughening line L-P, where the ratio L_2/K is sufficiently large, the surface is still smooth on average, because the height fluctuations are limited by the AF order of arrows in the backbone. Conversely if L_2/K is small, i.e. the energy for the generation of a step is large compared to the vertex energies, the 6V model is already in its rough phase when the backbone appears. So along the line R-L the system undergoes a conventional KT transition from the RSOS flat to the RSOS rough phase. The different phases in fig.3.1 are characterized by different order parameters: the Ising magnetization $\rho =< \exp(i\pi h_{\mathbf{R}}) >$, the staggered magnetization $\rho_s =< \exp(i\pi(h_{\mathbf{R}} + x + y) >$ and the order parameter ψ, measuring the AF arrows order in the backbone. $\psi =< e^{i\pi h_{\mathbf{R}}}(h_{\mathbf{R}} - h_{\mathbf{R}'}) >$, $\mathbf{R}'$ being a nearest neighbor to site $\mathbf{R}$ on the

square lattice. ρ is nonzero only in the RSOS flat phase, ρ_s is nonzero only in the BCSOS rough and flat phases, ψ is nonzero only in the BCSOS flat and DOF phases. The physical significance of ρ_s is that of a reconstruction order parameter. The significance of ρ is that of a sublattice or parity order parameter, and is identical to P_{EO}. The parameter ψ is more elusive and has not clear correspondence with others discussed so far. The critical lines in fig.3.1 corresponds to the vanishing of the different order parameters and can be located numerically by the finite-size scaling behaviour of interface free energies $\eta^{\pm}(a)$. $\eta^{\pm}(a)$ are defined as the difference in free energy of semi-infinite strips of width N with periodic boundary conditions and boundary conditions $h_{x,y} = \pm h_{x+N,y} + a$.

den Nijs and Rommelse decompose the $\eta's$ as follows:

$$\begin{aligned}
\eta^{+}(1) &= \eta_s^{+}(1) + \eta_I^{F} \pm \eta_I^{AF} \\
\eta^{+}(2) &= \eta_s^{+}(2) + \eta_I^{F}(2) \\
\eta^{-}(1) &= \eta_s^{-}(0) + \eta_I^{F} \pm \eta_I^{AF} \\
\eta^{-}(0) &= \eta_s^{-}(1)
\end{aligned} \tag{3.3}$$

with + (-) for even (odd) values of N. η_I^F is the free energy of one Ising-Bloch wall (step) and is finite in the RSOS flat phase and zero everywhere else. It is the only contribution to the step free energy in the absence of the backbone cluster; it vanishes along the line R-L-P. η_I^{AF} is the free energy of a string of ferromagnetic bonds in the AF ordered Ising phase, it is finite in the BCSOS flat and rough phase and zero everywhere else; it vanishes along the line S-M-I. The $\eta_s^{\pm}(a)$ are associated with the presence of the 6V model on the infinite backbone cluster, it represents the additional free energy due to the presence of "wrong" vertices on the backbone, induced by the additional step imposed by the boundary condition. It is nonzero only when the backbone exists in its smooth phase, i.e. in the BCSOS flat and DOF phases (except for $\eta_s^{-}(0)$ which is zero everywhere).

$\eta_s^{\pm}(a)$ vanishes at the roughening of the 6V model, but also on the preroughening line where the backbone disappears. So at the preroughening temperature T_{PR}, $\eta_I^F = 0$ and the step free energy $\eta^+(1)$ vanishes; above T_{PR}, $\eta^+(1)$ increases due to a finite value of $\eta_s^+(1)$ and it vanishes again at T_R. den Nijs and Rommelse show numerically that $\eta^+(1)$ indeed increases above T_{PR} along the line P-I in figure 3.1 in the limit $L_2 \to \infty$ (see fig. 11b in ref. [29]). $\eta_s^+(1)$ will have a maximum between T_{PR} and T_R, it is produced by the presence of two competing effects: by increasing the temperature above T_{PR}, the average lattice constant of the backbone decreases (the backbone net thickens), implying an increase in the density of "wrong" vertices induced by an additional step. On the other hand by increasing T, the free energy $\eta_s^+(1)$ of the 6V interface decreases on a lattice with fixed average density, due to the usual contribution of the meander entropy. The competition between the two effects produces the maximum in the step free energy. The preroughening line has been identified numerically as the threshold where η_I^F vanishes and $\eta_s^{\pm}(a)$ becomes finite. Hence, Rommelse and den Njis [29] provide a proof of the existence of the preroughening transition by showing that $\eta^-(1)$ vanishes, approaching T_{PR} from below and at the same time $\eta^-(0) = \eta_s^-(1)$ vanishes, approaching T_{PR} from above. We remark that the 6V model defined on the backbone does not have a critical point at the PR transition. Criticality at preroughening comes from the temperature dependence of the average lattice constant of the backbone a_b; it is expected to diverge at T_{PR} with a critical exponent deducible from the behaviour of $\eta_s^+(1)$. As a matter of fact near T_{PR} we can neglect the temperature dependence of the meander contribution to $\eta_s^+(1)$; $\eta_s^+(1)$ is roughly proportional to the number of wrong vertices per unit length, induced by the additional step, i.e. $\eta_s^+(1) \sim \frac{1}{a_b}$.

In subsequent work, den Nijs also showed that the inclusion of an hard-core attraction between antiparallel steps of the form $L_1 \sum_{<\mathbf{R},\mathbf{R}'>} \delta(|h_{\mathbf{R}} - h_{\mathbf{R}'}| - 1)$ modifies the phase

diagram of fig. 3.1: by taking for example $L = L_1 = \frac{L_2}{4}$, for large L the lines L-P and M-I merge in a line corresponding to a first order transition from the RSOS flat phase to reconstructed flat phase. The resulting phase diagram is shown in fig.3.2.

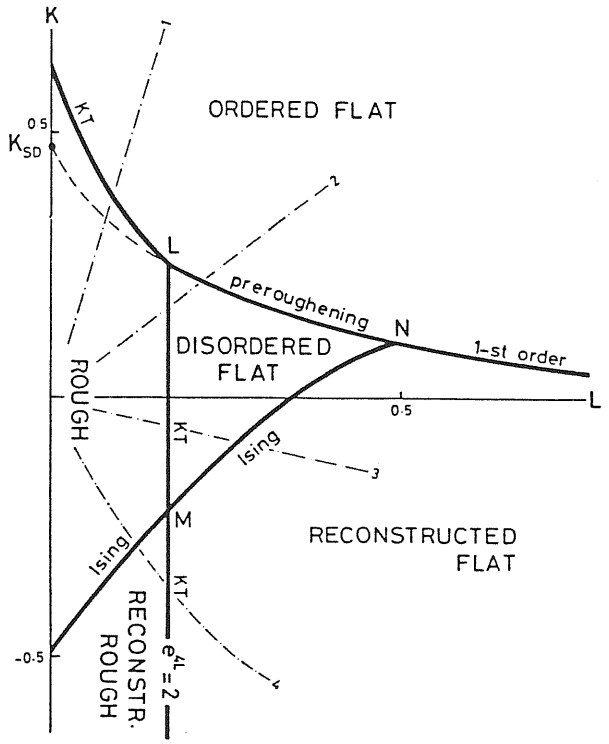

Figure 3.2: Phase diagram of hamiltonian (3.1), with attraction between antiparallel steps (see text). The dashed line is the $u_2 = 0$ line. The dash-dotted lines represent characteristic experimental paths. The figure is taken from ref. [43].

den Nijs and Rommelse showed numerically [29] that the critical exponents at point P along the PR line in fig.3.1 (in the limit $L_2 \to \infty$) do not belong to the KT universality class. This result suggest that the preroughening line has continuously varying critical exponents. In a successive paper den Nijs [43] confirm this expectation by studying a continuous version of a modified sine-Gordon model expressed by:

$$H = \int d\mathbf{r} \frac{1}{2} K_g (\nabla \phi_{\mathbf{r}})^2 - u_2 \cos 2\pi\phi_{\mathbf{r}} - u_4 \cos 4\pi\phi_{\mathbf{r}} \tag{3.4}$$

$\phi_{\mathbf{r}}$ represents the local average height. The hamiltonian (3.4) without the u_4 term is the usual interpolation between the SOS models and the Gaussian model [23]. $u_2 > 0$ favours integer heights, while $u_2 < 0$ and $u_4 > 0$ favour half integer heights. The average height is shifted by 1/2 in the DOF phase with respect to the flat phase, so the additional u_4 term introduces the possibility of a preroughening transition. On the preroughening line $u_2 = 0$. Renormalization group analysis of hamiltonian (3.4) provides a line of fixed points with $u_2 = 0$ and varying K_g (see fig.3.2). The critical exponents are shown to change along the critical line, due to the variation of K_g (see ref. [43] for further details).

Finally we mention that den Nijs and Rommelse proposed that the preroughening transition can be detected by scattering experiments. They showed that the coherent part of the specular peak in antiphase is expected to vanish in the DOF phase, while the incoherent part has a Lorentian shape and diverges as a power law at the roughening transition. We remark that up to now no sharp experimental evidence of a preroughening transition has been provided.

3.2 Application to the fcc(110) surfaces

Let us now try to apply these concepts in detail to an fcc(110) surface. There is an important difference between the sc(100) considered by den Nijs and the fcc(110). In the phase diagram of fig.3.2, which applies to sc(100), the order parameter ρ, vanishing at the preroughening, is zero in the reconstructed phase, so at deconstruction only the vanishing of ρ_s is required. Conversely in the fcc(110) surfaces the order parameter vanishing at T_{PR} is P_{EO} (eq.(1.2)) which is nonzero in the MR 2x1 phase. So, if we contemplate a deconstruction transition where P_{EO} is finite (scenarios (i)-(iii)), another phase boundary

must separate the DOF phase from the deconstructed phase, in a diagram of the type depicted in fig.3.2. Hence either the phase diagram should be richer than that, or simply P_{EO} should also vanish together with P_{2x1} at the deconstruction temperature. In the latter case the deconstruction should be of the type described in scenario (iv), i.e. produced by a proliferation of the unbounded monoatomic steps of the reconstructed phase and not by the proliferation of compact domain walls, as instead happens on the Ising critical line in the sc(100) phase diagram (fig.3.1). A numerical study of an hamiltonian for the fcc(110) surface seems necessary to elucidate this point.

Levi and Touzani [36] mapped the fcc(110) surface on a 6V model with additional repulsive interactions between adjacent vertices. The ground state is the MR phase or the 1x1 phase, depending on the strength of the vertex-vertex interaction. The presence of a reconstructed phase at nearby higher energy than the ground state suggest that the model should display a preroughening transition. The authors searches only for roughening, and detected a KT roughening transition , through the finite-size scaling analysis of an estimator of the step free energy. T_R is located by the change in sign of this estimator. This procedure is known to produce a correct value of T_R for a KT roughening, but may be unable to signal the vanishing of the step free energy at an isolated temperature , as should find at the preroughening transition. Mazzeo *et al* [44] have recently studied an anisotropic BCSOS hamiltonian with an additional interaction, which should play the role of the parameter L_2 in eq. (3.1). Further work is necessary to map out the full phase diagram of this latter model; in section 3.6 we will discuss the results obtained so far.

3.3 The models of Villain and Vilfan

Scenarios (i) and (ii) have been studied by Villain and Vilfan [31, 33]. They calculate the free energy of steps and walls, not by solving the bulk problem defined by the differ-

ent boundary conditions shown in figure 1.2, but just by considering the configurational entropy of the (one dimensional) interface. This procedure was discussed previously by E.Muller-Hartmann and Zittartz [68]; they show that for the 2D Ising model the interface free energy obtained from the solution of the bulk problem is equal to the free energy obtained by summing over all the configurations of the interface, supposed to traverse all the sample without bending backwards (i.e. overhangs are forbidden). This approximation is assumed by Villain and Vilfan to produce a correct evaluation of the critical temperature also for system different from the 2D Ising model. In this procedure step-step interaction is neglected. The transition temperature can be obtained as the temperature above which the free energy of the interface vanishes. The infinite defects in figure 1.1 are ground state configurations of the interface, which at finite temperature is interrupted by kinks. The interface jumps to neighboring atomic rows through intermediate excited states. Figure 3.3 a,b and 3.3 c,d describe a possible configuration with intermediate excited states for a 3x1 compact wall and a 3x1 step respectively. Villain and Vilfan assign an energy W_0 to the breaking of a bond along $[1\bar{1}0]$ (W_0 is equal to the parameter v_1 of Ising hamilatonian (B.2) in appendix B. As we will see in appendix C, total energy calculations with phenomenological many body potentials, produces a value for W_0 much greater that the energy per particle of the defects in fig.1.1. Since direct transition between ground state in neighboring rows requires the simultaneous breaking of several bonds along $[1\bar{1}0]$, their contribution to the partition function of the interface is neglected by Villain and Vilfan. Using a saddle point approximation for the interface partition function, they obtain the following expression for the critical temperatures, as a function of the defects energy in figure 1.1:

Deconstruction transition due to 1x1 compact wall:

$$k_B T_{D_1} = \frac{1}{2}\sqrt{\delta\delta'}\, exp(\frac{W_0}{k_B T_{D_1}}) \tag{3.5}$$

Roughening due to 1x1 step:

$$k_B T_{R_1} = \frac{1}{2}\sqrt{\gamma'\varepsilon'}\, exp(\frac{W_0}{k_B T_{R_1}}) \tag{3.6}$$

Deconstruction due to 3x1 wall, assuming $\delta = \delta'$, $\eta = \eta'$:

$$k_B T_{D_3} = \eta(\sqrt{1 + \frac{\delta}{\eta}} - 1)\, exp(\frac{W_0}{k_B T_{D_3}}) \tag{3.7}$$

Roughening due to 3x1 step:

$$k_B T_{R_3} = \frac{1}{2}\sqrt{\gamma\varepsilon}\, exp(\frac{W_0}{k_B T_{R_3}}) \tag{3.8}$$

The subscripts over T_D, and T_R assign the kind of defect involved. By letting $\frac{\delta}{\eta} \to 0$, in formula (3.7) one recovers formula (3.5), so (3.7) holds for all values of chirality. From the comparison of expressions (3.5)-(3.7), one notes that T_D can be lower than T_R even if the energy of a compact domain wall is equal or higher than twice the energy of a step. This occurs, provided that the intermediate excited states for the meandering of a step have energy sufficiently higher than the intermediate excited states of the domain wall. We remark also that there are two channels for the jump of the 3x1 domain wall as depicted in fig.3.3b. This double possibility increases the meander entropy of the 3x1 domain wall with respect to the 3x1 step. Only the lowest temperature amongst the set deduced from (3.5)-(3.7), makes really sense: the condition $T_{D_1} < T_{D_3}$ and $T_{D_1} < T_{R_3}, T_{R_1}$ indicates the occurring of a deconstruction transition driven by 1x1 wall, an anaguously the condition $T_{D_3} < T_{D_1}$ and $T_{D_3} < T_{R_3}, T_{R_1}$ indicates a deconstruction transition driven by 3x1 compact defect.

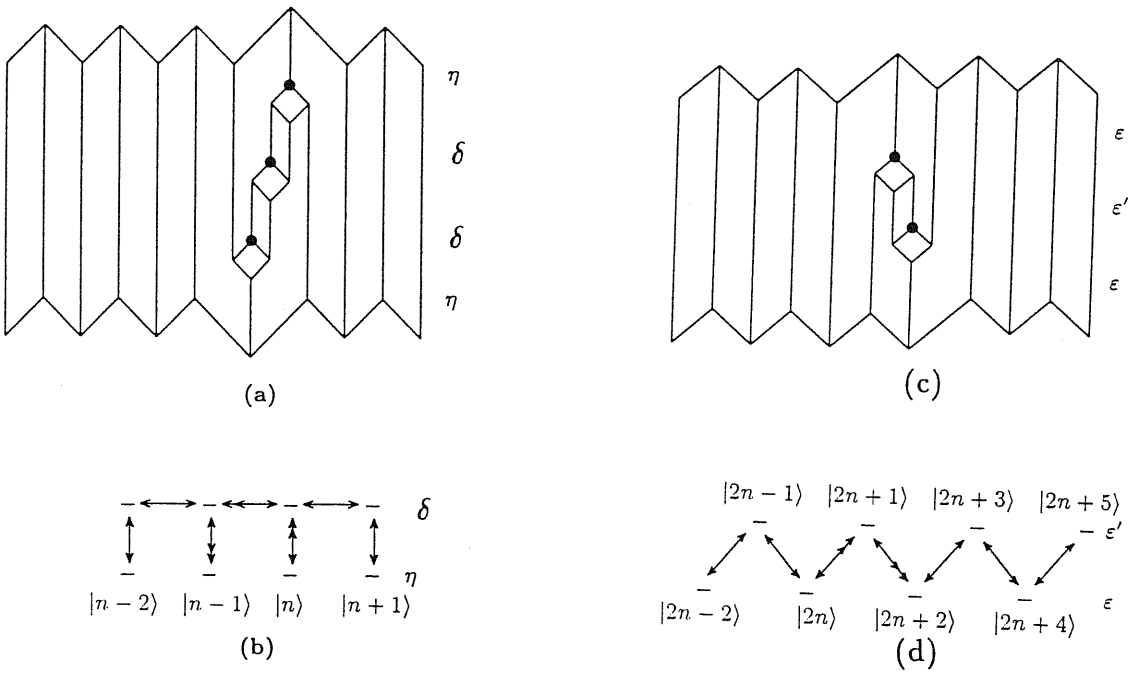

Figure 3.3: (a) Top view of the surface with a typical kink of the 3x1 compact wall. Circles represent broken bonds along $[1\bar{1}0]$. (b) Energy level of the domain wall. Possible transitions between different wall positions are shown by arrows. Double arrows describe the process shown in (a). (c) Top view of the surface with a typical kink in the 3x1 step. (c) The same as in (b) for the 3x1 step. Greek letters denote the energies of the states, as in fig.1.1. These figures are taken from ref. [34].

Vilfan and Villain [33] also analysed scenario (iii) for 3x1 extended domain wall. They calculate the partition function of a system composed by two 3x1 steps with opposite sign. Each step is assumed to traverse the surface in the x direction without bending backwards. The pair is described for each value of x by the state $|m,n>$, where m and n are the steps coordinates; the "motion' of the pair in the x direction is described within the transfer matrix formalism. The transfer matrix is then an operator on the states $|m,n>$, and its elements are expressed as a function of the energies of defects in figure 1.1. The eigenvectors of the transfer matrix are expressed on the basis as $\sum_{n,m} c_{n,m}|m,n>$. The bound state is considered stable if the eigenvector corresponding to the maximum eigenvalue has coefficients on the basis $|n,m>$ of type $c_{n,m} \sim exp(-\alpha|n-m|)$. By increasing the temperature there are two effects. On the one hand, a bound pair of steps becomes unstable at a certain temperature where the largest eigenvalue corresponds to a couple of unbound steps. On the other hand the wall free energy decreases by increasing temperature and could vanish before the unbinding of the pair. In the latter case an Ising deconstruction transition is expected before the roughening transition identified with the unbinding of the steps. As in the former analysis of compact domain walls, the free energy of an interface strongly depends on the energies of the intermediate excited states necessary for the meandering. The condition for the occurrence of an Ising deconstruction transition before roughening is thus a complicate algebraic expression involving most of the energies parameters in fig.1.1. The binding of the steps is not due to long range interactions, since there is only short range interaction ($\eta \leq 2\varepsilon$ in figure 1.1). However the larger meander entropy of the compact 3x1 domain wall with respect to the 3x1 step, which favours the crossing of the two steps, gives rise to an effective long-range entropic attraction. The phase diagram proposed by Villain and Vilfan [33] is depicted in fig.3.4 for two possible choices of the energies of intermediate excited states . The separation between T_D and

T_R widens by decreasing the energy of a 3x1 compact domain wall with respect to the 3x1 step, but still T_D can be lower than T_R even if $\eta = 2\varepsilon$, due to different energies of the intermediate excited states for the meandering of a wall and a step. In other words antiparallel steps can be bound even if there is no energetic attraction between them (pure entropic attraction). In the analysis by Villain and Vilfan the condition $T_D \leq T_{EO} = T_R$ is assumed.

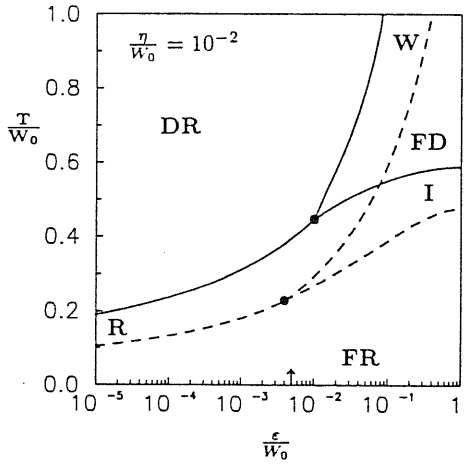

Figure 3.4: Phase diagram of the striped model of Villain and Vilfan [34]. Solid lines are for $\varepsilon' = \delta = \infty$, and dashed lines are for $\varepsilon' = 2\varepsilon, \delta = 3\varepsilon'/2$. R, I and W are the roughening , Ising, and wetting (roughening) critical lines, respectively. The arrow indicate the case $\varepsilon = \eta/2$. The figure is taken from ref. [34].

The model is not able to tell what happens when l_w, increasing monotonically above T_D, starts to compete with the reconstruction correlation length. Furthermore the analysis of the critical behaviour at roughening is beyond the scope of the model. However an important message which comes out from the investigation of Villain and Vilfan is that, by tuning the energy of intermediate excited states, it should be possible to move from a scenario where two phase transition are predicted to a scenario where only the roughening

transition survives.

3.4 The four-state clock step model of den Nijs

An alternative model for the deconstruction and roughening described in scenarios (i)-(iii) has been recently proposed by den Nijs [39, 40]. It contemplates also a possible description of scenario (v), i.e. of a simultaneous deconstruction and roughening, but still with critical behaviour of the reconstruction order parameter in the 2D Ising universality class. Instead of considering hamiltonians, e.g. an SOS model, den Nijs prefers a "coarse grained" description of the system. He defines a rectangular lattice oriented along the grooves of the missing rows; its lattice constant is large compared to the MR unit cell, but small compared to the reconstruction correlation length. He associates to each unit cell on the lattice a height and a four-state variable $\theta = 0, \pm 1/2\pi, \pi$ which describes the phase of the order parameter $< \rho_{\mathbf{Q}} >$, in the four degenerate ground states. The boundary between the unit cells can be a wall or a step, depending on the value of $d\theta$. He introduces a hamiltonian with interactions between cells, assigning an energy to the boundary along [001] which represents steps and wall energies, and energies to the boundaries along $[1\bar{1}0]$ which represent kink energies. We remark that in this model the wall has zero size on the coarse grained scale, being the boundary between adjacent cells. He considers the following partition function:

$$\begin{aligned} Z &= \sum_{\{\theta_{n,m}\}} \exp(\sum_{n,m}[K_m \cos(\theta_{n,m} - \theta_{n,m+1} - \Delta) + Q_m \cos(2\theta_{n,m} - 2\theta_{n,m+1}) \\ & K_n \cos(\theta_{n,m} - \theta_{n+1,m}) + Q_n \cos(2\theta_{n,m} - 2\theta_{n+1,m})] Z_{6V}(\{d\theta = \pm\frac{1}{2}\pi\}, L). \end{aligned} \quad (3.9)$$

This is a four-state clock model, where K_m, Q_m and Δ assign steps and wall energies. Δ represents the chirality, i.e. the energy difference between 1x1 and 3x1 steps. K_n and

Q_n represent the energies of the kinks. Every configuration of the θ variables is weighted by a six vertex (6V) model which includes the height degrees of freedom. The 6V arrows represent the change in height at the steps. The vertices are defined on the annealed fluctuating lattice, formed by the $d\theta = \pm\frac{1}{2}$ boundaries of the clock model (similar as in the DOF). We remark that a couple of parallel and antiparallel steps have the same configuration of θs, and so the same energy in the clock model. Only step-step hard-core interaction, assigned by the 6V model, is sensitive to the additional height degrees of freedom. L in (3.9) represent the parameter of the six vertex model, favoring up-down-up step order.

The model is quite complex, and up to now only the simplest case has been examined via the analysis of interface free energies, in finite-size transfer matrix framework. Let us call $\eta(d\theta, dh)$ the free energy of the interface introduced through the boundary condition $d\theta$ and dh along [001]. The vanishing of $\eta(\pi, 0)$ indicates the disappearance of long range reconstruction order, while the the vanishing of $\eta(0, 2)$ indicates surface roughening. One can then simplify the model, assuming zero chirality, isotropic interactions between cells along $[1\bar{1}0]$ and [001], and neglect step-step interactions (L=0). Only two parameters survive: the wall energy E_w and the step energy E_s. The phase diagram as determined by den Nijs is shown in fig.3.5.

For $E_w < 2E_s$ there is an Ising deconstruction transition followed by a KT roughening transition, while for $E_w > 2E_s$ the deconstruction and roughening lines merge together. The universality class of the transitions is assigned by the universal finite-size scaling amplitude of interface free energy: den Nijs finds $N\eta(\pi, 0) = \frac{\pi}{4}$ which is characteristic of the 2D Ising deconstruction, and $N\eta(0, 2) = \pi$ corresponding to a KT roughening, N being the stripe size. For $E_w < 2E_s$ one finds $T_D < T_{EO} = T_R$. The wall width can not widen above T_D, since it has zero dimension. Surprisingly, this finite-size scaling behaviour of

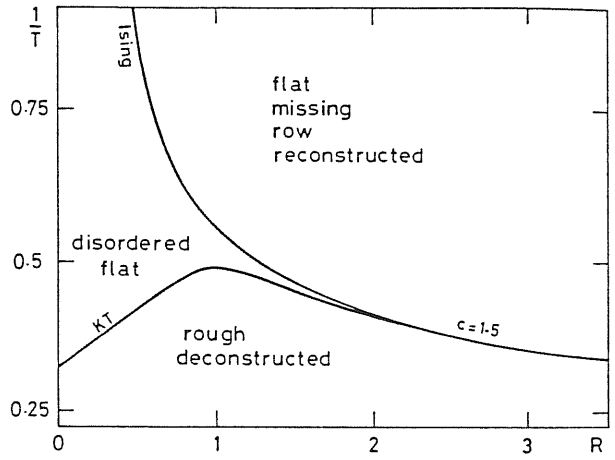

Figure 3.5: Phase diagram of the four-state chiral clock-step model with $R = E_w/E_s$, and temperature T in units of E_s. The figure is taken from ref. [39].

the interface free energy of steps and walls still hold along the critical line of simultaneous deconstruction and roughening in fig.3.5.

When $E_w > 2E_s$ the $\eta(\pi, 0)$ interface is reasonably composed by a couple of independent steps in the simplified model analysed numerically. Neglecting step-step interaction (as the model does) the chemical potentials of a couple of parallel or antiparallel steps is expected to vanish simultaneously. This should explain naively why the critical line $\eta(\pi, 0) = 0$ and $\eta(0, 2) = 0$ merge for $E_w > 2E_s$. Moreover power law fit of the temperature derivative $d(N\eta)/dT \sim N^{\frac{1}{\nu}}$ gives $\nu_{EO} = \nu_{2x1} = 1$ at simultaneous deconstruction and roughening. den Nijs provides some evidences that a small, but finite chirality does not change the critical properties.(see ref. [39] for more details). Hence, the experimental data on Pt(110) by Robinson *et al* [30] can be consistent with a simultaneous deconstruction and roughening. Information on height-height correlation function are not available from the numerical results presented. This information is necessary to predict the behaviour of

integer peaks at roughening.

The phase diagram of den Nijs (fig.3.5) and of Villain and Vilfan (fig.3.4) are indeed very similar. The position of the multicritical point N, occurring at $E_W = 2E_S$ in fig.3.5, is actually dependent on the energies of intermediate excited states for the meandering of walls and steps, as shown in section 3.3. This effect should be recovered in the general model (3.9) of den Nijs, by introducing the anisotropy of the surface, i.e. $Q_n \neq Q_m$ and $K_n \neq K_m$ in (3.9).

den Nijs does not discuss the role of the P_{EO} order parameter. The deconstructed phase in fig.3.5 is actually a DEF phase; all the observations concerning the critical line assigned by the condition $< P_{EO} >= 0$, presented in section 3.2, still apply to the phase diagram of the 4-state clock-step model. Furthermore den Nijs does not analyse the role of vertex energies in the phase diagram of the four-state clok-step model. Following the arguments by Rommelse and den Nijs [42], we predict that, for a sufficiently large value of L in (3.9), the KT line could split into a preroughening line, where P_{EO} vanishes, plus a true roughening line, corresponding to the roughening of the six vertex model in (3.9). Assigned a value to L , there is a maximum value of E_s above which the DOF is no more stable.

So, by fixing L and E_w such that the multicritical point where the roughening and preroughening lines merge lies below R=2, a qualitative phase diagram of the model could be described by fig3.6. By decreasing E_s in fig. 3.6 (E_w fixed) the system moves from the scenario $T_D < T_{EO} = T_R$ to the scenario $T_D < T_{EO} < T_R$ where T_{EO} corresponds to a transition from the the deconstructed phase of the pictures (i)-(iii) to the DOF of scenario (iv). By decreasing further E_s the scenario $T_D = T_{EO} < T_R$ is realized. Concluding, we suggest that the model by den Nijs with $L \neq 0$ can be used to analyse the properties of the phase transition between DEF and DOF proposed in chapter 1.

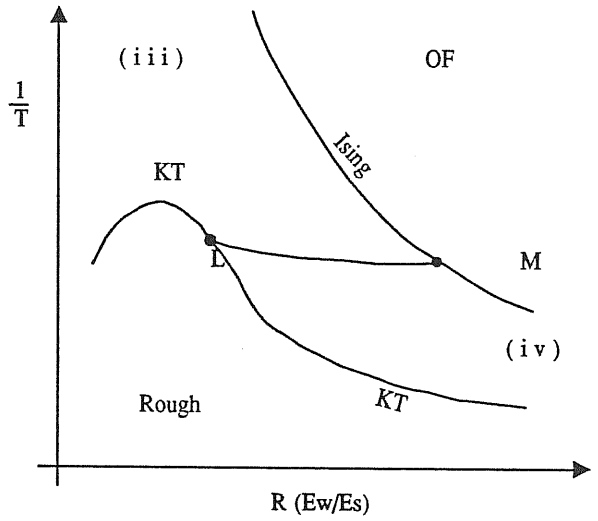

Figure 3.6: Tentative phase diagram for the model producing the phase diagram in fig.3.5, with an additional step-step interaction L. E_w and L are fixed to suitable values (see text). OF, R, (iv) and (iii) represent, respectively, the MR flat, the rough, the DOF of scenario (iv) and the deconstructed phase of scenarios (i)-(iii). L-M is the critical line where T_{EO} vanishes.

3.5 The strong chirality limit and the global phase diagram

In the previous section results for the zero chirality limit of the model hamiltonian (3.9) have been presented. On the opposite limit of infinite chirality the problem can be mapped onto a system of quantum fermions in one dimension, as firstly pointed out by Villain and vilfan [34, 35]. In this section we present the results obtained from this mapping by Villain and Vilfan [34, 35] and recently by Balents and Kardar [41]; finally the global phase diagram for all values of chirality, as recently proposed by den Njis [45] is sketched.

In the limit of strong chirality only one type of step is considered. As already discussed, in the 2x1 surface overhangs and hence simple closed terraces are forbidden, while more complex islands as in fig.1.3 c-d are possible. Neglecting finite terraces, we are led to a model of lines oscillating along the $[1\bar{1}0]$ without overhangs, and crossing the whole sample from the bottom to the top. There are two types of lines, corresponding to up and down steps. Villain and Vilfan [34, 35] assumed that lines of the same sign cannot cross, while lines of opposite sign can cross with some crossing energy c, which can be positive, negative or zero. For $c < 0$ a pair of steps forms a bound state at $T = 0$. The situation is analogous to the models for commensurate-incommensurate transitions (CIT) [70, 71, 72, 73], the only essential difference being the number of species allowed for each line. The statistical mechanics of directed lines in two dimension can be mapped into the quantum mechanics of fermions in one dimension, as discussed by [70, 71, 72, 73]. Since in our case there are two type of steps, the fermions are spin-1/2 particles. The mapping can be sketched as follows. Consider a rectangular array of N_y rows of N_x sites each, y being along $[1\bar{1}0]$ and x along [001]; the partition function of the system with q steps up and p steps down is $Z(q,p) = Tr\Theta_{qp}^{N_y}$, where $\Theta_{qp}^{N_y}$ is the transfer matrix acting on the orthonormal vectors

$|x_{1\uparrow}\, x_{1\downarrow}\, x_{2\uparrow}\, x_{2\downarrow} \ldots . x_{q\uparrow}\, x_{p\downarrow} >$. $x_{i\uparrow}$ is the position along x of the i-th step up. Calling μ_o

the energy per atomic spacing along y of a step and γ_o the energy of a kink, it is easy to show that in the limit $\beta\gamma_o \gg 1$ the following relations hold [73, 71, 35]:

$$\Theta \simeq e^{-\beta H} \tag{3.10}$$

where

$$\begin{aligned} H &= -\beta^{-1} e^{-\beta\gamma_o} \sum_{i\sigma} (c^+_{i+1,\sigma} c_{i,\sigma} + c^+_{i-1,\sigma} c_{i,\sigma}) \\ &+ \mu_o \sum_{i\sigma} n_{i,\sigma} + c \sum_{i\sigma} n_{i,\sigma} n_{i,-\sigma} \end{aligned} \tag{3.11}$$

$\sigma = \uparrow, \downarrow$ and $c_{i,\sigma}, c^+_{i,\sigma}, n_{i,\sigma}$ are respectively creation, destruction and number operators of one fermion at site i. The steps are hence associated to the world lines of the fermions. In the limit of $N_y \to \infty$ the free energy per site of the system with q step up and p step down is $f(q,p) = E_o/N_x$, E_o being the ground state energy of hamiltonian (3.11). Then the true free energy of the system and the concentration of steps is obtained by minimizing $f(q,p)$ with respect to the number of steps q and p. The hamiltonian (3.11) describes the one dimensional hubbard model for spin-1/2 particles, which has been exactly solved by Lieb and Wu [74]. For $c = 0$, and $c = \infty$ the solution is straightforward. It has been discussed by Villain and Vilfan [35]: a Pokrovsky-Talapov (PT) roughening transition is expected at temperature T_R assigned by

$\mu_o - 2\beta^{-1} e^{-\beta\gamma_o}$ = free energy of a single step = 0

For $T < T_R$ the density of steps n is zero, while for $T > T_R$ $n \sim |T - T_R|^{\frac{1}{2}}$ and the free energy per site f is $f \sim -|T - T_R|^{\frac{3}{2}}$. Above T_R the surface is rough, but it is a "floating" or "incommensurate" solid with respect to reconstruction order. This means that $< P_{2x1} >= 0$, but the reconstruction correlation function decays as a power law, e.g. [45],

$$G(x,y) =< P_{2x1}(x+x_o, y+y_o)P^*_{2x1}(x_o,y_o) >\sim e^{i\Delta Q x_r - 2x_\theta} \qquad (3.12)$$

where $P_{2x1}(\mathbf{R})$ is the local expression of the order parameter (1.1), as defined in appendix A. The critical exponent x_θ varies continuously inside the rough incommensurate (RI) phase. Comparing (3.12) with the expression for the incoherent scattering (A.5) in appendix A, one recognizes that ΔQ in (3.12) represents the shift of the reconstruction peak. In complete analogy with the CIT one finds that ΔQ is proportional to the step density, and so $\Delta Q \sim |T - T_R|^{\frac{1}{2}}$ for the PT critical behaviour. Very recently Balents and Kardar [41] applied the full power of the fermionic mapping of the problem: they deduced the full phase diagram for all values of the interaction energy c and they studied the stability of the system with respect to the proliferation of the closed islands in fig.1.3c, by including in the model the possibility of a simultaneous annihilation and creation of four fermions with total spin zero. Balents and Kardar discuss the continuum version of hamiltonian (3.11), namely

$$\begin{aligned} H &= \sum_\sigma \int dx \psi^+_\sigma(x)(-\frac{\gamma}{2}\partial_x^2 - \mu)\psi_\sigma(x) \\ &+ c\sum_\sigma \int dx \psi^+_\sigma(x)\psi_\sigma(x)\psi^+_{-\sigma}(x)\psi_{-\sigma}(x) \end{aligned} \qquad (3.13)$$

γ and μ being related to the parameter of hamiltonian (3.11) by $\gamma = 2\beta^{-1}e^{-\beta\gamma_o}$, and $\mu = 2\beta^{-1}e^{-\beta\gamma_o} - \mu_o$. Balents and Kardar solved the continuum version of the Lieb and Wu equations [74] in the limits of strong coupling ($n/c \gg 1$). In the limit of small coupling, where the above procedure is cumbersome, they applied a renormalization group (RG) analysis of hamiltonian (3.13). The phase diagram obtained by the authors, neglecting finite terraces, is depicted in fig.3.7a. The phase diagram boundary reflects only the topology and not the detailed shape of the phase space.

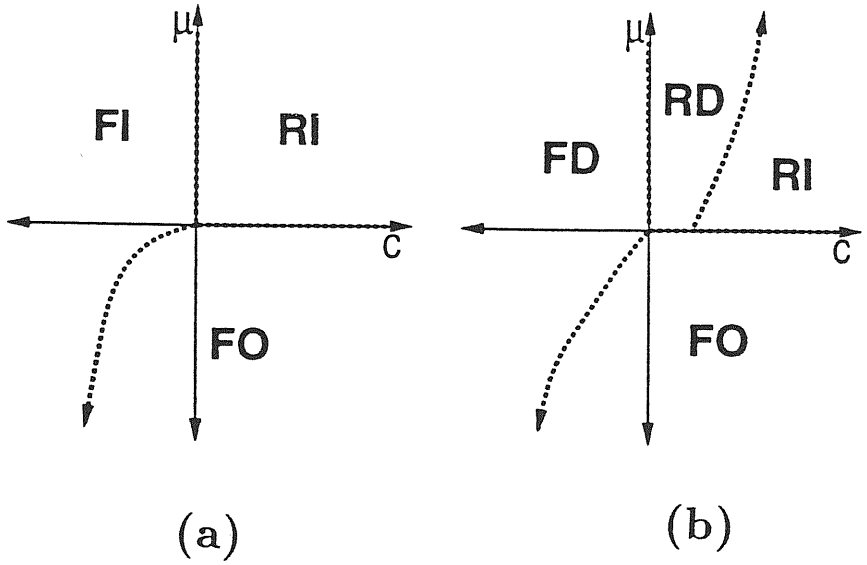

Figure 3.7: Phase diagram of the Hubbard model (3.11) without finite islands (a) and with finite islands (b), as proposed by Balents and Kardar. The figure is taken from ref. [41].

There is a flat ordered (FO) phase in which no steps are present, a flat incommensurate (FI) phase in which up and down steps are bound to form walls, and a rough incommensurate phase (RI). In the FI and RI phases the surface is deconstructed, but the correlation function decays as power law. In the rough phase the height-height correlation function diverges logarithmically, as in the conventional SOS models. The FI-FO and RI-FO transitions are both in the PT universality class, while the RI-FI boundary is an infinite order phase transition, different from the KT universality class. Balents and Kardar showed that choices for the step-step interaction different from the contact interaction in (3.11) can assign a KT universality class to the RI-FI boundary. The PT universality class of the deconstruction and roughening transitions is due to the extreme anisotropy of the system of travelling lines. The introduction of finite islands partly regain the spatial isotropy and can modify the critical behaviour. In fact, Balents and Karkar showed that for $c \leq 0$ the system is unstable with respect to islands formation, while it is stable for large positive c. The instability for $c \leq 0$ is easy to understand: in the regime the fermion lines are paired up into bound states of up and down steps. As this bound states act effectively as single lines the requirement for four fermion lines meeting at a vertex in fig.1.3c reduces to only two bound pairs intersecting. This is a much probable event. The stability for large positive c is also easily understood, as in this case the lines are completely mutually avoiding. The phase diagram proposed by Balents and Kardar, modified by the presence of islands is reported in fig.3.7b. The phase diagram in fig.3.7a still apply to (px1) reconstruction with $p > 2$, since finite islands have been shown to be irrelevant for these systems [41]. For the (2x1) case the FO-FI transition is now replaced in fig.3.7b by a conventional deconstruction transition into a flat disordered phase (FD), where finite islands proliferate and where the reconstruction correlations decay exponentially. The FD is a DEF phase in the language of chapter 1. The proliferation of

finite islands modify the critical behaviour of the deconstruction transition, which is now Ising-like as expected on symmetry ground for a systems of walls, as discussed in chapter 1. Anaguously the FI-RI transition is replaced by a conventional KT roughening into a rough disordered (RD) phase with reconstruction correlation decaying still exponentially. For $c \gg 0$ the surface first undergoes a PT transition into a rough phase with power law reconstruction correlations, and at higher temperature the proliferation of finite terraces induces a transition into the RD phase. In fig.3.7b is shown a boundary between the RD and the simple FO phase. The existence of this boundary should imply the instability of the FO phase with respect to islands formation also for small positive c. Unfortunately this range of values for c is outside the range of applicability of the RG approach with the inclusion of finite terraces. So the existence of the FO-RD transition at infinite chirality is still an open problem. Moreover Balents and Kardar show that if simple loops (fig.1.3b) were permitted the system would be unstable with respect to loop formation for all c. Actually, it is the condition of infinite chirality that has frozen out the possibility for steps to turn backwards. If we decrease the chirality, a step could turn backwards by changing from a 3x1 step to a 1x1 step. Hence for zero chirality the simple closed terraces are fully allowed and the results by Balents and Kardar imply that the PT roughening is fully replaced by a roughening into the RD phase. This is in agreement with the results of the 4-state clock-step model at zero chirality by den Njis.

Very recently den Nijs [45] deduced a phase diagram for the 4-state clock step model at infinite chirality which is essentially equal to fig.3.7b. In the limit of infinite chirality the 4-state clock-step model can be mapped into the fermionic problem previously discussed, including dislocations (i.e. finite islands). den Nijs decouple the fermionic hamiltonian into the sum of two terms, e.g. $H = H_r + H_d$. The phase diagram of each single term H_r and H_d can be deduced and the phase diagram of the full hamiltonian H is described

as the superposition of the phase diagrams of H_r and H_d. The result is equivalent to fig.3.7b, except for the boundary FO-RD which is absent in the phase diagram proposed by den Nijs. The superposition of the two phase diagram in an heuristic procedure and it does not exclude the existence of the boundary FO-RD at infinite chirality proposed by Balents and Kardar. From the topology of the phase diagram at infinite chirality, and from the phase diagram at zero chirality in fig.3.5, den Nijs sketched a global phase diagram for the 4-state chiral clock-step model (3.9). It is reported in fig.3.8: Δ is the chirality, $R = E_w/E_s$ and T is in unit of E_s.

den Nijs distinguishes three paths on the phase diagram. Path 3 in fig.3.8 describes the Ising-like deconstruction transition of scenarios (i)-(iii) and the subsequent KT roughening; the critical properties are not affected by the chirality. Across the line marked as L in fig.3.8 the sequence of phase transitions and their nature change. den Nijs distinguishes between path of type 4a and type 4b; both describe a simultaneous deconstruction and roughening, they correspond to the FO-RI and FO-RD transitions discussed by Balents [41]. The existence at low chirality and the precise location of the critical line L are the major uncertainties in the structure of the phase diagram in fig.3.8. Path 4a corresponds to the simultaneous deconstruction and roughening predicted by the 4-state clock-step model at zero chirality: the correlations of the reconstruction order parameter decay exponentially above $T_D = T_R$ and the shift of the reconstruction peaks is expected to increase above T_R as $\Delta Q \approx |T - T_R|$. Along path 4b, at strong chirality, the surface roughens via a PT type transition leading to an incommensurate solid with respect to the reconstruction order; the reconstruction peaks start to shift at the PT transition as $\Delta Q \approx |T - T_R|^{\frac{1}{2}}$. At higher temperature the reconstruction degrees of freedom melt via a KT transition; the correlation change from power law to exponential and the line shape of reconstruction peaks consequently changes from power law to lorentzian. Scenario (v)

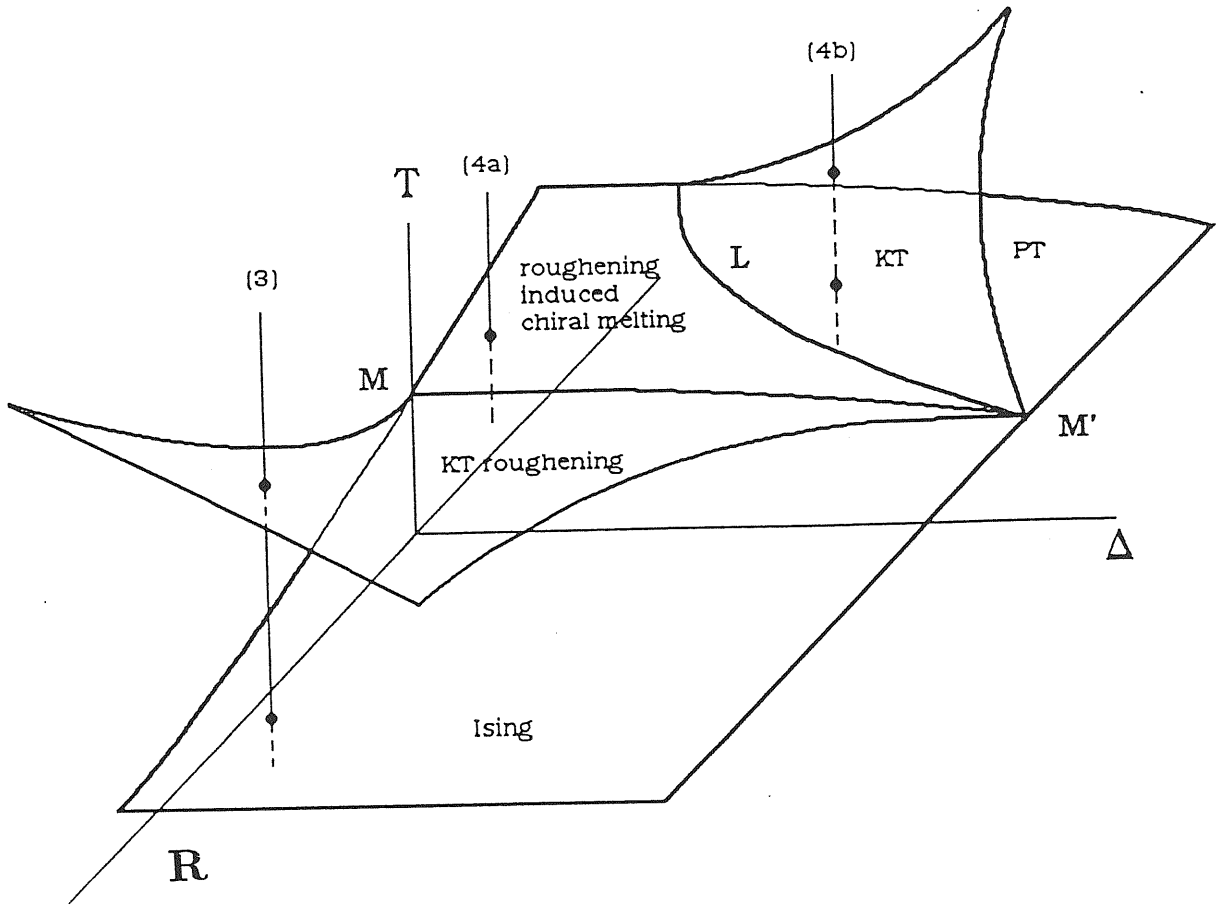

Figure 3.8: Schematic structure of the full phase diagram of the 4-state chiral clock step model, where $R = E_w/E_s$, Δ is the chirality, and the temperature T is measured in unit of the step energy E_s. The figure is taken from ref. [45].

described in chapter 1 can be thus split in two scenarios, say (v) and (v'), corresponding to paths 4a and 4b in fig.3.8.

Still in the global phase diagram in fig.3.8 there is room for the critical line $< P_{EO} >= 0$. This is expected to coincide with the roughening line, if step-step interaction is neglected in hamiltonian (3.9), but in real system (and in the 4-state clock-step model by assuming $L \neq 0$ in (3.9)) the mechanisms discussed in chapter 1 could split the $< P_{EO} >= 0$ line from the roughening one, and stabilize the DOF phase of scenario (iv). The experimental results on Pt(110) by Robinson *et al* [30], indicating a shift of the reconstruction peaks scaling as $\Delta Q \approx |T - T_R|$, is compatible with the condition of strong chirality if the deconstruction transition of scenario (iv) is assumed. Conversely, the previous analysis of fig.3.8 indicates that, by excluding scenario (iv), the results by Robinson *et al* on the shift should imply a small chirality limit, since they are compatible only with path 4a.

Finite terraces have been supposed to play an important role in the stabilization of the DOF of scenario (iv) , as we discussed in chapter 1; moreover they are the key ingredient for the location of the critical line L in fig.3.8. The role of finite terraces has been included only in an approximate way in the works discussed in this section. Its full characterization could come from Monte Carlo simulations of hamiltonian sufficiently rich to include all the mechanism discussed. A first step in this direction has been realized by Mazzeo *et al* [44], as we will discuss in the following section.

3.6 The model of Mazzeo-Jug-Levi-Tosatti

A recent attempt at modeling realistically and studying quantitatively a reconstructive fcc(110) surface has been made by Mazzeo, Jug, Levi and Tosatti (MJLT) [44], following earlier work of Jug e Tosatti [37], and Kohanoff *et al* [38]. Mazzeo *et al* present for the first time a Monte Carlo (MC) study of an SOS hamiltonian which displays both a roughening

and a reconstruction transitions. Their hamiltonian is the following:

$$\begin{aligned} H/J &= \sum_i (h_i - h_{i+\hat{\mathbf{x}}})^2 - K_2 \sum_i (h_i - h_{i+\hat{\mathbf{y}}})^2 \\ &+ \frac{K_3}{2}[\sum_i (h_i - h_{i+\frac{3}{2}\hat{\mathbf{y}}+\frac{1}{2}\hat{\mathbf{x}}})^2 + \sum_i (h_i - h_{i+\frac{3}{2}\hat{\mathbf{y}}-\frac{1}{2}\hat{\mathbf{x}}})^2] \end{aligned} \tag{3.14}$$

As in the BCSOS, the interaction between nearest neighbours is taken to be infinitely strong, imposing the usual six vertex constraint [48]. $\hat{\mathbf{x}}$ and $\hat{\mathbf{y}}$ are the basis vectors of the 1x1 Bravais lattice along $[1\bar{1}0]$ and [001] respectively. i runs over all surface lattice sites. h_i is the height at site i. J and $J\,K_2$ are equivalent to the parameters v_1 and v_2 of hamiltonian (B.2) in appendix B ($v_1 = 4J$, and $v_2 = 4J\,K_2$). In physical terms, large J stabilizes a straight, uninterrupted $[1\bar{1}0]$ top row, large K_2 favours the disappearance of a neighboring row (whence the missing row reconstruction) with formation of a (111) microfacet, and finally large K_3 stops the (111) faceting into simply a 2x1 reconstruction. Therefore $K_2 > 0$ stabilizes the MR phase with respect to the unreconstructed state, and $K_3 > 0$ stabilizes the MR phase with respect to higher order reconstructions. The $T = 0$ phase diagram of the above hamiltonian presents three possible ground states according to the values assumed by the parameter $K = K_2/K_3$. If $K < 0$ the 1x1 structure is stable , if K is in the range $0 < K < 4$ the surface is 2x1 reconstructed, whereas if $K > 4$ the surface facets, with a single (111) slanted face replacing the horizontal (110) state. For $K = -\infty$, ($K_3 = 0$ and $K_2 < 0$) the model is equivalent to the anisotropic six vertex model [5]. In the region of the phase diagram with $K < 0$, the additional interaction $K_3 > 0$ represents a hard core repulsion between parallel 2x1 steps, playing the same role of the parameter L_2 in the hamiltonian (3.1) by Rommelse and den Nijs. Following the general arguments of section 3.1, the unreconstructed surface described by hamiltonian (3.14) should display a preroughening transition for K_3 sufficiently large. MC simulation in this region of the

phase diagram is in progress [69]. No direct attraction between antiparallel steps is present for $K < 0$, so the first order transition line in fig.3.2 should be absent in the phase diagram of hamiltonian (3.14).

The disordering properties of the surface described by this hamiltonian have been fully analysed only in one point of the parameter space. In order to investigate a point representative of the Au(110) surface, Mazzeo *et al* choose the parameters of the hamiltonian (3.14) through a comparison of the surface energies for 1x1(110), 2x1(110), (100), (111) as deduced from model (3.14) with those obtained by MD simulations using the so-called glue model [16] (see appendix C). One obtains $J = 1005.2K$, $K_2 = 0.51$, and $K_2/K_3 = 2.3$. The MC work then yields a deconstruction transition at $T_D = 2.903\,J$ and indicates a 2D Ising critical behaviour from the analysis of the finite-size scaling properties of the specific heat C_v and of the susceptibility χ_{2x1} of the reconstruction order parameter, namely:

$$C_v(N, T_D) = A_1 + A_2 \ln N \tag{3.15}$$

$$\chi_{2x1}(N, T_D) = A_4\, L^{\gamma/\nu} \; with \; \gamma/\nu = 1.8 \pm 0.2 \tag{3.16}$$

the system size being $N \times N$ surface cells. The behaviour of P_{2x1} and ξ_{2x1} are reported respectively in fig.3.9a and 3.9b. The definition of P_{2x1} and P_{EO} adopted by Mazzeo *et al* are slightly different from the definitions (1.1)-(1.2) of chapter 1 [44, 69], but their critical behaviour is the same.

At a temperature around $T_R \approx 1.06 T_D$ a roughening transition is identified from the logarithmic divergence of the height-height correlation function, which has been successfully fitted according to relations (1.4) and (1.5), characteristic of a KT roughening.

While, as MJLT remark, the value of J deduced from surface energies is actually four times larger than the value required to reproduce the critical temperature observed experimentally ($T_D \approx 700K$), this discrepancy on energy scales does not invalidate the informa-

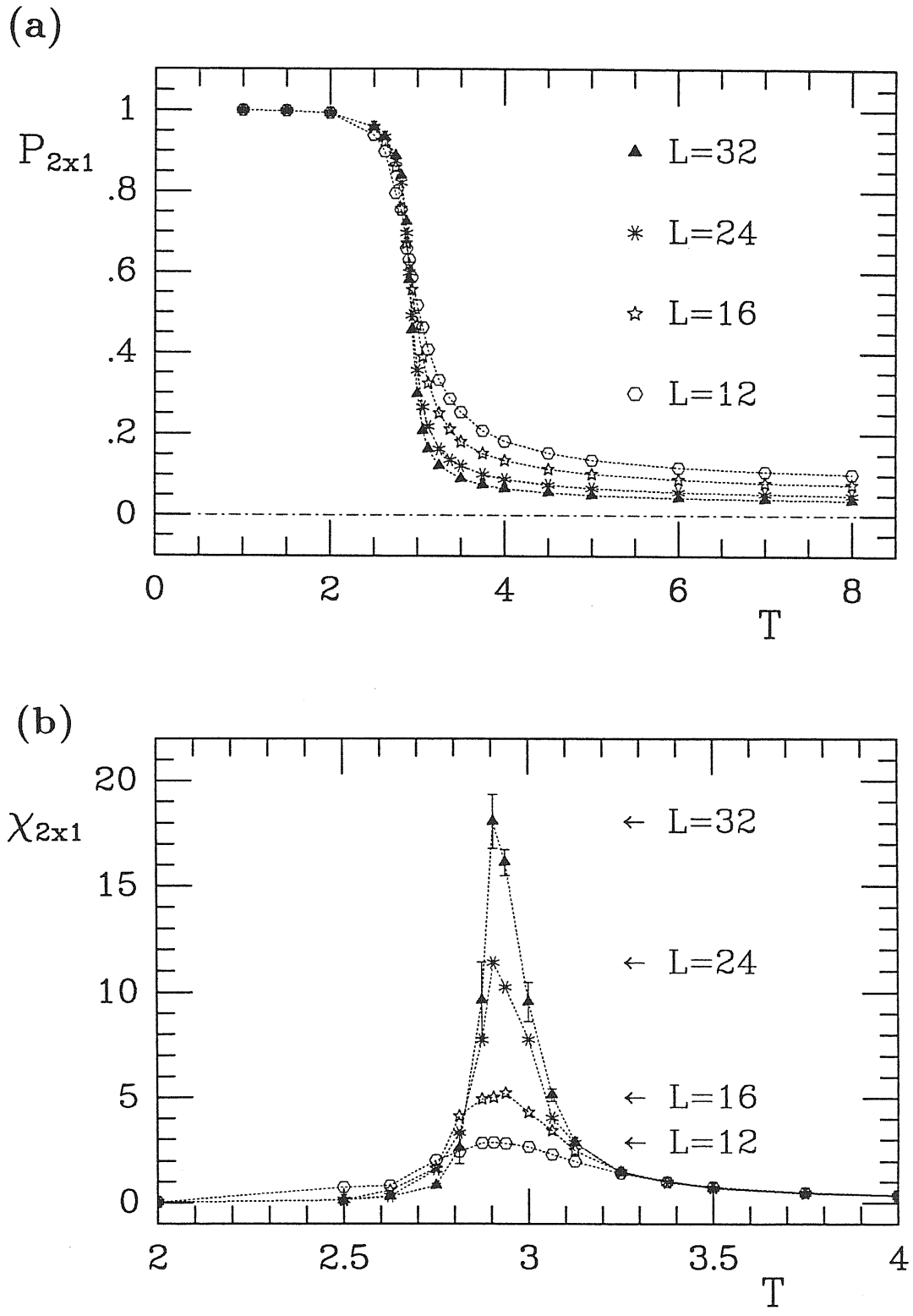

Figure 3.9: (a) Monte Carlo results by Mazzeo *et al* [44] for the order parameter P_{2x1}. The temperature is in unit of J. (b) Results for the susceptibility. The figures are taken from ref. [44].

tion obtained from MC results on the interplay between roughening and deconstruction, and the existence of two distinct transitions: an Ising-like deconstruction transition and a KT roughening.

We now wish to understand which one, amongst the scenarios (i)-(iv) previously discussed, applies to these MC results. Furthermore one may wonder if within the same model it would or not be possible to move from one scenario to another one, by tailoring the parameters of the hamiltonian (3.14) or by introducing new ones. In this respect some indications on the phase diagram of hamiltonian (3.14) can be obtained by inspection of the energies of the defects in figure 1.1. The following relations holds for the energies of the defects in figure 1.1 as deduced from hamiltonian (3.14):

$$\begin{aligned} \delta' &= \delta = 4J\,K_2 \;;\; \eta' = \eta = J(16K_3 - 4K_2) \\ \varepsilon &= \frac{\eta}{2} = \frac{\mu}{2} \;;\; \varepsilon' = \frac{\delta}{2} = \frac{\mu'}{2} \\ \gamma &= \frac{3}{2}\delta \;;\; \omega = \eta \;;\; \gamma' = \frac{5}{2}\delta \end{aligned} \tag{3.17}$$

The energy of the 3x1 wall is 24% lower than the energy of the 1x1 wall with the value of K_2 and K_3 obtained from the glue model for Au. So a condition of small chirality is reasonably fulfilled. From eq. (3.17) one sees that no step-step hamiltonian interactions is present at $T = 0$. The vertex energies associated to the intersection of parallel and antiparallel steps are both zero ($\omega = \eta = 2\varepsilon$). However the 6% temperature gap between deconstruction T_D and roughening T_R is real. In section 3.3 we have seen that two antiparallel steps can be bounded just by a difference in the meander entropy of steps and walls (see fig.3.4). We can not completely exclude that the disordering process detected by Mazzeo *et al* follows scenario (ii)-(iii); however in our opinion the MC results can be better attributed to scenario (iv), mainly for two reasons:

a) Applying the analysis of Villain and Vilfan in section 3.3, with the choice of defects energies assigned by eq. (3.14) with the parameter chosen by Mazzeo *et al*, it turns out that the step free energy vanishes before the vanishing of the free energy of a compact or extended 3x1 wall (formulas (3.7) and (3.8) in section 3.3, and formula (3.8b) in ref [33]). So the models by Villain and Vilfan predict that steps are unbound in the point of the parameter space explored by Mazzeo *et al.*

b) The order parameter P_{EO} independently behaves as P_{2x1}, i.e. it vanishes at T_D. Its susceptibility also has a maximum at T_D, the intensity scaling with the size in an Ising fashion (see fig.3.10) [69].

Neither of the preceding arguments is conclusive: an analysis *á la* Villain and Vilfan is obviously oversimplified, it gives useful indications on the structure of the phase diagram, but probably it cannot locate accurately the positions of the critical lines. For what concerns point b), we observe that, due to finite-size effects, the order parameters in fig.3.10a are not zero at T_D, as defined by the maximum of their susceptibility. By inspection in MC snapshots, one notes that at T_D mainly 3x1 compact walls and 1x1 microregions are present; there are only few small terraces. Large terraces appear at higher temperature, still below T_R, where the reconstruction order parameter is small [69]. Actually also 1x1 microregions reduce the intensity of both the P_{EO}, and the P_{2x1} order parameters; so the peak in χ_{EO} at T_D does not unambiguously prove the existence of the DOF phase of scenario (iv). However we remark that in a scenario where deconstruction is provided by a mixture of compact domain walls and 1x1 microregions, the P_{EO} order parameter can not vanish. Hence, if we consider fig.3.10 as a clear indication that P_{EO} and P_{2x1} should

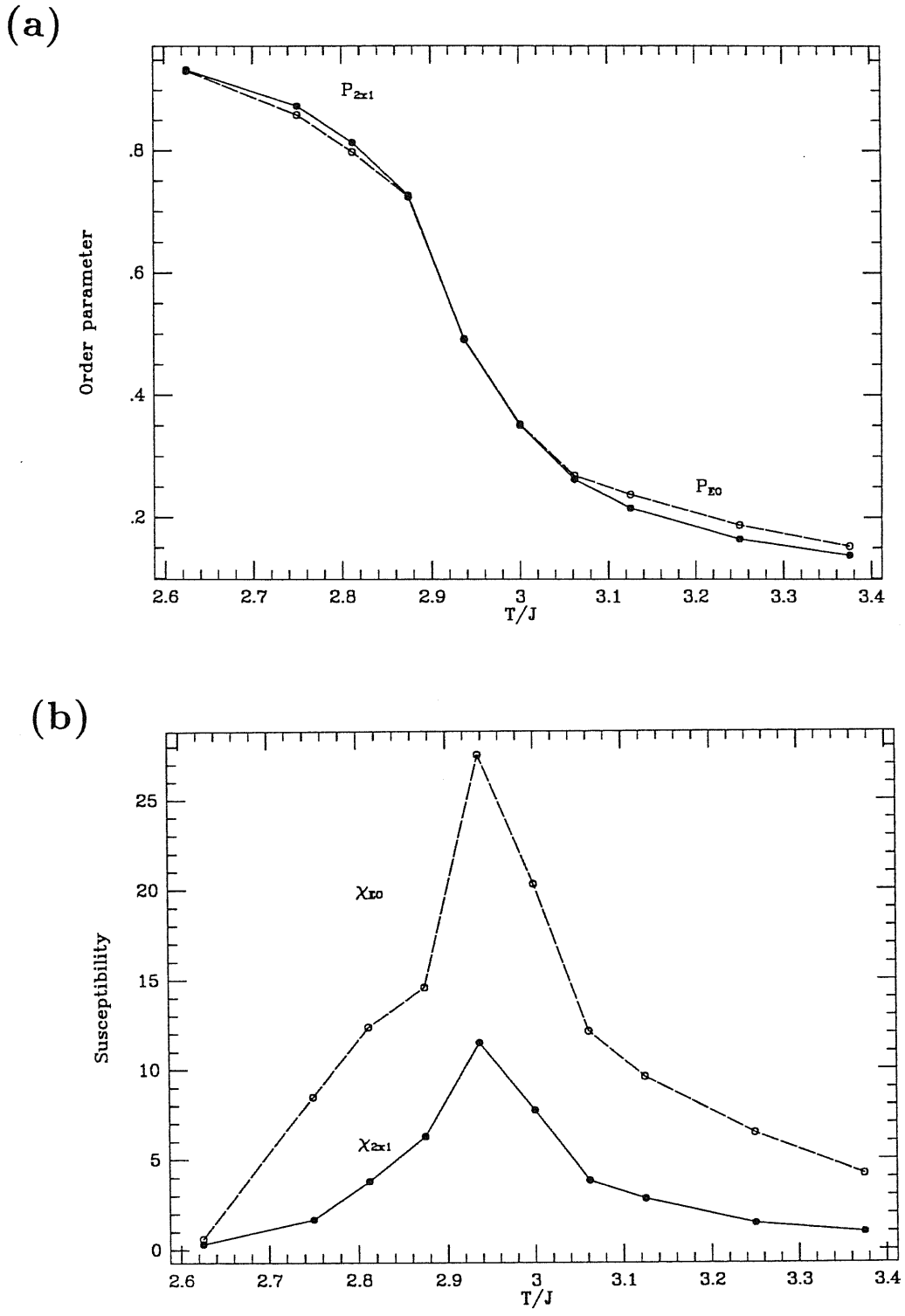

Figure 3.10: (a) Comparison between P_{EO} and P_{2x1} for N=24 in the model by Mazzeo *et al* [69]. (b) the same as in (a) for the susceptibilities.

behave in the same fashion also in the thermodynamics limit, the MC results strongly suggest the presence of the DOF phase: the decostructed phase of scenario (iv) is the only deconstructed flat phase able to destroy the P_{EO} order parameter that we know of so far. We guess that by increasing the system size to values much larger than $N = 32$, the MC snapshots at T_D should evolve towards configurations compatible with the picture of scenario (iv).

A further test on the structure of the deconstructed phase should come from a MC simulation in a point of the parameter space with larger K_2. Larger K_2 means stronger chirality and presumably smaller concentration of 1x1 microregions. In this condition, terraces are the only defects present on the surface which can destroy the P_{EO} order parameter. However an unambiguous evidence of the presence of a DOF phase should come from the analysis of the step free energy. As discussed in chapter 1, the step free energy is expected to vanish at the deconstruction-"preroughening" T_D; it will then increase again above T_D, and vanish again and definitively at T_R (see section 3.1). Such a study, not available for hamiltonian (3.14), either via thermodynamics integration in MC simulation or via transfer matrix formalism, should provide crucial insight into the disordering process of both reconstructed and unreconstructed fcc(110).

As was repeatedly said, according to eq. (3.17), all energetic interaction between steps are absent in the hamiltonian studied by Mazzeo *et al.* Thus the DOF should be stabilized by a lower meander entropy of a 4x1 step with respect to the 3x1 compact wall. This effect favours vertices 5-6 with respect to vertices 1-2; under this conditions vertices 3-4 are unfavored due to the terrace-mediated interaction, as described in chapter 1 (see fig.1.6). The path for the meandering of the 4x1 step is displayed in fig.3.11, along with the energies of intermediate excited states (compare with fig.3.3b). We expect that for a suitable choice of the intermediate excited states the 4x1 step could have lower meander

entropy than the 3x1 wall. Actually we have not proven that this happens for the point chosen by Mazzeo *et al.* In order to support the picture of scenario (iv) for hamiltonian (3.14), it is necessary to compute the free energy of vertex 5 and vertex 1. This will probably be the subject for a future work.

Within the model hamiltonian (3.14), only entropic effects due to different path for the meandering can favour the bonding between antiparallel steps (see section 3.3) or the stabilization of the DOF with respect to the rough phase, if steps are unbound. The entropic effects are controlled by a subtle interplay between the energy of the intermediate excited states and the number of possible path for meandering (see fig.3.3 and 3.11). Hence, it is very hard to speculate what the phase diagram of the hamiltonian studied by Mazzeo *et al* will look like in the plane (K_2, K_3). We propose that the introduction of a step-step energetic interaction provides a better way to explore the different scenarios discussed in chapter 2. A possible choice of the step-step interaction may be provided by the following additional term to hamiltonian (3.14):

$$\begin{aligned} H'/J = \; - \; & \Delta \sum_i [\delta(|h_i - h_{i+\hat{\mathbf{y}}}| - 2)\delta(h_{i+\hat{\mathbf{y}}} - h_{i+2\hat{\mathbf{y}}})\delta(|h_{i+2\hat{\mathbf{y}}} - h_{i+3\hat{\mathbf{y}}}| - 2)] \\ [\; & K_2\delta(h_{i+\frac{1}{2}\hat{\mathbf{x}}+\frac{3}{2}\hat{\mathbf{y}}} - h_{i\frac{3}{2}\hat{\mathbf{x}}+\frac{3}{2}\hat{\mathbf{y}}}) + K_3\delta(|h_{i+\frac{3}{2}\hat{\mathbf{x}}+\frac{3}{2}\hat{\mathbf{y}}} - h_{i\frac{5}{2}\hat{\mathbf{x}}+\frac{3}{2}\hat{\mathbf{y}}}| - 2)] \end{aligned} \quad (3.18)$$

Note the extreme non-two-body nature of this kind of term, unlike all other terms in (3.14). It reflects a rather nonlocal physical requirement. The virtue of this kind of additional term is simply to introduce an additional energy to the compact walls, without modifying the other defects in fig.1.1, namely $E_{wall} = (2 - \Delta)\, E_{step}$ (i.e $\eta = (2 - \Delta)\varepsilon$ and $\eta' = (2 - \Delta)\varepsilon'$).

For $\Delta > 0$ sufficiently large, one expects that domain walls are largely favoured with respect to steps; pairs of antiparallel steps are bound and the deconstruction transition

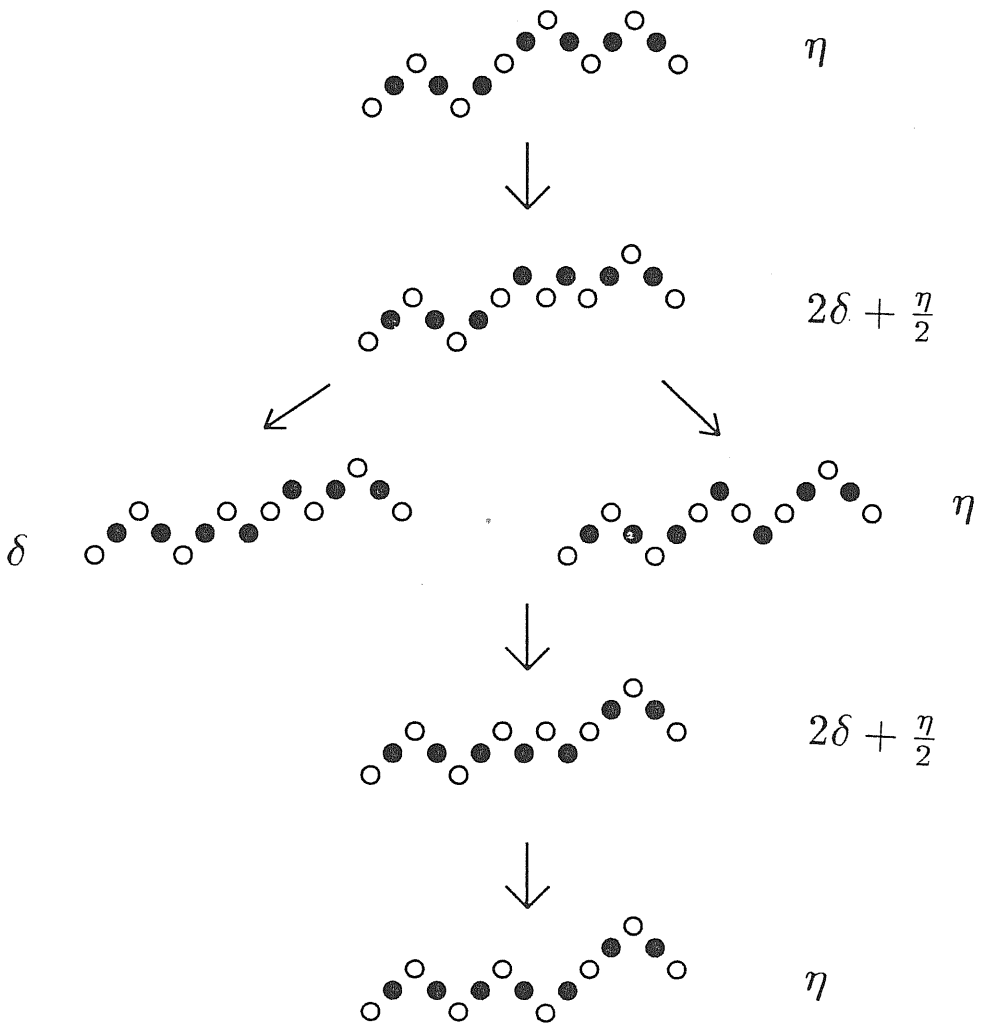

Figure 3.11: Intermediate excited states for the meandering of a 4x1 step.

follows the scenarios (i)-(iii). A positive Δ stabilizes further the DOF phase with respect to roughening, since it unfavours the crossing between parallel steps. Hence we expect that a new scenario $T_D < T_{EO} < T_R$, which was speculated upon in chapter 1, could be realized. Now, the peak of χ_{EO} should correspond to the transition from the deconstructed phase of scenario (i)-(iii) to the DOF of scenario (iv).

Conversely for $\Delta < 0$ antiparallel steps repel each other. For $|\Delta|$ sufficiently large the DOF is unstable and a simultaneous deconstruction and roughening is expected. Thus by tuning just the parameter Δ, one could explore the scenarios $T_D = T_{EO} < T_R$, $T_D < T_{EO} < T_R$ and $T_D = T_{EO} = T_R$, within the framework adopted by Mazzeo *et al*, providing critical exponents and correlation functions.

Conclusions

Many of the existing concepts in the theory of MR deconstruction/roughening are essentially summarized in the global phase diagram in fig. 3.8. The present work represents an endeavor at extending and clarifying further the physical situation, without really attempting any comprehensive review of the earlier contributions. In particular we have discussed the role of the order parameter P_{EO}, not considered up to now in literature for the MR reconstructed surfaces, and its relevance for the analysis of the structure of the deconstructed phase. We have discussed the different ways by which the critical line $< P_{EO} >= 0$ could enrich the phase diagram of fig.3.8, and specifically the possibility of the stabilization of a DOF phase analogous to the disordered flat phase proposed by Rommelse and den Nijs for the sc(100) surface. In conclusion four different deconstructed phase are possible:

(1) the DEF phase, where $< P_{2x1} >= 0$, but $< P_{EO} >\neq 0$ (scenarios (i)-(iii))

(2) the DOF phase, where $< P_{2x1} >=< P_{EO} >= 0$ (scenario (iv))

(3) the rough disordered (RD) phase where $< P_{2x1} >=< P_{EO} >= 0$, and the reconstruction degrees of freedom are melt

(4) the rough incommensurate (RI) phase, where $< P_{2x1} >=< P_{EO} >= 0$ (scenario (v')), but the surface is an incommensurate solid with respect to the reconstruction degrees of freedom (power law correlations).

Since there are two kinds of disordered flat phase (DEF and DOF), we have proposed the possible occurrence of a phase transition from the DEF to the DOF before roughening.

The critical exponents are different for transitions leading to different deconstructed phases; as discussed in chapter 2, they can be detected experimentally from the analysis of the shift and width of the half-integer peaks and from the lineshape of the integer peaks. The possible phase transition DEF $\rightarrow$ DOF could be detected indeed from the analysis of the specular peak in antiphase. We have emphasized the role of finite terraces in the stabilization of the DOF phase, and on the cross-over between the phase transitions leading to the RD and RI phases. A complete analysis of a model which includes exactly the contribution of finite terraces seems necessary to properly locate the critical line L in the global phase diagram in fig.3.8, and to prove the stabilization of the DOF phase in scenario (iv). This should come from Monte Carlo simulation of SOS hamiltonian, sufficiently rich to include all the mechanism discussed. We have proposed that the recent Monte Carlo simulation of the SOS model by Mazzeo *et al* could represent a realization of a deconstruction transition leading to the DOF phase of scenario (iv). A possible enrichment of the hamiltonian by Mazzeo *et al*, which could display the full sequence of phase transitions $T_D < T_{EO} < T_R$ has been presented. The ability of SOS hamiltonians to mimic many-body interactions in metals has been briefly discussed in appendix C.

Concerning the experimental data available on Au(110) and Pt(110), we can conclude that, while for Au(110) all the results suggest the occurrence of scenarios (i)-(iii), the situation is far less clear for Pt(110). The previous results by Robinson *et al* [30] on Pt(110) are consistent with both scenario (iv) and (v), while the more recent results by Kern [67] exclude scenario (v), and can be better explained within scenario (iv), although (i)-(iii) are also possible. The analysis of the shift should be able to discriminate between scenarios (iv) and (i)-(iii) in the latter case.

From both experimental and theoretical sides further work seems necessary to achieve a satisfactory comprehension of the interplay between deconstruction and roughening on fcc(110)(2x1) surface, along the lines that we have tried to summarize in the present contribution.

Appendix A
Scattering intensity and the reconstruction order parameter

In this appendix we show that the coherent part of the reconstruction peak defined in eq. (2.5) is proportional to the square of the average order parameter as defined in (1.1). For sake of simplicity we restrict ourselves to an SOS model, and we take the shadowing factors in (2.1) appropriate for X-rays scattering, i.e. only the top rows contribute to the scattering intensities (see the discussion in chapter 2). We also show that for $\mathbf{Q}$ near the reconstruction points the incoherent part of the scattering, defined as the difference between the total scattering in equation (2.1) and the coherent part, is proportional to the fourier transform of the correlation function of the suitable defined local order parameter. We can define in every 2x1 unit cell $\mathbf{R}$ a local order parameter as follows:

$$P_{\mathbf{R}} = \sum_{\kappa=0}^{3} P_{\mathbf{R},\kappa}, \; and \; P_{\mathbf{R},\kappa} = e^{i\mathbf{G}\,\mathbf{X}(\kappa)}\,\alpha(\mathbf{R}\,\kappa) \tag{A.1}$$

where $\mathbf{G}$ are reconstruction points in the reciprocal space and α is 1 for top rows atoms, and 0 otherwise. κ indexes the four sublattices of the 2x1 phase, and $\mathbf{X}(\kappa)$ is the position of the κ sublattice in the unit cell. We neglect relaxation, and so the dependence of $\mathbf{X}(\kappa)$ on the unit cell index $\mathbf{R}$. Then one recognizes that the reconstruction order parameter $< \rho_{\mathbf{G}} >$ in chapter 1 coincide with the spatial and configurational average of the local order parameter $P_{\mathbf{R}}$. From the expression for the scattering intensities (2.1), and

for $q_z = 0$ one obtains:

$$< I(\mathbf{Q}) >= N \sum_{\mathbf{R}} e^{i\mathbf{Q}\,\mathbf{R}} \sum_{\kappa,\kappa'} e^{i\,(\mathbf{Q}-\mathbf{G})\,(\mathbf{X}(\kappa)-\mathbf{X}(\kappa'))} < \overline{P_{\mathbf{R},\kappa} P^{*}_{\mathbf{0},\kappa'}} > \qquad (A.2)$$

Decoupling the spatial and configurational averages as prescribed in chapter 2 one obtains from equation (A.1) and (A.2)

$$\begin{aligned} < I(\mathbf{Q}) >_{coherent} &= N \sum_{\mathbf{R}} e^{i\,\mathbf{Q}\,\mathbf{R}} \mid \sum_{\kappa} e^{i(\mathbf{Q}-\mathbf{G})\,\mathbf{X}(\kappa)} < \overline{P_{\mathbf{R},\kappa}} > \mid^2 \\ &= N^2\, \delta_{\mathbf{Q},\mathbf{G}} \mid < \rho_{\mathbf{G}} > \mid^2 \end{aligned} \qquad (A.3)$$

and

$$< I(\mathbf{Q}) >_{incoherent} = N \sum_{\mathbf{R}} e^{\mathbf{Q}\,\mathbf{R}} \sum_{\kappa,\kappa'} e^{i\,(\mathbf{Q}-\mathbf{G})\,(\mathbf{X}(\kappa)-\mathbf{X}(\kappa'))} < \overline{\delta P_{\mathbf{R},\kappa}\, \delta P^{*}_{\mathbf{0},\kappa'}} > \qquad (A.4)$$

in the limit $|\mathbf{Q} - \mathbf{G}| \rightarrow 0$ one deduces:

$$< I(\mathbf{Q}) >_{incoherent} \sim N \sum_{\mathbf{R}} e^{i(\mathbf{Q}-\mathbf{G})\,\mathbf{R}} < \overline{\delta P_{\mathbf{R}}\, \delta P^{*}_{\mathbf{0}}} > \qquad (A.5)$$

The right hand side of equation (A.5) is the fourier transform of the correlation function of the reconstruction order parameter, connected to the susceptibility χ through the fluctuation-dissipation theorem, namely

$$< I(\mathbf{Q}) >_{incoherent} \sim N\, k_B\, T\, \chi(\mathbf{Q} - \mathbf{G}) \qquad (A.6)$$

We remark that by taking in (A.1) the shadowing factors appropriate for atom scattering, i.e. eq. (2.2), one obtains a slightly different definition of the local order parameter. Equations (A.3)-(A.4) still holds, and apply now to atom scattering. Since the new local order parameter still assumes the same values of the order parameter (1.1) in the

four degenerate 2x1 ground states, one expects that the critical exponents deducible from (A.3)-(A.6) near T_c are actually the same for the two choice of the shadowing factors.

Appendix B
The lattice gas model

In this appendix we introduce the first model proposed for the deconstruction transition of Au(110) [53, 54].

The model includes only defects (b) and (b') in fig.1.1; just the outermost layer is supposed to be involved in the deconstruction. We assign an occupation number $n_{i,j}$ of the lattice sites in the outermost layer, where the indexes i and j run on lattice sites along $[1\bar{1}0]$ and [001] respectively. The following hamiltonian is defined:

$$H = v_1 \sum_{i,j} (n_{i,j} - n_{i+1,j})^2 - v_2 \sum_{i,j} (n_{i,j} - n_{i,j+1})^2 \qquad \text{(B.1)}$$

$v_1, v_2 > 0$. At half coverage the ground state of (B.1) has the MR structure. v_1 is the energy required by the breaking of a bond along $[1\bar{1}0]$, and v_2 is the energy per atom of the excitations (b) and (b') in figure 1.1. We put $n_{i,j} = (1 + \sigma_{i,j})/2$, $\sigma_{i,j} = \pm 1$. It is straightforward to recognize that the gran canonical partition function of hamiltonian (B.1) with zero chemical potential is equal to the canonical partition function of the following anisotropic Ising hamiltonian

$$H_{Ising} = \frac{v_1}{2} \sum_{i,j} \sigma_{i,j}\sigma_{i+1,j} - \frac{v_2}{2} \sum_{i,j} \sigma_{i,j}\sigma_{i,j+1} \qquad \text{(B.2)}$$

Since $< \sigma >$ is always zero for the anisotropic Ising model above, the average coverage

is always 1/2 for zero chemical potential. Thus one can use the result of the Ising model (B.2) to describe the deconstruction phase transition in the gran canonical ensemble of hamiltonian (B.1) with the constraint of average coverage 1/2. From Onsager solution one obtains [55]

$$\sinh \frac{v_1}{T_D} \sinh \frac{v_2}{T_D} = 1 \tag{B.3}$$

and the correlation length

$$\xi = \xi_0^+ t^{-1},\ 0 < t = \frac{T - T_D}{T_D} \ll 1 \tag{B.4}$$

For square lattice the non universal factor ξ_0^+ is [50]

$$\xi_0^+ = 2 / (\frac{v_1}{T_D} \cosh \frac{v_1}{T_D} \sinh \frac{v_2}{T_D} + \frac{v_2}{T_D} \cosh \frac{v_2}{T_D} \sinh \frac{v_1}{T_D}) \tag{B.5}$$

The 2D universality class of the deconstruction transition is actually predicted for all lattice gas hamiltonians for atoms in the outermost layer of fcc(110). This result comes only from symmetry consideration as shown by Bak [20] and Schick [21]. The particular choice of hamiltonian (B.1) let us to obtain not only the universality class, but all thermodynamical properties from the solution of the 2D Ising model. Even for the deconstruction transition in scenario (i) this model seems too naive: many body interactions in the lattice gas sense are expected to play a role. More sophisticated lattice gas models have been proposed later, including many body adatom-adatom interactions calculated from phenomenological many body potential (EAM) [56] or tight binding schemes [54]. Actually the Monte Carlo simulations with these models show that hamiltonian (B.1) gives indeed a good estimate of the transition temperature, if the parameters v_1 and v_2 are deduced from the breaking of an infinite row and from the energy of the defect in figure 1.1c, respectively.

Appendix C
Molecular Dynamics study of defects energies and deconstruction transition with many-body classical potentials

In this appendix we discuss to which extent a SOS model, as hamiltonian (3.14), is able to describe the true hierarchy of the energy of defects in fig.1.1 for a real surface. In order to do this we compare the defects energy as predicted by hamiltonian (3.14) with the energies deduced by molecular dynamics simulation with two different phenomenological classical potential, namely the glue model [16, 18, 17] and the Voters' potential [46] for gold. It turns out that the results are strongly potential dependent; hence we have investigated the structure of the deconstructed phase obtained with both the previous continuum models. Unfortunately the kinetics of the deconstruction transition is very low, so the thermodynamical characterization of the phase transition by molecular dynamics is very computer demanding. Moreover, the detection of the roughening transition, necessary for the discrimination between the scenarios proposed in chapter 1, seems up to now infeasible in standard molecular dynamics simulations with a fixed number of particles. Nevertheless we have obtained a picture of a deconstrucetd phase by warming up the sample at temperature higher than the expected T_D, where the kinetics is much faster. The deconstructed

phases for the Voters' and glue models are indeed very different.

Let us briefly describe the form of these phenomenological classical hamiltonians. In these hamiltonians, the total energy of a system including N atoms in an arbitrary geometry is function only of atomic positions, by means of an appropriate analytic classical expression whose form is such to mimic the forces induced by the electronic system on the ions. In these models one makes the energy of an atom dependent upon a "coordination" or "density" variable n_i, characterizing the local environment in which the atom is immersed. In this way, one could easily model the dramatic changes in the nature of the forces that occur when an atom is brought from the bulk to the surface, which is a key ingredient in the physics of metals. Following this idea, several many-body Hamiltonians of the form

$$V = \frac{1}{2} \sum_{\substack{i,j=1 \\ (j \neq i)}}^{N} \phi(r_{ij}) + \sum_{i}^{N} U(n_i) \tag{C.1}$$

where n_i is in turn constructed as a superposition of two-body-like contributions

$$n_i = \sum_{\substack{i=1 \\ (j \neq i)}}^{N} \rho(r_{ij}) \tag{C.2}$$

have become rather popular in recent years in modeling metals [75, 76, 77, 16, 17, 46] and particularly noble metals. The various scheme proposed differ widely in the implementation of the three functions $\rho(r)$, $U(n)$, $\phi(r)$. In the "embedded-atom method" [75], ϕ and U are fitted, while ρ is assumed to be the density distribution around an isolated atom taken from Hartree-Fock calculations. In the glue model [16, 17] and in the potentials by Voter and Chen [46] , all the three functions are included in the fitting procedure. The parameters of the hamiltonian are fitted on bulk and diatomic molecules properties, except for the glue model, where the surface energy has been included among

the quantity to be fitted.

All these hamiltonians have been applied to surface geometries, with various degrees of success. For instance, Voter and Chen [46] obtain occurrence of the missing-row reconstruction on the (110) surface for Au and Pt, and absence of such reconstruction for Ni, Pd, Cu, Ag and Al, which exactly corresponds to the experimental evidence. The glue model seems up to now the best parametrization of hamiltonian (C.1) for gold. It is the only parametrization that predicts the experimentally observed reconstruction of (100), (111), of magic vicinal surface of (110) [17] and that stabilizes the 2x1 reconstruction of (110) surface with respect to faceting into the (111) surface [18] [1].

The $T = 0$ missing-row structure of Au(110)(2x1) as given by the glue model was detailed in ref. [18]. The topmost row is shrunken by $\approx$ 27%, the second are slightly inward paired, and the third layer buckling magnitude is about 26%. Experiments [12] indicate a somewhat smaller relaxation 18 – 20%, and no second-layer inwards pairing, suggesting too large contractive forces in the glue model. Moreover the glue model predicts a small ($\approx 0.26\mathring{A}$) sliding distortion of the top rows along their own direction, which up to now has not been detected experimentally. In the glue model the average sliding distortion disappears at an Ising-like critical temperature $T_c \approx 230K$. The Voters' potential does not present the sliding distortion and produce inward relaxation of the top rows of 16%.

In table I are compared the surface energies per atom at $T = 0$ as deduced from the glue model [18, 78], Voters' potential [78] and ab initio pseudopotential calculation [15, 79].

[1] Roefles *et al* [56] have proposed a modification of hamiltonian (C.1), including in the argument of the "embedding energy" U a gradient correction of the form $U(n_i + \beta|\nabla n_i|^2)$. By tailoring the parameter β, they obtained a (2x1) phase lower in energy than the (1x1), and stabilized with respect of the faceting in the (111) surface. They used this hamiltonian to deduced the parameters of a lattice gas model with many-body interactions. The lattice gas model can describe only scenario (i) for the deconstruction; this scenario is probably less favoured, since in their model the energy of the 3x1 wall is lower than the energy of the 1x1 wall.

	Glue	Voter	ab initio
γ_{100}	1064.3 (128.5)	461.2 (55.68)	678.4 (83.0)
γ_{111}	692.9 (122.5)	312.9 (60.52)	465.6 (86.13)
γ_{1x1}	717.4 (107.4)	354.4 (58.99)	504.4 (81.76)
γ_{2x1}	629.0 (96.6)	341.2 (47.99)	478.8 (64.91)

Table I. Surface energies in *mev/atom* and in *mev/Å*^{2} (in parenthesis) for (100), (110)(1x1), (110)(2x1), (111) surfaces of gold. The energies refer to the glue model [18, 78], the Voters' potential [78] and ab initio calculations [15, 79].

For Voters' and ab initio potentials the surface energy of (111) surface is lower than those of the (110)(2x1) surface, so one deduces that the (110)(2x1) surface is unstable with respect to faceting into the (111) surface. The difference between γ_{2x1} and γ_{111} in ab initio calculation is of the same order of magnitude of the expected numerical error. Hence, although probably stabilized, the 2x1 phase should be very close in energy to the higher order reconstructed phases. When the (110) surface is unstable, as for the Voters' potential, the study of the defects energy and of the deconstruction transition on the (110)(2x1) metastable surface could seem meaningless. Nevertheless we have studied defects energies at $T = 0$ and the structure of the deconstructed phase at high temperature for both the glue model (where the (110)(2x1) is stable) and the Voters' potential with the aim of comparing, for two different continuum model, the role of relaxation and interactions between defects. As a first step let us deduce the parameters of the model hamiltonian (3.14) from the the energies of infinite surfaces in table I; then the comparison between the energies of defects calculated within the SOS hamiltonian with those obtained by molecular

dynamics simulation will give us some indications on the importance of relaxation and interactions between defects. The parameters J, $J_2(J \cdot K_2)$ and $J_3(J \cdot K_3)$ of hamiltonian (3.14) by Mazzeo *et al* can be expressed in terms of surfaces energies per atom as follows:

$$J = \frac{\gamma_{100} - \gamma_{1x1}}{4} \; ; \; J_2 = \frac{\gamma_{1x1} - \gamma_{2x1}}{2} \; ; \; J_3 = \frac{\gamma_{111} - \gamma_{1x1} + 2J_2}{8} \qquad \text{(C.3)}$$

In table II are reported the values of J, JK_2 and JK_3 deduced from the surface energies in table I.

	Glue	Voter	ab initio
J	86.7	26.7	43.5
J_2	44.2	6.6	12.8
J_3	19.0	-1.8775	1.55

Table II. Parameters J, J_2, and J_3 of hamiltonian (3.14), deduced from relations (C.3) and surface energies in table I.

We have mentioned in section 3.6 that T_D, obtained by Mazzeo *et al* with the parameters in table II from the glue model, is four times greater than the experimental value. Table II suggests that J and J_2 deduced from the glue model may be simply too large.

We have calculated the energies of defects in fig.1.1 at $T = 0$ with a molecular dynamics steepest descent procedure. The atoms are arranged in a slab 16 layers thick, with in-plane periodic boundary condition. Four layers on one surface are fixed to bulk positions at $T = 0$. The energies $\delta, \delta', \eta, \eta'$ of defects (b),(b'),(c) and (c') in fig.1.1, are calculated in a configuration with two identical defects, infinite along $[1\bar{1}0]$, separated by a distance of $28a_o$. Decreasing the distance bewteen the defects from $28a_o$ to $8a_o$, the energy δ increases

of 8%. The energies μ and μ' of defects (i) and (l) in fig.1.1 are obtained from a sample composed by two terraces, large $18a_o$ and $16a_o$ respectively, separated by a distance of $15a_o$. The energy required to break a bond along $[1\bar{1}0]$ is evaluated from the sample depicted in fig.C.1. We assign $W_o = \frac{(\gamma - \gamma_{2x1}).A}{8}$, where γ and A are the surface energy and area of the sample in fig.C.1. W_o is equal to $4J$ for hamiltonian (3.14).

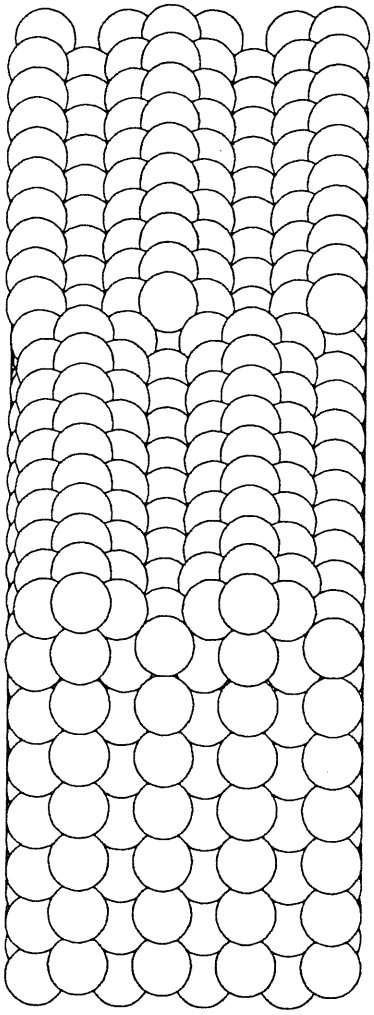

Figure C.1: Sample used to evaluate the energy W_o required to break a bond along $[1\bar{1}0]$. $W_o = \frac{(\gamma - \gamma_{2x1}).A}{8}$, where γ and A are surface energy and area of the fully relaxed sample. In-plane periodic boundary conditions are applied.

The energies of the fully relaxed defects are summarized in table III.

	Glue		Voter	
	MD	SOS	MD	SOS
δ	30	177	28	26
δ'	106	177	28	26
η	38	127	-	-
η'	144	127	-	-
ε	22	63	-16	-28
ε'	64	88	15	13
$W_o = 4J$	369	347	153	107

Table III. Energy per atomic spacing along $[1\bar{1}0]$ of defects in figure 1.1 at $T = 0K$. The energy are in *mev*, and are calculated for both glue and Voters' potentials with a molecular dynamics steepest descent (MD column), and with hamiltonian (3.14) by Mazzeo *et al* (column SOS), with the parametrization of table II.

Surprisingly there is a strong asymmetry between the energies of defects (b) and (b'), and (c) and (c') for the glue model. This asymmetry is absent in the Voters' model. We note that, in the glue model, δ is much lower from the values predicted by hamiltonian (3.14). The energy gain is due to a large in-plane relaxation of the top rows of the defect, which produce a release of surface stress. In the glue model the surface stress is negative for 1x1 surface ($\partial\gamma/\partial\varepsilon = -118\, mev/\mathring{A}^2$, ε = strain along [001]), while it is positive for the 2x1 surface ($\partial\gamma/\partial\varepsilon = 81\, mev/\mathring{A}^2$). The surface stress is strongly reduced by an expansion of 8.5% of the distance between the two top rows of the defect (b), and by a contraction of the 2x1 region, extending as far as $14a_o$ from the defect. Hindering the in-plane contraction

or expansion of all the top rows, one obtain $\delta \approx 130\, mev$ (cfr. Table III). The energy gain is mainly due to relaxation in a region of $4a_o$ around the defect. This effect is responsible for the peculiar hierarchy of defects energy, anticipated in chapter 1 : $E^{wall}_{1x1} < E^{wall}_{3x1}$, but $E^{step}_{1x1} \gg E^{step}_{3x1}$. Conversely, in the Voters' potential the distance between the two top rows of the defect (b) does not expand, the surface stress being small and positive for both the 1x1 and 2x1 surfaces ($18.9\, mev/\mathring{A}^2$ and $24.5\, mev/\mathring{A}^2$, for 2x1 and 1x1 respectively).

Table III reports the energies of defects infinite along $[1\bar{1}0]$. Now one may wonder what happens if we consider defects finite along the rows. In order to investigate this point we have calculated the energy of a finite defect, obtained by breaking a row and displacing ten atoms of the row in the adjacent groove. The sample used is shown in figure C.2, it contains 20 atoms along $[1\bar{1}0]$ and it is $24a_o$ large, periodic boundary conditions are applied as usual. The energy of the defect should be $10(\delta + \delta') + 4W_o$. The energy obtained by the relaxation of the sample with the glue model is 38 % higher than the aforementioned value, indicating a strong deviation from the SOS prescriptions, while it is only 6 % higher for the Voters' potential.

Furthermore we have investigated the renormalization of the energies of the defects due to the crystal expansion, simply by assigning to the fixed layers at the bottom of the sample the bulk lattice constant predicted by the model at $850K$. This calculation is meaningful in the quasi-harmonic approximation. Within the glue model we have obtained for example a decrease of 30 % in the energy of the defect in fig.C.2 with respects to its value with the zero temperature lattice constant. Conversely the parameter W_o decreases only of 10 %, by increasing the lattice parameter. Still the renormalization of the defects energy within the Voters' model is negligible.

Summarizing, we have found in the glue model large deviations from the prescriptions of the SOS model (3.14): namely, an asymmetry between "up" and "down" walls, a strong

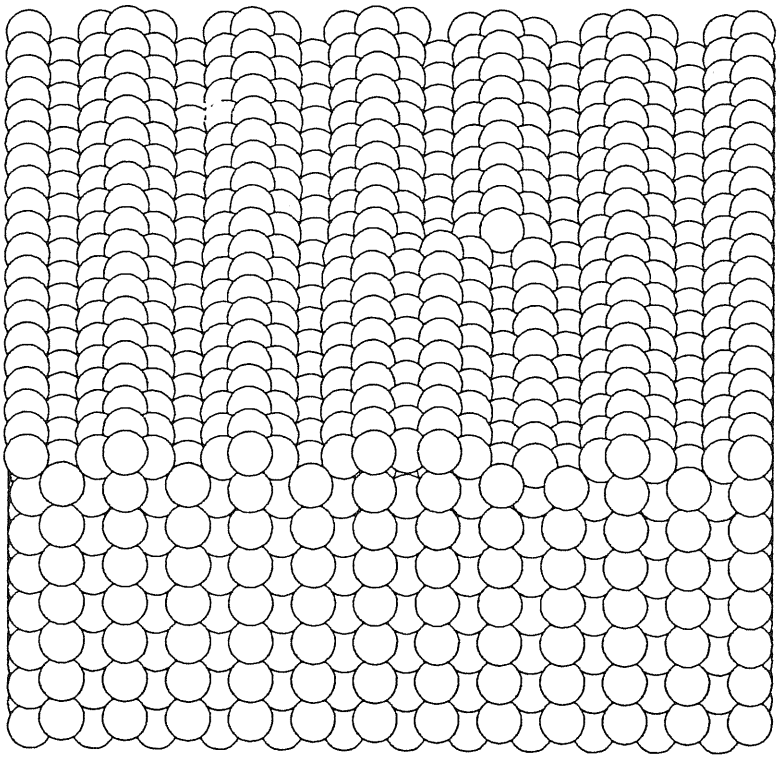

Figure C.2: Sample used to evaluate the energy of a defect finite along $[1\bar{1}0]$ (see text). In-plane periodic boundary conditions are applied.

renormalization of the defects energy with the lattice parameter (hence with temperature), a strong interaction between finite defects, as deduced from the surface energy of sample in fig.C.2, a large deviation of the MD results from the energies predicted by hamiltonian (3.14) fitted to the energies of infinite surfaces (see table II). All these "anomalies" are far less pronounced in the Voters' potential. Hence we attribute these features to large in-plane relaxation along [001] around the defects, due to the larger surface contractive forces of the glue model with respect to the Voters' potential. From the above results one concludes that the ability of the SOS model in reproducing the correct energetics of defects of a continuum model, depends on details of the many-body potential: while the SOS predictions are fairly well realized by the Voters' potential, they are largely wrong for the glue model.

The surface contractive forces are responsible also for a striking difference in the structure of the deconstructed phases of glue and Voters' potentials. In figure C.3 is reported the final configuration of a molecular dynamics run at constant temperature ($T = 980K$), 1.75 nsec long (250.000 MD time steps, a time step being $7\,10^{-3}$ psec). The potential used is the glue model and the sample is composed by 3720 particles arranged in a slab 16 layers thick; the 4 bottom layers fixed at the bulk positions (the lattice constant is the theoretical one at the working temperature). Figure C.4 reports the final configuration of a simulation with the Voters' potential at $T = 990K$, 0.35 nsec long (50.000 MD time step), for the same sample of fig.C.3. The starting configuration is, in both cases, the final result of a MD schedule of heating from the ground state at $T = 0$, it is essentially reconstructed, and contains a small amount of defects. For comparison, figure C.5 reports a snapshot of the sample at 400 K.

The sample in figures C.3 and C.4 are probably not well equilibrated, more than 50.000 and 10.000 times steps are necessary, respectively for the glue and Voters' potential, in

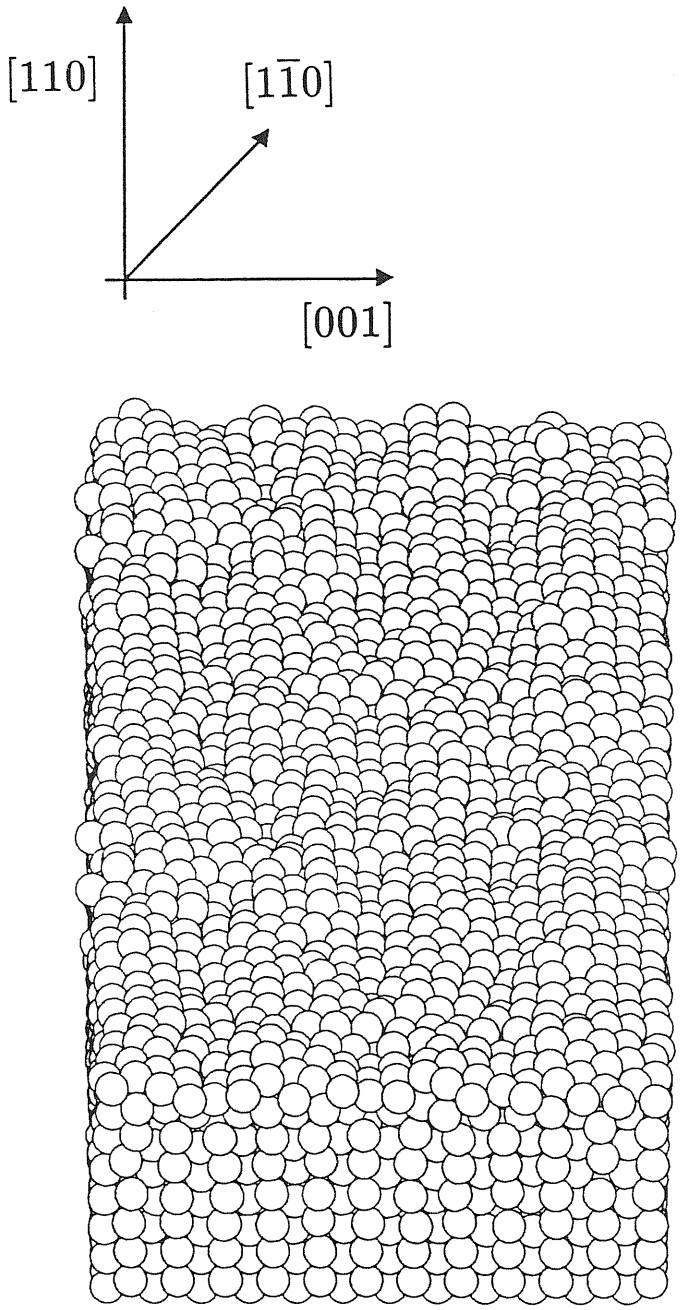

Figure C.3: Final configuration of a MD run at $T = 980K$ for the glue model. In the figure are reported 2 MD unit cells along the [1$\bar{1}$0] direction for sake of clarity.

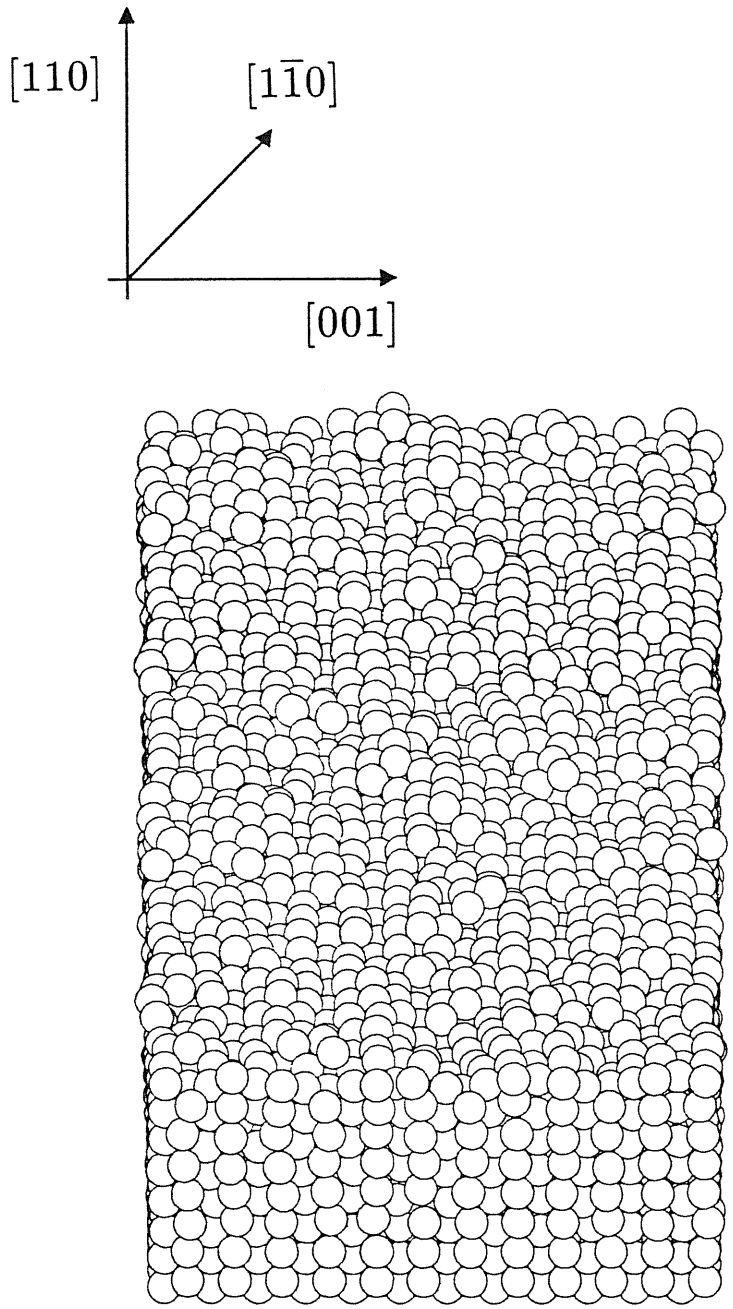

Figure C.4: The same as figure (C.3) for the Voters' potential at $T = 990K$.

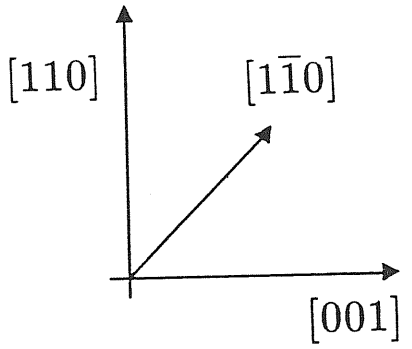

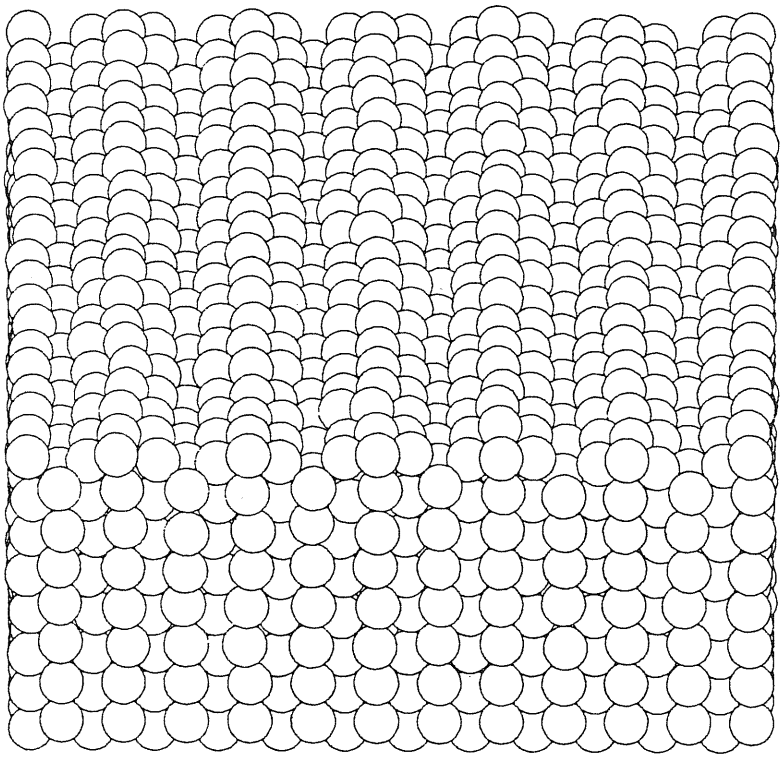

Figure C.5: Snapshot of a MD run at $T = 400K$ for the glue model. The sample has the same dimension as the samples of figures (C.3) (C.4).

order to detect diffusion and/or generation of defects at 980 K. Nevertheless by doubling the length of the run the characteristic features of the deconstructed phases do not change, so we expect than figures C.3 and C.4 are good pictures of the deconstructed phases for both the models. The reconstruction order in the samples of figure C.3 and C.4 is evidently lost (cfr. fig.C.5), but while in fig.C.4 a strong resemblance with a SOS model survives, the surface of fig.C.3 looks very different.

In figure C.3 defects of type (b) and (c) are evident, but the surface has lost the registry with the underlying bulk lattice. In the glue model when a defect of the type depicted in fig.C.2 appears, the atoms of rows in the second layer, adjacent to the defect, relax into the hole, hiding the row in the third layer. In fig.C.6 is reported the same defect as in fig.C.2, nucleated at 980 K. The relaxation around the defect are evident.

Driven by the previous mechanism, two atomic rows have disappeared from the surface in fig.C.3, the relaxation produce an increase in the distance between the adjacent top rows, inducing an incommensuration with the bulk. This incommensuration can be seen in the elastic scattering intensity (2.1). The elastic scattering intensity has been calculated from expression (2.1) by averaging over 100 configurations taken every 100 time steps from a molecular dynamics trajectory. The shadowing factors are taken equal to one for "surface atoms" and zero otherwise, by defining "surface atoms" those which are not vertically shadowed by any other atom, once a conventional spherical radius r_o is attached to each atom. The choice $r_o = 1\mathring{A}$ let us obtain a scattering intensity (2.1) displaying very clearly bulk permitted and reconstruction peaks for a reconstructed sample. The quantity $< I(\mathbf{Q}, q_z) >$ (cfr. (2.1)) is reported in fig.C.7 as a function of Q_x along [001], with $q_z = Q_y = 0$, for the sample at 970 K and at 500 K, within the glue model.

Figure C.8 is the analogous of figure C.7 for the Voters' potential.

In fig.C.7 a doublet appears very clearly in correspondence of the integer peak $Q_x = \frac{2\pi}{a_o}$.

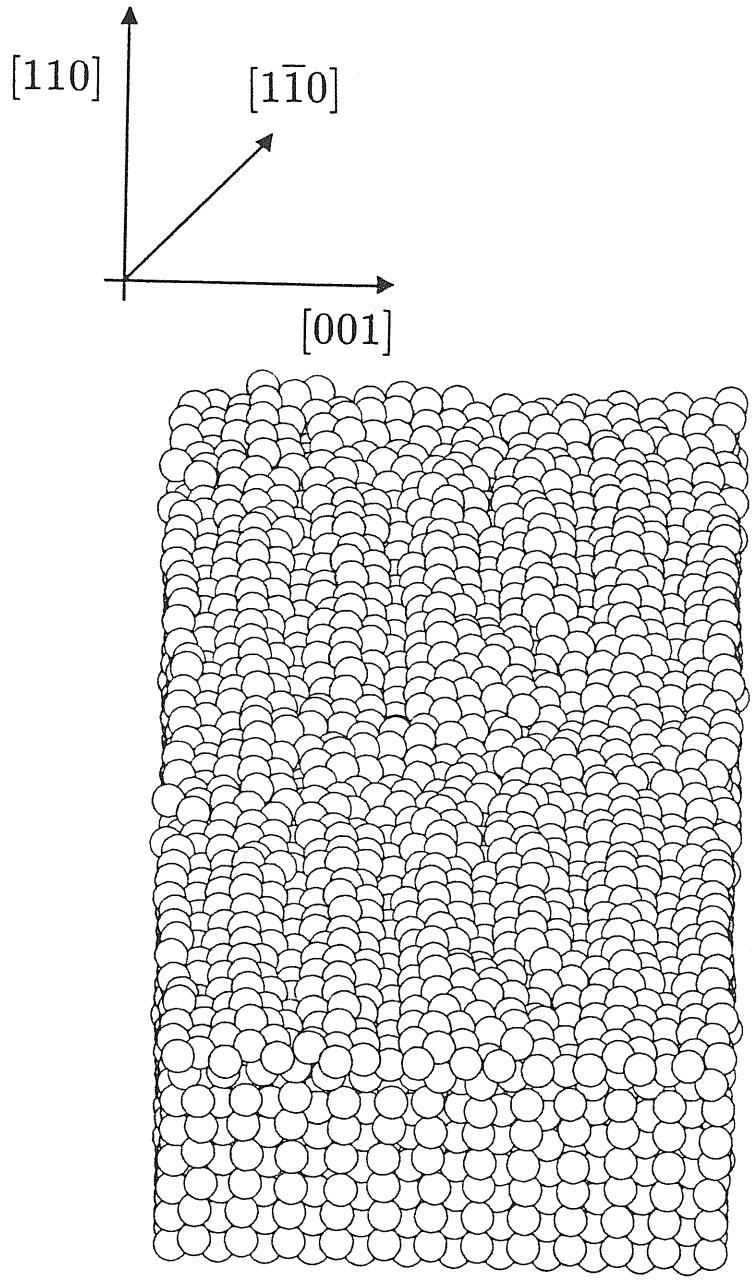

Figure C.6: Configuration at $980K$, averaged over 500 time steps (roughly 10 phonon periods) of a sample with a spontaneous nucleation of a defect of the type reported in figure (C.2). In the figure are reported 2 MD unit cells along the $[1\bar{1}0]$ direction for sake of clarity.

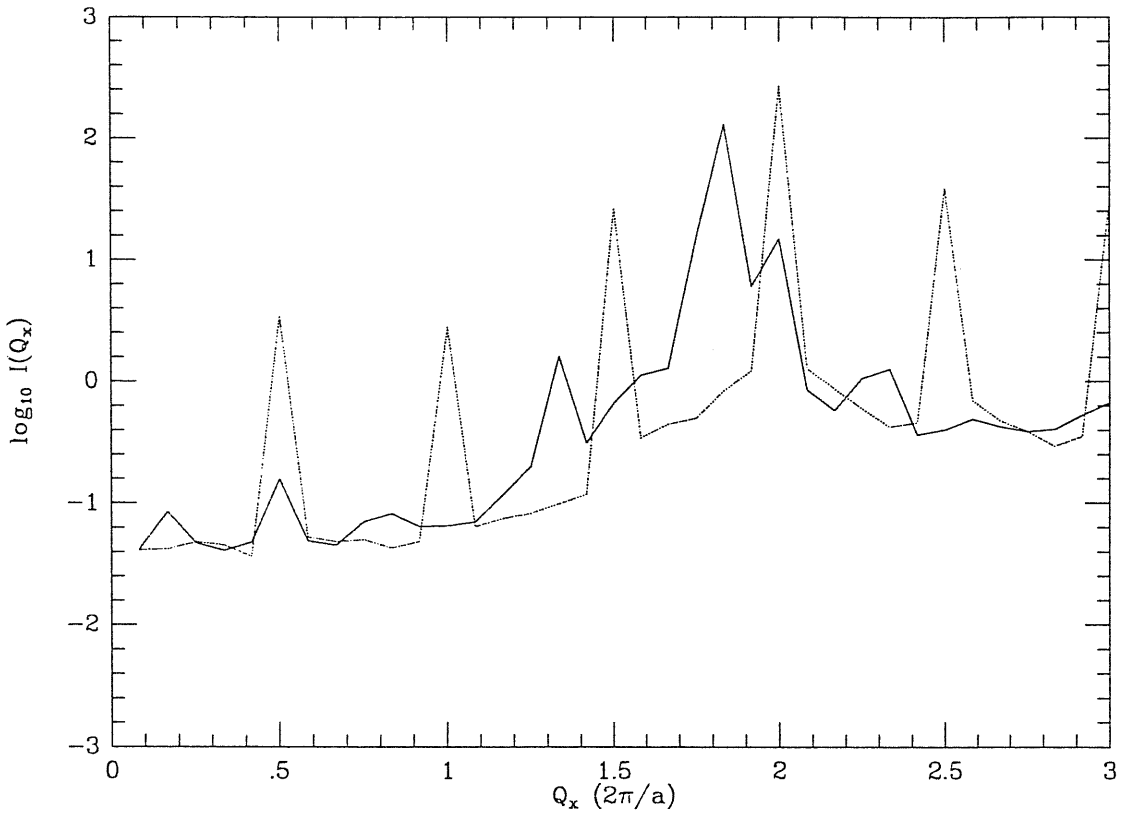

Figure C.7: Elastic scattering intensity $I(Q_x)$ calculated from MD run for the glue model (see text). Q_x is along [001]. Continuous line refers a simulation at $980K$ starting from the configuration in (C.3). Dotted line refers to a simulation at $400K$ starting from the sample in figure (C.5).

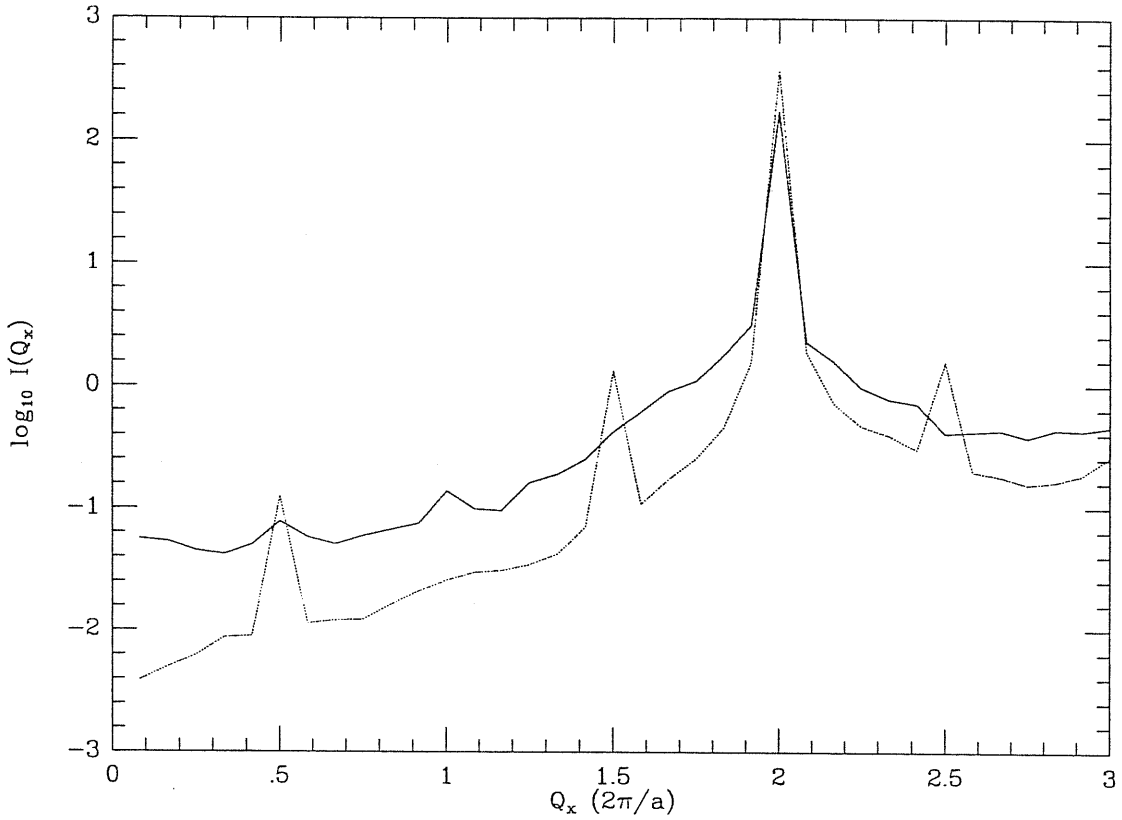

Figure C.8: The same as figure (C.7) for the Voters' potential. Continuous line refers to a simulation at $990K$ starting from the sample in figure (C.4), while dotted line refers to a simulation at $500K$.

The lowest and more intense peak of the doublet corresponds to $Q_x = \frac{2\pi}{a'}$, where a' is exactly the renormalized surface lattice constant, obtained dividing the sample length along [001] by the number of surface rows visible in fig.C.3. This effect is present for different sample sizes for the glue model. Conversely the registry with the underlying lattice is conserved in the deconstructed phase for the Voters' potential, as illustrated by fig.C.8: the reconstruction peaks disappear, but the integer peak does not move. Since the incommensuration has never been observed experimentally on Au(110) we expect that it is a failure of the glue model, and that a more plausible picture of the real deconstructed phase is provided by the Voters' potential result in fig.C.4. Since for the Voters' potential the 2x1 phase is not stable with respect to faceting into the (111), fig.C.4 can describe just the deconstruction of a *metastable* 2x1 surface [2].

The ability to reproduce the structure of the deconstructed phase seems thus a strigent test for the quality of phenomenological continuum potentials. A parametrization of the phenomenological many-body hamiltonian C.1, able to describe properly the deconstructed phase of Au(110)(2x1) is thus still lacking.

[2] As a subsidiary result of the MD simulation of the deconstruction transition, we have characterized the mechanism by which the defects in fig.C.2 appear at 990 K within the Voter' model. The process is identical to the cross-channel exchange mechanism, proposed for adatom migration on the unreconstructed fcc(110) surfaces [80, 81, 82]: an atom in the second layer jumps in the channel produced by the missing row, and an adjacent atom in the top row replaces the atom in the second layer. In the final configuration one vacancy is formed in the top row, and one adatom is present in the adjacent channel, but this configuration is produced through an exchange between atoms of the first and second layer. Recently Liu *et al* [82] have calculated the self-diffusion coefficient for adatoms on the (110)(1x1) surface of several metals including Au and Pt within the Voters' model. By using molecular static simulations they have calculated attempt frequency and saddle point energy for the exchange mechanism, subsequently used in standard transition state theory. Our MD simulation confirms that the exchange mechanism is the dominant one up to 990 K for interchannel diffusion. Moreover we have observed that the adatoms in the channel act as nucleation center for the generation of new adatoms via the exchange mechanism.

Acknowledgements

First of all I would like to express my thanks to my supervisors Prof. Erio Tosatti and Dr. Furio Ercolessi , for their guidance and encouragement during the course of this work. I am also grateful to Prof. Andrea Levi and Prof. Giancarlo Jug for illuminating discussions. A special aknowledgemet is owed to Dr. Giorgio Mazzeo for his constant critical advice on this work, and for providing his original results prior to publication. I thank Dr. Balents and Prof. den Nijs for sending their preprint prior to publication.

Bibliography

[1] B. H. Hayden, K. C. Prince, P. J. Davie, G. Paolucci and G. M. Bradshow, Solid State Commun. **48**, 325 (1983).

[2] S. M. Francis and N. V. Richardson, Surface Sci. **152/153**, 63 (1985).

[3] M. Copel, W. R. Graham, T. Gustafsson and S. M. Yalisove, Solid State Commun. **53**, 695 (1985).

[4] J. W. M. Frenken, R. L. Krans, J. F. van der Veen, E. Holub-Krappe and K. Horn, Phys. Rev. Lett. **59**, 2307 (1987).

[5] A. Trayanov, A.C. Levi and E. Tosatti, Surf. Sci. **233** 184 (1990); Europhys. Lett. **8**, 657 (1989).

[6] S. G. J. Mochrie, Phys. Rev. Lett. **59**, 304 (1987).

[7] P. Zeppenfeld, K. Kern, R. David and G. Comsa, Phys. Rev. Lett. **62**, 63 (1989).

[8] G. A. Held, J. L. Jordan-Sweet, P. M. Horn, A. Mak and R. G. Birgeneau, Phys. Rev. Lett. **59**, 2075 (1987).

[9] I. K. Robinson, E. Vlieg, H. Hornis and E. H. Conrad, Phys. Rev. Lett. **67** 1890 (1991).

[10] Y. Cao and E. H. Conrad, Phys. Rev. Lett. **64**, 447 (1990).

[11] R. Koch, M. Borbonus, O. Haase, and K. H. Rieder, Phys. Rev. Lett. **67**, 3416 (1992).

[12] W. Moritz and D. Wolf, Surf. Sci. **163**, L655 (1985); C. M. Chan and M.A. Van Hove, Surf Sci. **171**, 226 (1986); T. Engel and J.H.Weave, Surf. Sci. **1164**, 403 (1985); L. D. Marks, Phys. Rev. Lett. **51**, 1000 (1983); G. Binnig, H. Roher, Ch. Gerber and

E. Weibel, Surf. Sci. **131**, L379 (1983); I. K. Robinson, Phys. Rev. Lett. **50**, 1145 (1983); J. Moller, H. Niehus and W. Heiland, Surf. Sci. **166**, L111 (1986); M. Copel and T. Gustafsson, Phys. Rev. Lett. **57**, 723 (1986).

[13] E. C. Sowa, M. A. van Hove and D. L. Adams, Surf. Sci. **199**, 174 (1988); G. L. Kellog, Phys. Rev. Lett. **55**, 2168 (1985); P. Fery, W. Moritz and D.Wolf, Phys. Rev. B **38**, 7275 (1988).

[14] H. J. Broksch and K. H. Bennemann, Surf. Sci. **161**, 321 (1985).

[15] K. M. Ho and K. P. Bohnen, Phys. Rev. Lett. **59**, 1833 (1987).

[16] F. Ercolessi, M. Parrinello and E. Tosatti, Phylos. Mag. A **58**, 213 (1988).

[17] E. Tosatti and F. Ercolessi, Mod. Phys. Lett. **B 5**, 413 (1991).

[18] M. Garofalo, E. Tosatti and F. Ercolessi, Surf. Sci. **188**, 321 (1987).

[19] S. M. Foiles, Surf. Sci. **191**, L779 (1987).

[20] P. Bak, Solid State Comm. **32**, 581 (1979).

[21] M. Schick, Progr. Surf. Sci. **11**, 245 (1981).

[22] H. van Beijeren and I. Nolden, in *Structure and Dynamics of Surfaces II*, Eds. W. Schommers and P. von Blanckenhagen (Springer-Verlag, Heidelberg, 1987) p. 259.

[23] J.D. Weeks, in *Ordering in Strongly Fluctuating Condensed Matter Systems*, NATO ASI **B50**, Ed. T. Riste (Plenum, New York, 1979).

[24] J.C. Campuzano, M.S. Foster, G. Jennings, R.F. Willis and W. Unertl, Phys. Rev. Lett. **54**, 2684 (1985).

[25] D.T. Keane, P.A. Bancel, J.L. Jordan-Sweet, G.A. Held, A. Mak and R.J. Birgeneau, *Surf. Sci.* **250**, 8 (1991).

[26] J. Sprösser, B. Salanon and J. Lapujoulade, Europhys. Lett. **16**, 283 (1991).

[27] D. Cvetko, A. Lausi, A. Morgante, F. Tommasini and K.C. Prince, Surf. Sci. **269/270**, 68 (1991).

[28] E. van de Riet, H. Derks and W. Heiland, Surf. Sci. **234**, 53 (1990).

[29] U. Romahn *et al*, Surf. Sci. **251/252**, 656 (1991).

[30] I. K. Robinson, E. Vlieg and K. Kern, Phys. Rev. Lett. **63**, 2578 (1989).

[31] J. Villain and I. Vilfan, Surf. Sci. **199**, 165 (1988)

[32] J. Villain and I. Vilfan, Phys. Rev. Lett. **65**, 1830 (1990).

[33] J. Villain and I. Vilfan, Surf. Sci. **257**, 368 (1991).

[34] J. Villain and I. Vilfan, Europhys. Lett. **12**, 523 (1990); **12**, 741 (1990); **13**, 285 (1990).

[35] J. Villain, J. L. Rouviere and I. Vilfan, in: *Phase Transition in Surface Films*, Eds. H. Taub , H. Lauter and S. C. Fain, pag. 210 (Plenum, New York, 1990).

[36] A.C. Levi and M. Touzani, Surf. Sci. **218**, 223 (1989).

[37] G. Jug and E. Tosatti, Phys. Rev. **B41**, 969 (1990); G. Jug and E. Tosatti, Physica **A 175**, 59 (1990).

[38] J. Kohanoff, G. Jug and E. Tosatti, J. Phys. **A23**, L209 (1990); J. Kohanoff, G. Jug and E. Tosatti, J. Phys. **A23**, 5625 (1990).

[39] M. den Nijs, Phys. Rev. Lett. **66**, 907 (1991).

[40] M. den Nijs, in: *Phase Transition in Surface Films*, Eds. H. Taub , H. Lauter and S. C. Fain, pag. 247 (Plenum, New York, 1990).

[41] L. Balents and M. Kardar preprint (1992).

[42] K. Rommelse and M. den Nijs, Phys. Rev. Lett. **59**, 2578 (1987); Phys. Rev. **B40**, 4709 (1989).

[43] M. den Nijs, Phys. Rev. Lett. **64**, 435 (1990).

[44] G. Mazzeo, Magister Thesis, S.I.S.S.A. (1990), Trieste; G. Mazzeo, G. Jug, A. Levi and E. Tosatti, Surf. Sci. **273**, 237 (1992).

[45] M. den Nijs preprint (1992).

[46] A. F. Voter and S. P. Chen, Mat. Res. Soc. Symp. Proc. **82**, 175 (1987), and to be published.

[47] S. T. Chui and J. D. Weeks, Phys. Rev. **B14**, 4978 (1976).

[48] H. van Bejeren, Phys. Rev. Lett. **38**, 993 (1977).

[49] H. E. Lieb, Phys. Rev. Lett. **18**, 1046 (1967); H. E. Lieb and F. Y. Wu, in *Phase Transition and Critical Phenomena*, Eds. C. Domb and M. S. Green, pag. 331 (Academic, New York 1972).

[50] R. J. Baxter, *Exactly Solved Models in Statistical Mechanics* (Academic, London 1982).

[51] C. Jajaprakash and W. F. Saam, Phys. Rev. **B30**, 3916 (1984).

[52] J. H. van der Merwe and G. J. Shiflet, Surf. Sci. **256**, 171 (1991); G. J. Shiflet and J. H. van der Merwe, Surf. Sci. **256**, 187 (1991).

[53] J. C. Campuzano, A. M. Lahee and G. Jennings, Surf. Sci. **152/153**, 68 (1985).

[54] M. Guillope' and B. Legrand, Surf. Sci. **215**, 577 (1989).

[55] K. Huang, *Statistical Mechanics* (J. Wiley, New York 1987), pag. 368.

[56] L. D. Roelofs, S. M. Foiles, M. S. Daw and M. I. Baskes, Surf. Sci. **234**, 63 (1990).

[57] R.F. Willis, in *Dynamical Phenomena at Surfaces, Interfaces and Superlattices*, Eds. F. Nizzoli, K.H. Rieder and R.F. Willis (Springer-Verlag, Berlin, 1985).

[58] A.C Levi, R. Spadacini, G.E. Tommei, in *The Structure of Surfaces II*, Vol. 11, Eds. J.F. van der Veen and M.A. Hove (Springer-Verlag, Berlin, 1988)

[59] P. Fenter and T. M. Lu, Surf. Sci. **154**, 15 (1990).

[60] J. Villain, D. R. Grempel and J. Lapujoulade, J. Phys. F **15**, 809 (1985).

[61] H. N. Yang, T. M. Lu and G. C. Wang, Phys. Rev. **B 43**, 4714 (1991).

[62] H. N. Yang, T. M. Lu and G. C. Wang, Phys. Rev. Lett. **63**, 1621 (1989).

[63] D. E. Clark, W. N. Unertl and P. H. Kleban, Phys. Rev. **B 34**, 4379 (1986).

[64] E. G. McRae, T. M. Buck, R. A. Malic and G. H. Wheatley, Phys. Rev. **B 36**, 2341 (1987).

[65] J. K. Gimzewski, R. Berndt and R. R. Schlittler, Surf. Sci. **247**, 327 (1991); J. K. Gimzewski, R. Berndt and R. R. Schlittler, Phys. Rev. **B 45**, 6844 (1992).

[66] T. Gritsch, D. Coulman, R. J. Behm and G. Ertl, Surf. Sci. **257**, 297 (1991).

[67] K. Kern, private communication.

[68] E. Muller-Hartmann and J. Zittartz, Z. Phys. B **27**, 261 (1977).

[69] G. Mazzeo, private communication.

[70] S. N. Coppersmith *et al*, Phys. Rev. Lett. **46**, 549 (1981).

[71] H. J. Schulz, B. I. Halperin and C. L. Henley, Phys. Rev. **B 26**, 3797 (1982).

[72] V. L. Pokrovsky and A. L. Talapov, Phys. Rev. Lett. **42** , 65 (1979).

[73] J. Villain, in *Ordering in Strongly Fluctuating Condensed Matter Systems*, edited by T. Riste (Plenum, New York, 1980), p.221.

[74] E. H. Lieb and F. Y. Wu, Phys. Rev. Lett. **20**, 1445 (1968).

[75] M. S. Daw and M. I. Baskes, Phys. Rev. **B 29**, 6443 (1984); S. M. Foiles, M. I. Baskes and M. S. Daw, Phys. Rev. **B 33**, 7983 (1986); Phys. Rev. **B 37**, 10378 (1988).

[76] M. W. Finnis and J. E. Sinclair, Phil. Mag. **A 50**, 45 (1984); Phil. Mag. **A 53**, 162 (1986).

[77] D. Tomanek and K. H. Bennemann, Surf. Sci. **163**, 503 (1985).

[78] F. Ercolessi, Philosophiae Doctor Thesis, S.I.S.S.A - I.S.A.S. Trieste, 1988, unpublished.

[79] N. Takeuchi, C. T. Chan, and K. M. Ho Phys. Rev. **B 43**, 14363 (1991); Phys. Rev. **B 43**, 13899 (1991).

[80] G. De Lorenzi, G. Jacucci and V. Pontikis, Surf. Sci. **116**, 391 (1982).

[81] D. W. Basset and P.R. Webber, Surf. Sci. **70**, 520 (1978).

[82] C. L. Liu, J. M. Cohen, J. B. Adams and A. F. Voter, Surf. Sci. **253**, 334 (1991).